Order Number 8801700

Raman spectroscopy and Raman optical activity of organic molecules

Davies, Mark Allen, Ph.D.

City University of New York, 1987

U·M·I
300 N. Zeeb Rd.
Ann Arbor, MI 48106

PLEASE NOTE:

In all cases this material has been filmed in the best possible way from the available copy. Problems encountered with this document have been identified here with a check mark ✓.

1. Glossy photographs or pages _____
2. Colored illustrations, paper or print _____
3. Photographs with dark background _____
4. Illustrations are poor copy _____
5. Pages with black marks, not original copy ✓
6. Print shows through as there is text on both sides of page _____
7. Indistinct, broken or small print on several pages ✓
8. Print exceeds margin requirements _____
9. Tightly bound copy with print lost in spine _____
10. Computer printout pages with indistinct print _____
11. Page(s) _____ lacking when material received, and not available from school or author.
12. Page(s) _____ seem to be missing in numbering only as text follows.
13. Two pages numbered _____. Text follows.
14. Curling and wrinkled pages _____
15. Dissertation contains pages with print at a slant, filmed as received ✓
16. Other _____

_____

_____

UMI

RAMAN SPECTROSCOPY AND RAMAN OPTICAL ACTIVITY OF ORGANIC MOLECULES

by

MARK ALLEN DAVIES

A dissertation submitted to the Graduate Faculty in Chemistry in partial fulfillment of the requirements for the degree of Doctor of Philosophy, The City University of New York.

1987

This manuscript has been read and accepted for the Graduate Faculty in Chemistry in satisfaction of the dissertation requirement for the degree of Doctor of Philosophy.

6/10/87
Date

Max Hiam
Chair of Examining Committee

4/27/87
Date

G. M.
Executive Officer

William E. Hartman

David L. Burnside

Ricky Henkelman
Supervisory Committee

The City University of New York

Dedicated to my parents.

Acknowledgments

Several individuals contributed, perhaps more than they realize, to this work. First and foremost, many thanks go to Professor Max Diem, my adviser on this project, for his advice, encouragement, and unflagging enthusiasm. Dr. Reza Oboodi "broke me in" on the Raman Optical Activity spectrometer. We spent many days together chasing elusive signals during the summer and fall of 1984, at times getting frustrated but never losing our sense of humor. Finally, I thank Dr. James Calienni for performing the excellent optical resolution of chlorofluoroacetic acid.

Table of Contents

List of Tables

List of Tables, cont'd.

List of Figures

List of Figures, cont'd.

CHAPTER 1. INTRODUCTION

A. Scope and Objectives

Raman Optical Activity, the differential, inelastic scattering of left and right circularly polarized radiation by asymmetric or dissymmetric molecules, is one of the most recent additions to the ever growing array of techniques used in molecular spectroscopy and conformational analysis. X-ray diffraction proved to be a very powerful technique for use in solid phase studies. However, Pease and Watson (1) indicated that the conformation of small peptides in solution may not be the same as that in the solid state, due to the influence of high solvation energies. Electronic circular dichroism was used by a number of workers (2,3,4) to study samples of poly-amino acids, peptides,and proteins. Information on (very small differences in) conformational angles was obtained for samples with chain lengths ranging from a few residues to several dozen residues. This technique proved to be less useful in studies on very small peptides with irregular structures because of its lack of selectivity; that is, different amide electronic transitions with opposite CD signs were superimposed, rendering the data uninterpretable. Electronic CD also requires the presence of at least one group absorbing in the ultraviolet or

visible region of the spectrum. Usually, this is a carbonyl or peptide group.

NMR spectroscopy seems to work best in relatively rigid molecular systems; signals obtained during the relatively long time scale of the experiment are actually a time average of signals due to many rapidly equilibrating conformations.

Raman Optical Activity, henceforth called ROA, circumvents many of the problems mentioned above. The sample may be a liquid. An electronic absorber is not required. An important advantage of Raman scattering experiments is that all 3N-6 normal coordinates, where N is the number of atoms in the molecule, can be excited; i.e., there are 3N-6 possible ROA signals. Raman scattering is a fast process, taking place on a picosecond time scale.

The goal of the work described in this thesis was to develop the technique of ROA into a new chiroptical tool. This development includes instrumental aspects and studies on model systems. Optical alignment procedures were developed and refined. A detailed alignment procedure for the device producing circular polarization, the electro-optic modulator, is described. Samples chosen for study were organic liquids. The first liquid, (-)-α-pinene, was chosen in order to test the system for the presence of experimental artefacts in total ROA spectra. Such a spectrum, the total ROA spectrum, previously thought to be unobservable, is shown. The second, (-)-chlorofluoroacetic

acid, was chosen because its small size and relatively small number of normal modes (18) make it amenable to definitive vibrational assignment and normal coordinate analysis. ROA spectra obtained could be interpreted in terms of the normal coordinate analysis.

B. Introduction to Optical Activity

In 1812, Jean Baptiste Biot (5) repeated an experiment first performed by his colleague, Francois Arago, in 1811 (6). Plane polarized white light, produced by reflection off of a glass plate, was passed through quartz. The light was polarized perpendicular to the symmetry axis (optic axis) of the crystal. The light passing through the quartz was examined by observing it through a piece of calcite. It was observed that when the calcite was rotated, different colors appeared. Biot, unlike Arago, interpreted the effect. He said that the appearance of colors was due to rotation of the plane of polarization about the axis of travel. Furthermore, the angle of rotation depends upon the wavelength of light used. This effect is known today as optical rotatory dispersion. Biot also discovered that quartz crystals occur in two forms, the physical properties of which are similar except in one respect: each form rotates light in a direction opposite to that of the other form. We now call these two forms of quartz left handed

and right handed. A compound which rotates light clockwise (when viewed looking towards the source of light), is called dextrorotatory; compounds rotating plane polarized light in a counterclockwise direction are said to be levorotatory.

Biot continued his experiments using liquids in which he immersed the quartz. He then discovered that liquids themselves can be optically active. Among the liquids he examined were turpentine, lemon oil, alcoholic solutions of camphor and aqueous solutions of sugar and tartaric acid. Because some of the liquids, such as lemon oil, were found naturally in one form and were randomly oriented in the liquid state, Biot reasoned that optical activity is a property of the individual molecules. To test this theory, he heated turpentine and attempted to measure the optical rotation of the vapor. He observed that isolated gas phase molecules do indeed rotate plane polarized light (7). Biot, through his measurements to determine the optical rotation of quartz, found that optical rotation is inversely proportional to the square of the wavelenth of light passed through a given path length of quartz. Drude modified this law and (1) bears his name:

$$\theta = \Sigma_j A_j/(\lambda^2-\lambda_j^2). \qquad [1\text{-}1]$$

A_j is a constant, λ_j is the wavelength of an absorption, and λ is the wavelength of incident light. Even modern theories of optical rotation in transparent media have this form.

Augustin Fresnel put forth the first theory of optical rotation. This followed his discovery of circularly polarized light. A more detailed discussion of circular polarization is given in chapter 3; here, only general concepts are summarized. The tip of an electric field vector lying in a plane perpendicular to the direction of propagation traces out a helix as time passes (Fig.1-1). When viewed along the propagation direction, the helix appears as a circle (Fig.1-2). Fresnel reasoned that linearly polarized light can be thought of as the sum of left and right circularly polarized beams of equal amplitude propagating coherently. The orientation of the plane of polarization depends upon the relative phases of the two components. The phase difference is, in turn, due to a velocity difference between the two circular components in an optically active medium. If, at a given instant, the electric field vectors of both circularly polarized components are parallel to the plane of polarization of the incident light, then at the same point in time, electric field vectors at some point z=l in the medium are inclined at angles $\theta^R=-2\pi cl/\lambda v^R$ and $\theta^L=2\pi cl/\lambda v^L$, respectively, to the plane of polarization. Here, c represents the velocity of light, λ is the wavelength, and v is the velocity of propagation. R and L denote circular polarization states. The angle of rotation is:

$$\alpha=1/2(\theta^R+\theta^L)=\pi cl/\lambda((1/v^L)-(1/v^R)). \qquad [1\text{-}2]$$

Here, l represents the path length of the sample. The

above equation is valid in transparent media. Since n=c/v,where n is the refractive index,

$$\alpha=\pi/\lambda\,(n^{L}-n^{R})\,. \qquad [1\text{-}3]$$

The refractive index is a complex quantity; that is, it can be described by a number containing a real part and an imaginary part. The real part of the refractive index describes the index of optical rotation and optical rotatory dispersion. The imaginary part describes the absorption.

Because absorption and refractive index are so closely related, it was reasoned that optically active samples should absorb left and right handed light differently. This effect, called circular dichroism (CD), was first observed by Haidinger (8) in 1847 in amethyst crystals.

In 1848, Pasteur used the term dissymetric to describe crystals of tartrate salts he had been studying. Dissymmetric compounds are not necessarily asymmetric; the former can possess rotational symmetry axes but no planes or centers of symmetry. He performed the first optical resolution of a racemic compound, a tartrate (Mitscherlich's salt), into its component mirror images (enantiomers) and observed that each one rotated light in the opposite direction. Thus, Pasteur was the first to recognize that crystals which are not superimposable on their mirror images exhibit optical rotation (9). Furthermore, he attributed optical activity of quartz to dissymmetry of the crystal lattice. This was confirmed by fusing the quartz, causing optical activity to disappear. He attributed the optical activity

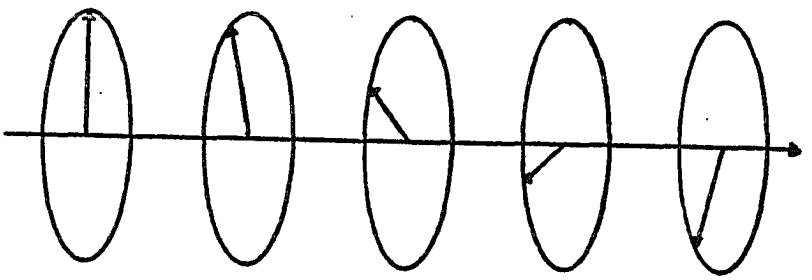

Figure 1-1. Circular Polarization of Light

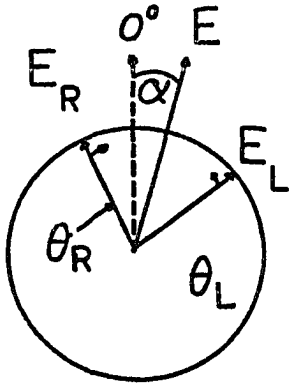

Figure 2. View of a Circularly Polarized Beam of Light Along the Direction of Propagation

of organic liquids and solutions to dissymmetry in themolecular framework.

Cotton (10), in 1895, observed CD in solutions of copper and chromium tartrate. If left and right handed light is absorbed differently by the sample, a linearly polarized incident beam will emerge from the sample with elliptical polarization. Elliptically polarized light is obtained when left and right circular components of different amplitude are added vectorially. The amplitude difference arises due to preferential absorption of one of the circular components (Fig. 3). A parameter, called the ellipticity ψ, is used to describe elliptically polarized light. It is defined as:

$$\tan\psi = (E_R - E_L)/(E_R + E_L). \qquad [1\text{-}4]$$

The amplitide attenuation of a light beam by absorption in a medium of refractive index n and path length l is given by:

$$E = E_0 \exp(2\pi n l/\lambda). \qquad [1\text{-}5]$$

R and L , as usual, denote right and left polarization states and E denotes the electric field vector. E_0 is the incident electric field strength. For differential absorption, the ellipticity is given by:

$$\tan\psi = \tanh(\pi l/\lambda (n_L - n_R)). \qquad [1\text{-}6]$$

Both circular dichroism and optical rotation are functions of the wavelength of light passing through the medium. The types of curves these functions exhibit are shown in Figure 4. The ellipticity maximum coincides with the

inflection point of the rotatory dispersion curve and is monosignate. Ideally, the inflection point of the ORD curve coincides with the CD maximum. The CD may, of course, be positive or negative. At wavelengths far from an absorption maximum, ORD is given by the Drude equation; this must be modified at absorption maxima. Absorpton bands close together yield CD and ORD curves which are complicated superpositions of the curves of each separate band.

Optical rotation measurements are presented as the specific rotation, defined as:

$$[\alpha] = \alpha V/ml; \qquad [1\text{-}7a]$$

where α is the measured optical rotation in degrees, V is the volume containing a given mass m of optically active material, and l is the path length in decimeters. CD spectra are displayed as the difference in molar extinction coefficients versus wavelength.

A dimensionless factor, g, called the dissymmetry factor was introduced by Kuhn (11). It is given by:

$$g = 2(\epsilon_L - \epsilon_R)/(\epsilon_L + \epsilon_R). \qquad [1\text{-}7b]$$

The epsilons are the extinction coefficients for each polarization state at a given wavelength. Note that the constants occurring in the equations for absolute absorption measurements drop out. Furthermore, in the case of identical coupled oscillators, g is a factor of molecular geometry only.

UV and visible CD bands can be related to the stereochemistry of the molecular skeleton, because CD

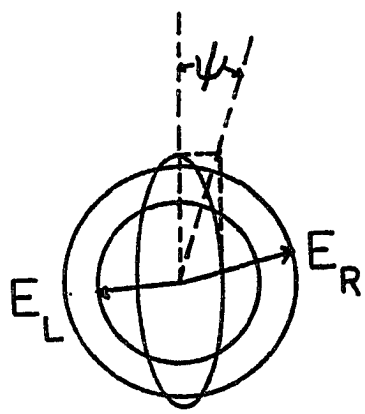

Figure 1-3. Elliptically Polarized Light Viewed Along the Propagation Direction

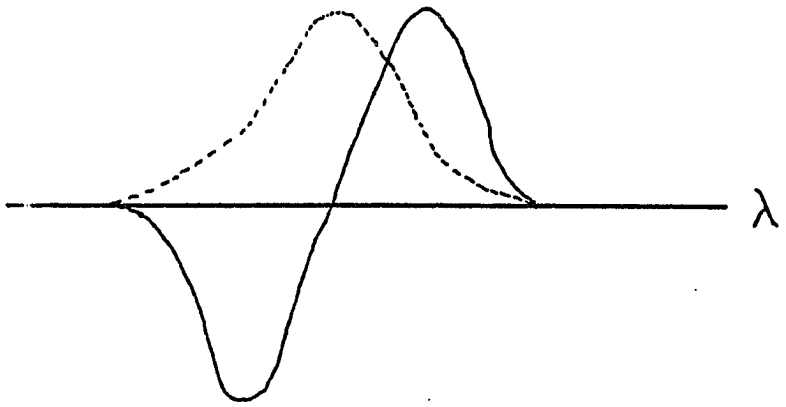

Figure 1-4. ORD and CD (Dashed) Curves

depends upon the spatial distribution of electronic states over the nuclear framework of the molecule. The sign and magnitude of Cotton effects were first related to molecular structure using the famous "octant rule", devised by Moffitt, Woodward, Moscowitz, Klyne, and Djerassi in 1961 (12). In this study, the carbonyl group in steroids was the absorbing "probe". The symmetry of the carbonyl (C=O) group, originally C_{2v} was lowered by asymmetric perturbation due to the molecular skeleton. Thus, it exhibits CD and ORD. Three nodal planes, two of which are the symmetry planes of the C_{2v} point group and the third being a nodal plane through and perpendicular to the C=O bond axis, split the area surrounding the C=O group into octants. The electronic CD and ORD were correlated with the position (octant) the perturbing group occupied. Furthermore, changes in the magnitude and sign of Cotton effects as the perturber moved from one octant to the other were predicted.

Although ORD and CD effects, collectively known as the Cotton effect, have been known for some time, experiments designed to measure them have not been applied until the 1950's, when photomultiplier tubes were developed. Before that time, visible and UV spectra were recorded on photographic plates. The introduction of electro-optic modulators, used to create circular polarization and switch between polarization states, in the 1960's, made measurement of UV/visible CD and ORD routine.

It seems quite resonable that if optically active molecules rotate plane polarized light and absorb circularly polarized light differently, there should also be manifestations of optical activity in scattering phenomena as well. The idea of Rayleigh (elastic scattering) and Raman (inelastic scattering) optical activity is not at all a new one. In 1923, Gans (13) considered Rayleigh scattering from optically active molecules and claimed to have observed optical activity effects in depolarization ratios. Two years later, de Mallemann (14) showed that these effects were due to optical rotation by the sample of the scattered beam. Gans also neglected to consider a crucial interference term generating ellipticity in scattered light as well as diffe rential scattering. Kastler (15) was the first to think about Raman difference for left and right circularly polarized light. Atkins and Barron (16) developed an explicit theory, involving interference between molecular polarizability and optical activity tensors which generate ellipticity in scattered light and circular intensity differences. Two years later, Buckingham and Barron (17) developed the theory in terms of a dimensionless Rayleigh and Raman circular intensity difference:

$$\Delta=(I_R-I_L)/(I_R+I_L). \qquad [1\text{-}8]$$

The first natural ROA spectra, reported by Moskovits, Bosnich, and Ozin (18) and by Diem, Fry, and Burow (19) were due to instrumental artefacts. The first real ROA spectra,

of 1-phenylethyl amine and 1-phenyl ethanol, were reported in 1973 by Barron, Bogaard, and Buckingham (20). The spectrum of phenylethyl amine was confirmed by Hug, Kint, Bailey, and Scherer in 1975 (21). Since then, natural ROA has been observed for and pinene (22) , methyl indanone (23) and fenchone, carvone, borneol, and camphor (24) and numerous other molecules. A series of substituted camphor species was studied by Barron (25). Resonance ROA, under the influence of a magnetic field, in ferrocytochrome C, a heme protein, was observed by Barron (26). The reason this experiment was possible is that ferrocytochrome C exhibits no CD in the particular absorption band excited in this experiment. The origins of artefacts in ROA spectra were carefully analyzed by Hug (27) and Barron and Vrbancich (28). Virtually all of the spectra of the above mentioned molecules were recorded using a polarization analyzer in order to observe the depolarized component. This is because instrumental artefacts, discussed in references 27 and 28, are inversely proportional to the depolarization ratio; thus, highly polarized bands can exhibit relatively large, spurious ROA signals. The first polarized ROA spectrum was observed by Hug (29). The first total ROA spectrum, recorded without using a polarization analyzer, was observed by Oboodi, Davies, Gunnia, Blackburn, and Diem (30).

C. Introduction to Optical Activity Theory

Optical activity can be explained using not only the technique of quantum mechanical perturbation theory, but also in terms of multipole moments induced in molecules when they interact with radiation. Several types of quantities are encountered when discussing the above mentioned moments. Those having a magnitude, but not associated with any direction in space, such as temperature, are scalars. Vectors differ from scalars in that they have a direction associated with a magnitude. Velocity is a familiar example of a vector. The magnitude of a tensor quantity can be specified can be specified only if at least two dimensions, corresponding to directions in space, are given. Molecular polarizabilities are tensor quantities. Unless otherwise noted, quantities given in this section with two or more subscripts are tensors. Spatial directions are given by the subscripts i, j, and k. These should not be confused with the unit vectors along the x, y, and z axes, respectively. When used as subscripts, the three letters can designate any axis in the coordinate system. A repeated subscript signifies a summation over that particular index. Such notation is known as the Einstein summation convention for tensors. For example, the electric polarizability tensor relates the induced dipole of a molecule to the applied electric field:

$$\mu=\alpha E. \qquad [1\text{-}9]$$

The physical significance of this equation is that the directions of the influence of E and the response are not necessarily the same; i.e., the induced dipole does not necessarily lie in the same direction as the vector E because the polarizability, α, is anisotropic. Thus, the induced dipole moment along the x axis of a molecule can be written:

$$\mu_x=\alpha_{ij}E_j, \qquad [1\text{-}10]$$

where the summation is carried out over j, j=i, j, k, and i=x. The Einstein convention simplifies this expression futher by omitting the summation symbol, this being understood because of the presence of the repeated subscript. Thus, the summation is shorthand for the following expression:

$$\mu_x=\alpha_{xx}E_x+\alpha_{xy}E_y+\alpha_{xz}E_z. \qquad [1\text{-}11]$$

If an electromagnetic wave propagates through a nonmagnetic, transparent, anisotropic medium (31),

$$D_i=\epsilon_{ik}E_k \qquad [1\text{-}12]$$

and

$$(1/\mu_0)B_i=H_i. \qquad [1\text{-}13]$$

The tensor ϵ is the permittivity of the medium and all components are positive. E and B are the electric and magnetic fields, respectively, of the wave in free space and D and H are the corresponding fields in the medium. Maxwell's equations for a wave of frequency ω are:

$$\mu i\omega H=c\nabla E \qquad [1\text{-}13]$$

and

$$\mu i\omega D=-c\nabla H. \qquad [1\text{-}14]$$

Vector subscripts have been omitted from D, E, and H for simplicity. The lower case i denotes an imaginary quantity. The speed of light is given by c. For a plane polarized beam, $H/c=k \times E$ and $D/c=-k \times H$. k is a propagation vector pointing in the direction of travel. A vector n is defined by:

$$k=\omega n/c. \qquad [1\text{-}15]$$

The magnitude of n is equal to the refractive index of the medium. H and D can be written as $H=n\ E$ and $D=-n\ H$. Then, $D=n \times E \times n=n^2E-(n\cdot E)n$. If the components of vector D in the above equation are equated with [1-11], three linear equations, one for each component of E, are finally obtained: $n^2E_i-n_in_k=\epsilon_{ik}E_k$. [1-16]

D can be written in terms of a bulk polarization P and a quadrupole polarization Q:

$$D_i=\epsilon_0E_i+P_i-(1/3)\nabla_jQ_{ij}. \qquad [1\text{-}17]$$

The bulk polarizations can, in turn, be related to the polarizations of the constituent molecules by:

$$P_i=N\mu_i, \qquad [1\text{-}18]$$

$$Q_{ij}=N\theta_{ij}. \qquad [1\text{-}19]$$

N is the number density of molecules. The oscillating multipole moments μ and θ are, in general, complex. They are given by (32):

$$\mu_i=\alpha_{ij}(E_j)+(1/3)A_{i,jk}(E_{jk})+G_{ij}(B_j)+... \qquad [1\text{-}20]$$

$$\theta_{ij}=a_{k,ij}(E_k)+d_{k,ij}(B_k)+... \quad . \qquad [1\text{-}21]$$

Equation [1-20] gives the induced electric dipole moment of the molecule; [1-21] describes the induced

electric quadrupole moment. In addition to these, magnetic dipole moments can also be induced. These are given by:

$$m_i=\chi_{ij}(B_j)+g_{ji}(E_j)+(1/3)D_{i,jk}E_{jk}+\cdots \quad . \qquad [1\text{-}22]$$

The quantities g, a, and d are, in general, complex. They are given by:

$$g_{ij}=G_{ij}+iG_{ij}', \qquad [1\text{-}23a]$$

$$a_{i,jk}=A_{i,jk}+iA_{i,jk}', \qquad [1\text{-}23b]$$

and

$$d_{i,jk}=D_{i,jk}+iD_{i,jk}'. \qquad [1\text{-}23c]$$

The quantities G, G', A, and A' are known as the dynamic molecular property tensors. G involves interference between the electric dipole and magnetic dipole matrix elements and is given by:

$$G_{ij}=(2/h)\Sigma(\omega_{jn}/\omega_{jn}^2-\omega^2)\mathrm{Re}((n|\mu_i|j)(j|m_j|n)). \qquad [1\text{-}24]$$

The sum is taken over all j not equal to n. Re denotes the real part of the expression. ω is the frequency of radiation interacting with the molecule. The expression for G' is almost identical to this one, except that the imaginary, rather than the real part, of the expression is evaluated. G' is negative. The expressions for A and A' take the same general form as those for G and G', respectively. The difference is that A involves interference between the electric dipole and electric quadrupole. Such interference terms are important not only in electronic optical activity of absorbing groups, but also in Raman optical activity. In order to obtain expressions for optical activity in terms of the dynamic molecular property tensors, a new tensor must be defined. This tensor is given

by:

$$\zeta_{ijk}=(1/c)[(1/3)i\omega(A_{i,jk}-a_{j,ik})+\epsilon_{jik}G_{ij}+\epsilon_{jki}g_{kj}]. \qquad [1\text{-}25]$$

The ϵ represents the Levi-Civita tensor. It has a value of 1 if the subscripts can be brought into the form ijk by a cyclic permutation of the subscripts. If such a form can be obtained only by non-cyclic permutation, the tensor takes on a value of -1. Repeated subscripts imply a zero value for the tensor.

Using this expression, equation [1-16] can be written in the form:

$$[(n^2-1)\delta_{ij}-\mu_0 c^2 N(\alpha_{ij}+n_k\zeta_{ijk}+\ldots)]E_k=0. \qquad [1\text{-}26]$$

Axes are now specified as i=x, j=y,and k=z. The direction of propagation is along the z axis. The equations for x and y axis components circularly polarized light can be used in the above equation to yield two equations for the refractive index which can be combined. Since the refractive index is a complex quantity, the real and imaginary parts can be separated. The separate parts can then be substituted into the phenomenological equations for optical rotation and circular dichroism given earlier to yield:

$$\Delta\theta\approx-(1/2)\omega\mu_0 lN[-c\alpha_{xy}(f)+(1/3)\omega(A_{x,yz}(f)-A_{y,xz}(f)) +G'_{xx}(f)+G'_{yy}(f)], \qquad [1\text{-}27]$$

and

$$\Delta\eta\approx-(1/2)\omega\mu_0 lN[-c\alpha_{xy}(g)+(1/3)\psi(A_{x,yz}(g)-A_{y,xz}(g)) +G'_{xx}(g)+G'_{yy}(g)]. \qquad [1\text{-}28]$$

The letters f and g represent dispersion and absorption lineshape functions, respectively. It was mentioned at the beginning of this section that the medium is anisotropic.

In an isotropic medium, the average of the tensor components over all space must be taken. When this is done, the quadrupole terms drop out and the following equations are obtained:

$$\Delta\theta \approx -(1/3)\omega\mu_0 lNG'_{ii}(f), \qquad [1\text{-}29]$$

and

$$\Delta\eta \approx -(1/3)\omega\mu_0 lNG'_{ii}(g). \qquad [1\text{-}30]$$

The first of these two equations is the Rosenfeld equation.

As mentioned earlier, ROA can be described in terms of the dynamic molecular property tensors. Light is propagating along the z axis. Scattering at 90 degrees;i.e.,along the y axis will be considered. The incident light induces oscillating electric and magnetic multipoles in the molecule, which are the source of the scattered light. The equation for the complex electric vector radiated in the y direction at a distance from the origin (molecule) is given by:

$$E_i^d = \omega^2\mu_0/4\pi y[\mu_i^0 - j_i\mu_y - (1/c)\epsilon_{iyj}m_j^0$$
$$-(i\omega/3c)(\theta_{iy}^0 - j_i\theta_{yy}^0)+\ldots]\exp(i\omega((y/c)-t)). \qquad [1\text{-}31]$$

The superscript d represents the distance from the origin. The subscript i denotes the direction of the electric vector, j is a unit vector in this direction,and ϵ is the Levi-Civita tensor. The intensity components of the scattered wave perpendicular to the scattering plane yz are denoted I_x; those parallel to the scattering plane are given by I_z. The equations for each component are:

$$I^d_x = (1/2\mu_0 c)E^d_x E^{d}_x{}^*, \qquad [1\text{-}32]$$

and

$$I^d_z = (1/2\mu_0 c)E^d_z E^{d}_z{}^*. \qquad [1\text{-}33]$$

The equation for each component (left or right) of circularly polarized light is substituted into the equations for the induced multipole moments and these, in turn, are used in the equations for the intensity components of the scattered light to yield the expressions for the circular intensity differences in scattered light:

$$\Delta_x = 2(7\alpha_{ij}G'^*_{ij} + \alpha_{ii}G'^*_{jj} + (1/3)\omega\alpha_{ij}\epsilon_{ikl}A^*_{k,lj}) / c(7\alpha_{mn}\alpha^*_{mn} + \alpha_{mm}\alpha^*_{nn}), \quad [1\text{-}34a]$$

and

$$\Delta_z = 4(3\alpha_{ij}G'^*_{ij} - \alpha_{ii}G'^*_{jj} - (1/3)\omega\alpha_{ij}\epsilon_{ikl}A^*_{k,lj} / 2c(3\alpha_{mn}\alpha^*_{mn} - \alpha_{mm}\alpha^*_{nn}). \quad [1\text{-}34b]$$

These equations assume a non-degenerate ground state and no static external magnetic fields. The tensor averages over all orientations have been taken. The equations for circular intensity differences given above are for Rayleigh optical activity. They can, however, be used for Raman optical activity if the molecular property tensors are replaced by the vibrational Raman transition tensors. Within Placzek's approximation, these are given by:

$$(v_m | \alpha_{ij}(Q) | v_n), \quad [1\text{-}35a]$$

$$(v_m | G'_{ij}(Q) | v_n), \quad [1\text{-}35b]$$

and

$$(v_m | A_{i,jk}(Q) | v_n). \quad [1\text{-}35c]$$

D. Symmetry and Optical Activity

While it is clear that molecular symmetry (or lack of it) is of enormous importance in vibrational spectroscopy and optical activity, it must be remembered that there are symmetries which determine the operation of physical processes. Wigner, in his classic paper (33), put forth the idea that if an experiment is subjected to a complete coordinate inversion or time reversal, the resulting experiment should be realizable. Since that time, it has been found that most physical laws, including those of electromagnetism, do conform to Wigner's theory. Such physical processes are said to conserve parity. One notable exception to this occurs during β-decay. The symmetry operation causing coordinate inversion (x,y,z to -x,-y,-z) is called parity, P. The operator T causes the time coordinate t to be replaced by -t. Reversibility with respect to time should not be confused with thermodynamic reversibility; thermodynamics is ultimately concerned with the probability of a reverse process. The reversibility discussed here is possible only if all motions occurring during a physical process can be reversed.

Scalars, vectors, and tensors can be described in terms of their behavior with respect to P and T. A polar vector is one whose sign is changed by P. The position vector r is an example of a polar vector. Axial vectors do not change

sign under P. Angular momentum, $L=r \times p$, is axial because P changes r to -r and p to -p. A position vector does not change sign under T and is said to be time even. Velocity and angular momentum do change sign under T and are time odd. Pseudoscalars are quantities having no directional properties, but which change sign under inversion.

The behavior of E and B, the electric and magnetic fields, under P and T, can be determined by analyzing the physical system used for their generation (Fig. 1-5). E is generated by two parallel plates, of infinite extent, each having equal and opposite charge densities. Under P, the plates change position. Since the charges are stationary, T has no effect. E is a polar, time even vector. B is generated by a cylindrical current sheet of infinite length. P does not reverse the sense of rotation of current as electrons move through the sheet. T, however, does reverse the direction of the current, thereby reversing the direction of B. B, therefore, is an axial, time odd vector.

Using such considerations, it can be shown that all optical activity experiments conserve parity and reversibility (34). In a simple optical rotation experiment, a plane polarized beam enters a medium which is chiral. The plane of polarization is rotated; as this happens, a helical pattern of electric field vectors is obtained. Under P, the sense of the helical pattern is reversed and the direction of propagation of the beam is reversed. The chiral medium is converted into its mirror image by P. The

direction of optical rotation is reversed; reversing the direction of propagation does not change the sense of optical rotation. It is known that replacing a sample with its enantiomer reverses the sense of optical rotation. Therefore, optical rotation conserves parity. Time reversal simply changes the beam direction; this does not affect an optical rotation experiment. Thus, reversibility is preserved.

Parity and time reversal symmetry are "modulated" by molecular symmetry. The unperturbed carbonyl group in formaldehyde, for example, has C_{2v} symmetry. The carbon and oxygen $2p_x$ orbitals form a π and a π^* orbital. The non-bonding orbital is the oxygen $2p_y$. Under C_{2v}, the π orbital transforms as B_1, the non-bonding orbital n as B_2, and the π^* as B_1 (Fig. 1-5). There are two electrons in both the n and the π orbitals in the ground state of the carbonyl group. The ground state symmetry is A_1. The first excited state has one electron in the π^* orbital and has A_2 symmetry. Since no component of the electric dipole moment operator μ transforms as A_2, the transition n to π^* is electronically forbidden. It is magnetically allowed, because the magnetic dipole moment operator transforms as a rotation R_z, which in turn transforms as A_2. There will, however, be no optical rotation, because the rotational strength is given by:

$$R_{AB}=\mathrm{Im}(a|\mu|b)\cdot(b|m|a)=0. \qquad [1\text{-}36]$$

This dot product is zero because μ and m transform

under different irreducible representations. Similar considerations show that the π-π^* transition is electronically allowed and magnetically forbidden. Schellman (35) points out that in most cases, the ground state wavefunction transforms as an axial vector and the excited state wavefunction as a polar vector. The product of these two is a pseudoscalar function, changing sign on reflection or inversion. The dot product of the operators μ (polar) and m (axial) must also be a pseudoscalar if the rotational strength is to be non-vanishing. In molecules containing planes of reflection or centers of inversion, the axial and polar vectors fall under different representations of the point group in question. Thus, the dot product of the electric and magnetic dipole moment operators is zero.

In the case of a symmetric molecule subjected to a static perturbation; i.e., a carbonyl group in the vicinity of a positive charge, the perturbation matrix element for the electronic transition 0-1 has a term of the form:

$$(0|\mu|1)\cdot[\Sigma\ (n|m|0)(1|V|n)]/\epsilon_n-\epsilon_1. \qquad [1\text{-}37]$$

The summation is carried out over excited states n. In order to have a non-zero rotational strength, the summation term must be non-zero. The form of the perturbing potential is important. V must transform as the dot product of 1 and n (or μ and m). The dot product will, of course, be a pseudoscalar. The potential functions can be written as expansions, one member of which must be a pseudoscalar. The pseudoscalar part of the function can be written:

$$V^{ps}=(1/n)\chi^{ps}(R)P_RV. \qquad [1\text{-}38]$$

The summation is carried out over the operations R of a given irreducible representation. $\chi(R)$ is the character of the pseudoscalar representation of R, and P_RV is the result of applying operation R to V. n is the number of operations of the group. The pseudoscalar part of the function generated by placing the point charge at positions around the absorbing group. The placement of the charge is dictated by the symmetry operations of the point group under consideration (for a C=O group, C_{2v}). Figure 1-6 shows how a point source can be decomposed into four parts, each belonging to one of the irreducible representations of C_{2v}. As the charge approaches one of the original symmetry planes of the C=O group all of the images of the point charge do so as well. The images then coalesce. Charges (and their symmetry generated images) lying in a symmetry plane, do not contribute to optical rotation.

Note that Figure 1-6b is the pseudoscalar representation, because the potential changes sign when being reflected through a symmetry plane.

Symmetry considerations allow one to deduce symmetry requirements for both Rayleigh and Raman optical activity. In Rayleigh optical activity, the corresponding components of the α and G' tensors must transform as the totally symmetric representation; for vibrational Raman optical activity, corresponding components of α and G' must span the irreducible representation of the particular normal

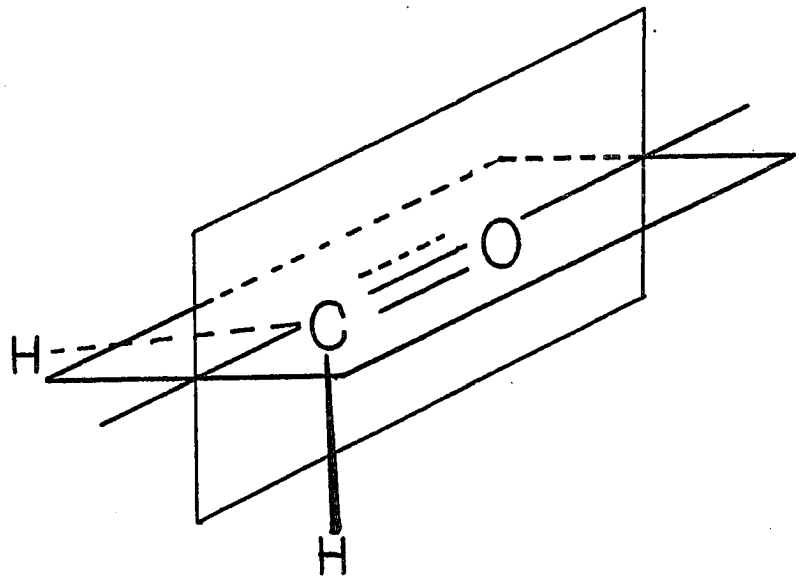

Figure 1-5. Formaldehyde and Symmetry Elements

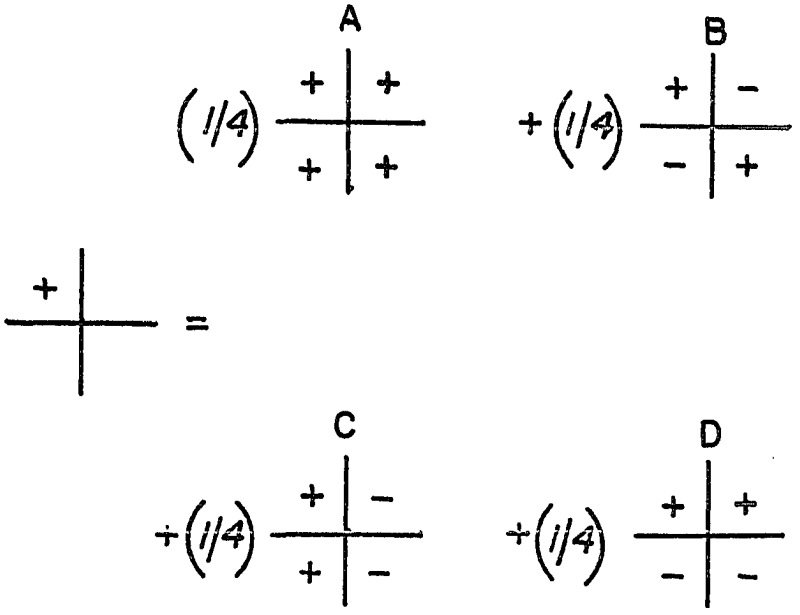

Figure 1-6. Decomposition of a Pseudoscalar Function

coordinate under consideration. Only for the chiral point groups C_n, D_n, O, T, and I, in which polar and axial tensors α and G' , respectively, have the same rank, can this requirement be met. Note that in the expression for Δ, ϵ and A terms are multiplied. Although A alone does not transform like G', the second rank axial tensor produced by the product of ϵ and A does. For this reason, all Raman active vibrations in a molecule should exhibit ROA.

CHAPTER 2. VIBRATIONAL SPECTROSCOPY OF CHLOROFLUOROACETIC ACID AND SODIUM CHLOROFLUOROACETATE

A. Introduction

Chlorofluoroacetic acid is one of the simplest chiral molecules known. It is a colorless, non-viscous, high boiling liquid at room temperature and, therefore, an ideal molecule for ROA studies. Having only eight atoms, this molecule exhibits 18 normal modes of vibration.

In order to better understand the ROA of this molecule, the ROA data must be interpreted in terms of an analysis of the vibrational spectrum. The infrared and Raman spectra of the acid are reported and interpreted in the following work. In order to simplify the analysis, the Raman spectra of the acid anion were studied first. Having only 7 atoms, the anion has three fewer (15) normal modes of vibration. Spectra of both H-CClFCOO$^-$ and D-CClFCOO$^-$ were recorded. Such isotopic substitution allows vibrations involving the C-H bond to be isolated and identified by observing the isotope effect on vibrational frequencies. Corresponding isotopic analogues of the parent acid were also studied.

Measured spectral frequencies, along with geometric parameters and vibrational force constants, were used as input for normal coordinate analysis of both the acid anion and the parent acid. The results of this analysis, along

with isotopic substitution studies, allowed assignment of all normal modes of both the anion and parent acid.

B. Sample Preparation

Chlorofluoroacetic acid was prepared according to the method of Young and Tarant (36). 50 g of 2-chloro-1,1,2 trifluoroethyl ethyl ether were placed in a 1 liter round bottom flask equipped with a stirrer, thermometer, and addition funnel and the ether was cooled to 0°C. 70 g of 96% sulfuric acid was added over a one hour period while the reaction mixture was stirred vigorously. Stirring was continued for an additional 90 minutes after the addition of the acid was complete. The reaction mixture was then poured over crushed ice. A yellowish white layer formed; this was the reaction mixture. This layer was saved and washed with H_2O until the pH was neutral. The resulting product, ethyl chlorofluoroacetate, was purified by distillation. The boiling point of the ester was 128-130°. Reaction yield was 75%.

The ethyl chlorofluoroacetate was then added to a 10% NaOH solution containing an equimolar amount of sodium while maintaining the temperature of the mixture below 15°C. After the addition was complete, the mixture was allowed to warm to room temperature and stirring was continued for another three hours. This mixture was then concentrated to

a pasty mass under water aspiration; toluene was then added to the paste to removed residual water by azeotrope formation.

100 ml of H_3PO_4 are then added to each mole of sodium chlorofluoroacetate formed in the previous step. It is important not to exceed this proportion, for when this mixture is heated, frothing of phosphoric acid occurs. This is so severe that the reaction was carried out on a smaller scale than that described in the literature. 6.53 g of the chlorofluoroacetate salt were used in the preparation of the acid. The mixture was heated at 50°C for 3 hours after P_2O_5 was added to the reaction mixture as a dehydrating agent and was added until it remained as a finely divided white powder; i.e., it did not dissolve. The distillation of the acid was carried out using a 50 ml round bottom flask with a micro disillation apparatus attached to either a vacuum pump or a water aspirator. Reduced pressures were used so that product decomposition was minimized. Though it is thought that the reduced pressure procedure intensifies the frothing of the reaction mixture, this was not found to be a problem if the scale of the reaction is kept small enough. A heat gun may be used to aid the distillation. Some water was present in the reaction mixture; this was the first fraction collected, boiling at 31°C under reduced pressure. The acid was the second fraction, boiling at 70-72°C. This fraction was re-distilled to yield 2.6 ml (3.9g) of chlorofluoroacetic acid. The product was characterized

by NMR. The line pattern is very simple; the acid proton exchanges rapidly with the D_2O solvent, yielding an HOD peak, and the aliphatic proton is split into a doublet by the ^{19}F nucleus. The splitting is 48 Hz. Chlorofluoroacetic acid is a colorless, non-viscous liquid at room temperature.

C. Raman and Infrared Spectra

All Raman spectra were recorded using a microcomputer controlled spectrometer designed and built at Hunter College. A detailed description of this instrument is given in (37); a brief description is given here. 5145 Å laser radiation, travelling vertically, passes through a focusing lens and through the bottom window of a rectangular quartz cell. The vertical image is collected at right angles to the incident beam and collimated with an f/1 lens. A second f/8 lens focuses the image onto the entrance slit of a Jarrell-Ash Model 25-100 subtractive dispersion double monochromator. The scan drive of the monochromator is driven by a computer controlled stepping motor. Raman signals are detected by a ITT FW 130 or a RCA 31034 A photon counting photomultiplier tube, cooled to -25°C in a thermoelectrically cooled PMT housing (Products for Research). A DC detection option, using a Victoreen 1001 microammeter, is available and is used for sample alignment.

Following detection, the signal is processed using a preamplifier-discriminator (EG&G Ortec Model 9103) and a 100 MHz photon counter (EG&G). Scan control, data manipulation, and graphic presentation of spectra are controlled by a North Star Horizon microcomputer, based on a Z-80 A processor. A half wave retardation plate, which can be rotated in and out of the laser path, is used instead of a polarization analyzer if depolarization ratio measurements are desired (see Table 2-1).

The Raman spectrum of the neat acid between 200 cm^{-1} and 2000 cm^{-1} was recorded in 30 minutes using a laser power of 400 mW at 5145 Å. The scan step size was $1cm^{-1}$. 20 slits were used. The low frequency region between 170 cm^{-1} and 230^{-1} was acquired with 300 mW of power at 5145 Å, $1cm^{-1}$ step size and a two second acquisition time per step. The same conditions were used for the α-deuterated analogue, except that the laser power was 500 mW and total acquisition times for both polarized and depolarized components was 2 hours. Aqueous solutions of the sodium salt of chlorofluoroacetic acid were studied using an H_2O/acid ratio of 100:1. Laser power was 500 mW at 5145 Å. As before, 1 cm^{-1} step sizes were used. Total acquisition time was 12 hours. The sample of acid in H_2O, 35:1 dilution, was studied with a laser power of 400 mW at 5145 Å and a data acquisition time of 2 hours.

Gas phase infrared spectra of chlorofluoroacetic acid and its analogue, deuterated at the aliphatic carbon, were

measured on a Beckman IR 4240 dispersive spectrometer (see Figures 2-11 through 2-14 and Tables 2-2 and 2-3). The sample was contained in a 10 cm pathlength pyrex cell equipped with thallium bromide iodide (KRS-5) windows. Samples were heated to between 68° and 72°C by wrapping the sample cell with resistively heated tape. The slitwidth at 3000 cm^{-1} was 1mm.

D. Spectral Interpretation

Simplification of the spectral assignment is possible if spectra of the sodium salt of the acid are recorded, because one atom ,and consequently three normal modes, are absent. Since the two structures are almost identical, many anion spectral assignments carry over to the acid. Acetate ions, produced by titrating the neat acid with NaOH, were dilute (100:1 in H_2O solution). Spectra of the acid diluted 35:1 in acetonitrile were also recorded. These spectra made possible observation of the O-H stretching vibration without interference from hydrogen bonding. All references to deuterated (d_1) spectra imply deuteration at the aliphatic carbon atom unless otherwise noted.

Assignment of certain bands was possible using a group frequency approach, coupled with comparisons of the intensities of corresponding lines in infrared and Raman spectra. The O-H stretch, occurring at 3528 cm^{-1} in

acetonitrile and 3578 cm^{-1} in the gas phase, is a case in point. It is expected to be very weak in Raman spectra, but very strong in absorption; such is the case in chlorofluoroacetic acid. Carboxylic acids and alcohols have O-H stretches occurring in this frequency region. The O-H stretching vibration is shown in Figure 2-1. Unless otherwise noted all Raman spectra are polarized. Several laser plasma emission lines appear in the spectrum.

The C-H stretch was observed at 3007 cm^{-1} in the neat acid. Deuteration shifted this frequency to 2212 cm^{-1}. Both of these lines are very weak infrared absorbers; in fact, the C-H stretch almost unobservable in the ir absorption and the C-D stretch is barely visible. The appearance of bands assignable to C-H stretches in the IR spectrum of the deuterated analogue are due to impurities deposited on the KRS-5 windows. These impurities are breakdown products from previous acquisitions of acid spectra.

A shoulder, approximately three-fourths as intense as the C-D stretch, occurs near 2260 cm^{-1}. This is assigned as a Fermi-Resonance enhanced combination band involving bands at 1269 cm^{-1} and 991 cm^{-1}. The C-H stretch is shown in Figure 2-2 and the C-D stretch in Figure 2-3.

Figures 2-4 and 2-5 show the middle and low frequency regions of the Raman spectra of protonated and deuterated neat chlorofluoroacetic acid. The broad band, centered above 1700 cm^{-1} in both spectra, is the C=O stretch. This band disappears in the protonated and deuterated anion

spectra, shown in Figures 2-6 and 2-7, respectively. This band appears very stongly in the ir spectra at 1805 cm^{-1}.

Figure 2-4 shows a weak, broad band at 1439cm^{-1}. It is difficult to observe in the deuterated neat acid spectrum, Fig. 2-5. This band disappears in anionic spectra, and is assigned as the C-O stretch. The anion spectra show a very intense peak at 1392 cm^{-1} (1393cm^{-1}, deuterated). This peak is the CO_2^- symmetric stretch. The asymmetric stretch occurs near 1600 cm^{-1}, and is obscured by the H_2O bending mode. The protonated spectrum, Fig. 2-6, shows a shoulder on the high frequency side of the 1392 cm^{-1} band; this is assigned as a Fermi Resonance enhanced combination band involving vibrations occurring at 928 cm^{-1} and 497 cm^{-1}.

Figure 2-6 shows clearly two bands at 1305 cm^{-1} and 1224 cm^{-1}. Both peaks are completely absent in Fig. 2-7, making them readily assignable as the C-H deformations. A normal coordinate analysis, to be discussed later, shows that the higher frequency member of this pair is the deformation occurring perpendicular to the plane containing the C-C bond and the C-H bond; the lower frequency band is the in-plane deformation. These bands shift to 957 cm^{-1} and 876 cm^{-1} upon deuteration. The higher frequency component is the strongest band in the deuterated neat acid spectrum, Fig. 2-5.

A weak band, occurring at 1253 cm^{-1}, but not observed in anionic spectra, is assigned as the C-O-H deformation. This band does appear in the ir spectrum at 1260 cm^{-1}

(protonated) and 1265 cm^{-1} (deuterated).

Intensity comparison, coupled with group frequency considerations, lead to assignment of the weak Raman band at 1083 cm^{-1} as th C-F stretch. This band shifts to 1121 cm^{-1} upon deuteration of the neat acid. It occurs at 1057 cm^{-1} in the protonated anion spectrum, and at 1112 cm^{-1} in the deuterated anion spectrum. It is the strongest band in the infrared spectrum, occurring at 1100 cm^{-1} in the protonated acid and at 1090 cm^{-1} in the deuterated analogue.

The line occurring at 927 cm^{-1} in neat acid was assigned as the C-C stretch. Deuteration shifts this vibration to 981 cm^{-1}. Such shifts to higher frequency are known to occur for C-C stretches. Such behavior also occurs in anionic spectra and in gas phase ir absorption (see Figures 2-5, 2-7, 2-11 through 2-14 and Tables 2-2 and 2-3).

The most intense line in the neat liquid spectrum (protonated) occurs at 811 cm^{-1}. This is the C-Cl stretch. Such a frequency may seem surprisingly high for this type of vibration, but Katon (38) has also observed C-Cl stretches near 800 cm^{-1}. Deuteration of the aliphatic carbon shifts this band to 755 cm^{-1} in the neat acid and 785 cm^{-1} in the anion. The intensity of this band was greatly reduced upon deuteration of the anion.

The line at 701 cm^{-1} in the neat acid was not readily assignable without resorting to a normal coordinate analy sis. This band also appears in anionic spectra. The analysis (see next section) shows that this vibration is a

skeletal mode. This vibration, along with the Cl- C-F deformation, exhibits large ROA in the neat acid (see Ch. 3).

The next band appears as a shoulder on the low frequency side of the 700 cm^{-1} band. It occurs near 620 cm^{-1} in the neat acid and at 611 cm^{-1} in its deuterated analogue. It is assigned as the COOH wagging mode. A vibration occurs at 636 cm^{-1} in the anion spectrum. It occurs at 620 cm^{-1} in the deuterated anion and is assigned as a COO^- wagging vibration. A similar assignment for acetic acid was made by Wilmshurst (39).

Normal coordinate analysis shows the vibration occurring near 500 cm^{-1} in both acid and anionic spectra to be a poorly defined superposition of a number of atomic motions.

The mode occurring at 380 cm^{-1} in the neat acid is responsible for a large ROA signal. It is assigned as the Cl-C-F deformation. Such deformations have previously been observed in this spectral region by Durig et. al. (40).

Two poorly resolved bands occur between 250 cm^{-1} and 300 cm^{-1}. Both are rather weak in the Raman spectra. One of these is a skeletal mode, but the other is readily assignable as the O-H torsion. This mode can be assigned by analogy to methanol, which exhibits a strong O-H torsional absorption at 270 cm^{-1} (41). Large amplitude motions predominate at the low frequencies. The 222 cm^{-1} Raman line is a complex skeletal mode, containing a large contribution from the COOH wagging force constant. An analogous mode occurs in the anionic spectra. The last of the 18 normal

modes of chlorofluoroacetic acid is calculated, via normal coordinate analysis, to occur at 120.1 cm^{-1}. This mode is the COOH torsion. Again, a vibrational analogue involving the CO_2^- is observed in the anionic spectra. This vibration was unobservable due to interference form the Rayleigh line.

The spectrum of chlorofluoroacetic acid in water is shown in Figure 2-8. Note the C-O-H deformation situated near 1320cm^{-1}. Also notice the carbonyl stretching mode. These lines are clear indication that the acid is not completely dissociated in water. Figure 2-9 shows the depolarized Raman spectrum of the neat, deuterated acid and is given for comparison with the polarized spectrum.

Figure 2-10 shows the polarized Raman spectrum of chlorofluoroacetic acid deuterated at the acidic position (CClFHCOO-D). All lines below 1200 cm^{-1} correspond to those observed at similar spectral positions in the undeuterated acid. A distinctive feature of this spectrum is the shift of the band assigned to the C-O stretch, occurring at 1439 cm^{-1} in the undeuterated acid, to 1390 cm^{-1}. The band near 1290 cm^{-1} was not expected to appear, because the C-O-H angle deformation, occurring at 1253 cm^{-1} in the undueterated acid spectrum, should shift to below 1000 cm^{-1}, as it does in the spectrum of acetic acid recorded by Wilmshurst (39). This sample was made by repeated exchange of the acid proton using a large excess of D_2O as solvent the D atom source. There may have been a small amount of

D_2O present in the sample when the spectrum was recorded. Therefore, the line near 1290 cm^{-1} is assigned to the D-O-D angle deformation mode, expected to occur between 1200 cm^{-1} and 1300 cm^{-1}. The C-O-D deformation may occur as a shoulder on the high frequency side of the band near 900 cm^{-1}.

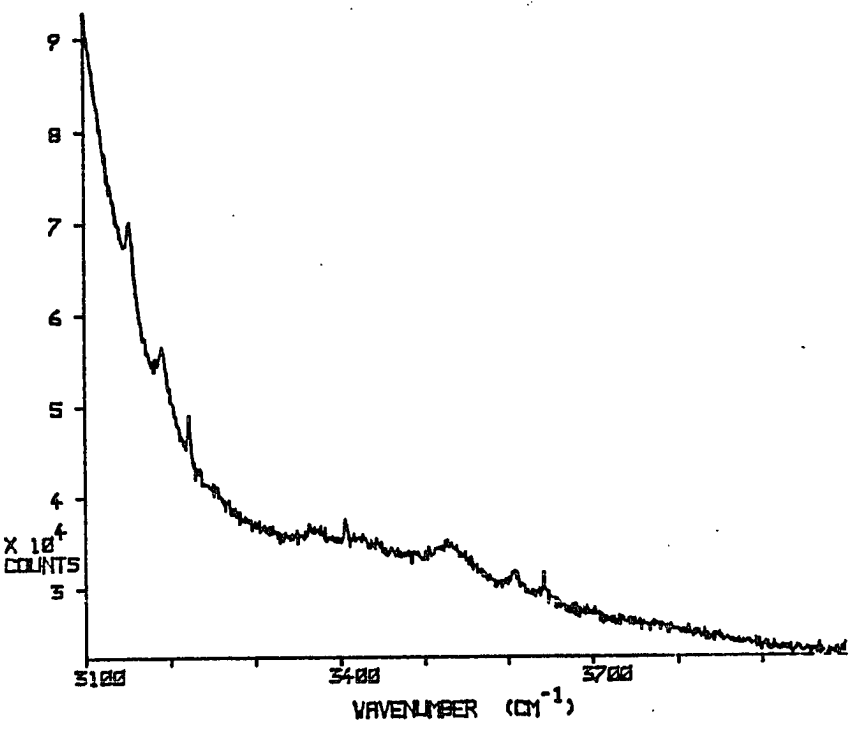

Figure 2-1. O-H Stretching Raman Spectrum

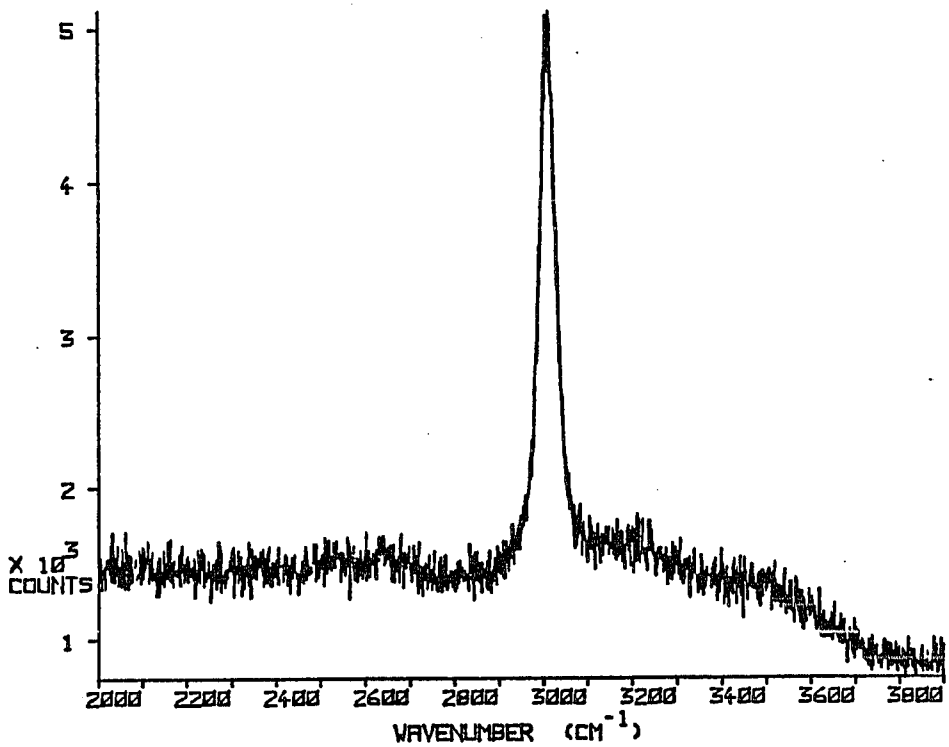

Figure 2-2. C-H Stretching Raman Spectrum

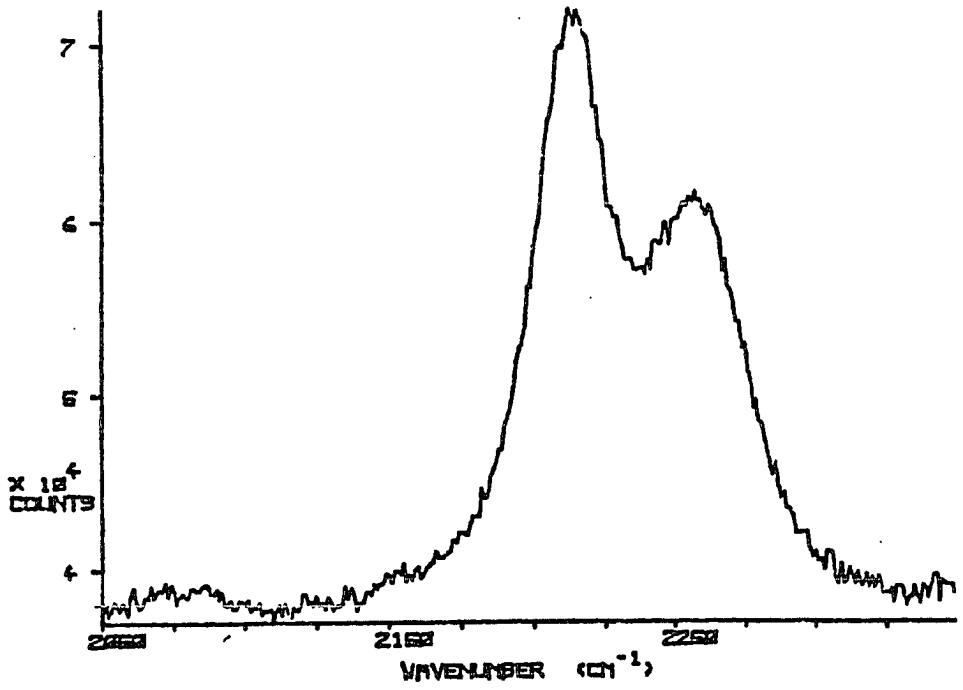

Figure 2-3. C-D Stretching Raman Spectrum

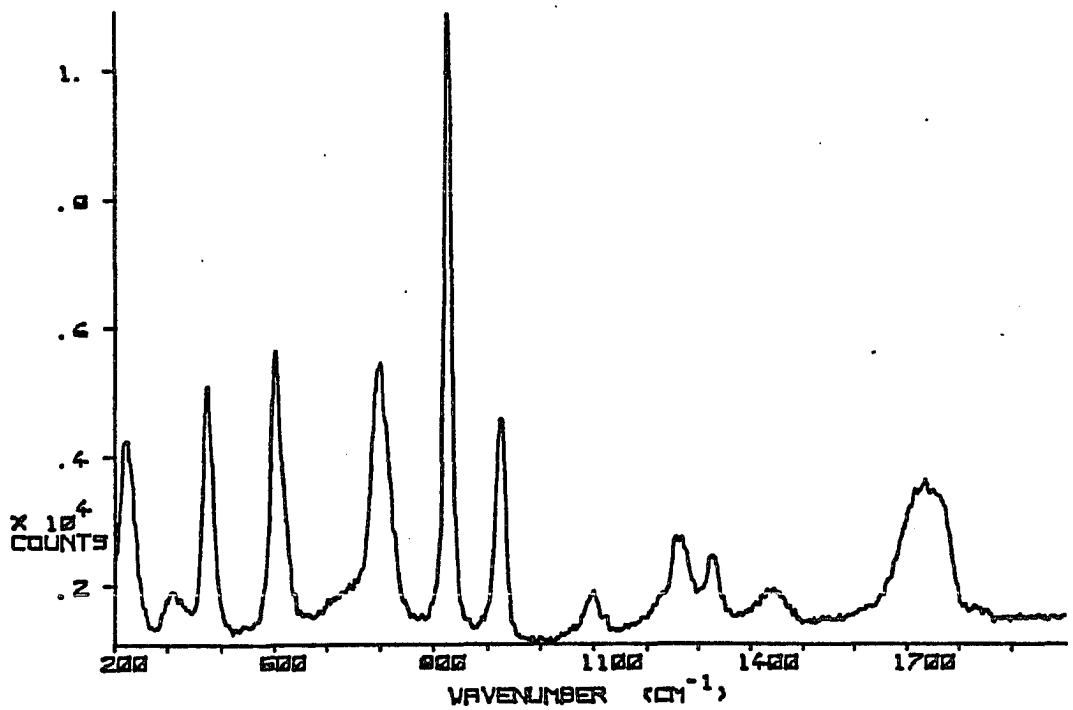

Figure 2-4. Mid-Frequency Raman Spectrum of Neat Acid

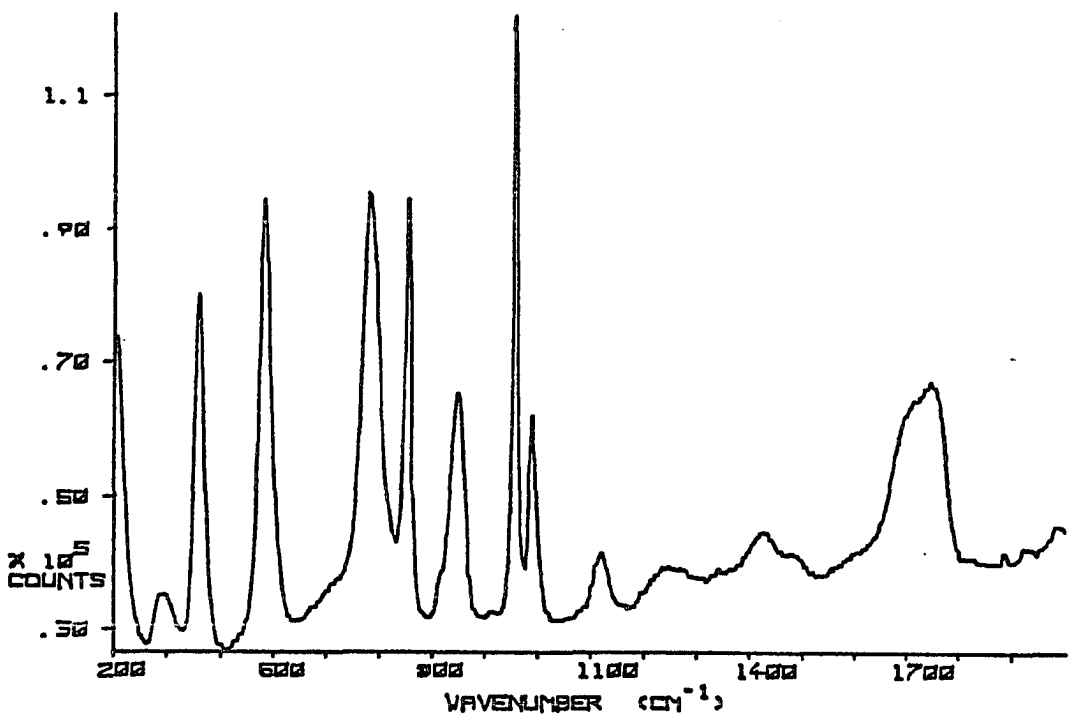

Figure 2-5. Mid-Frequency Raman Spectrum of Neat Acid (deuterated)

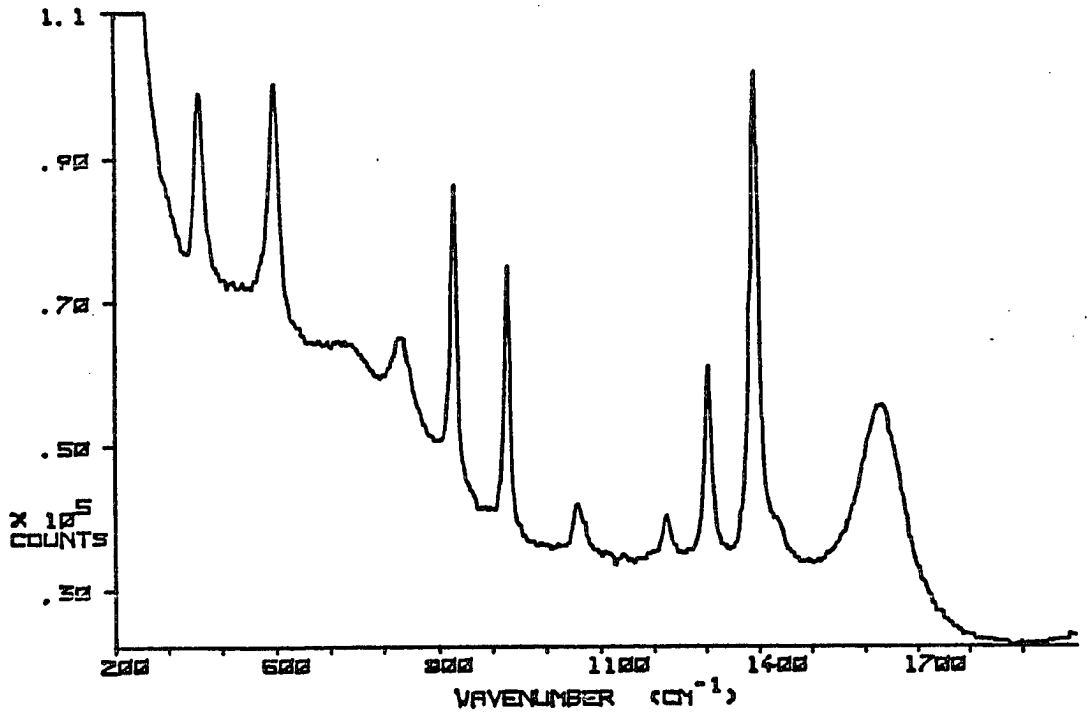

Figure 2-6. Mid Frequency Raman Spectrum of Acid Anion

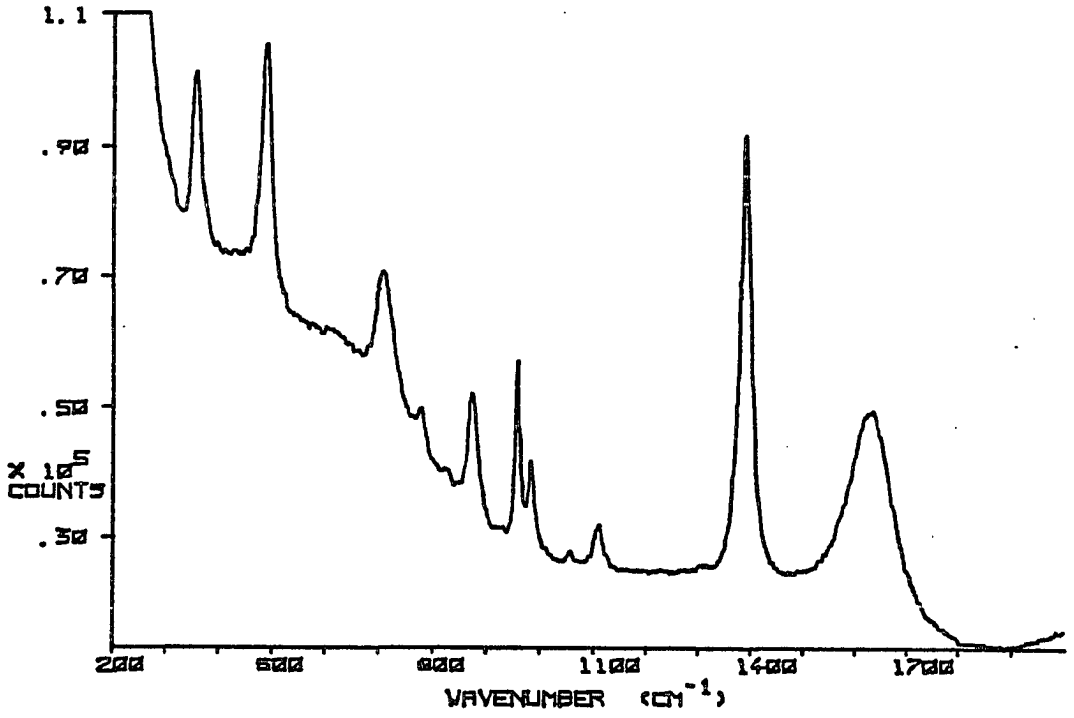

Figure 2-7. Mid Frequency Raman Spectrum of Deuterated Acid Anion

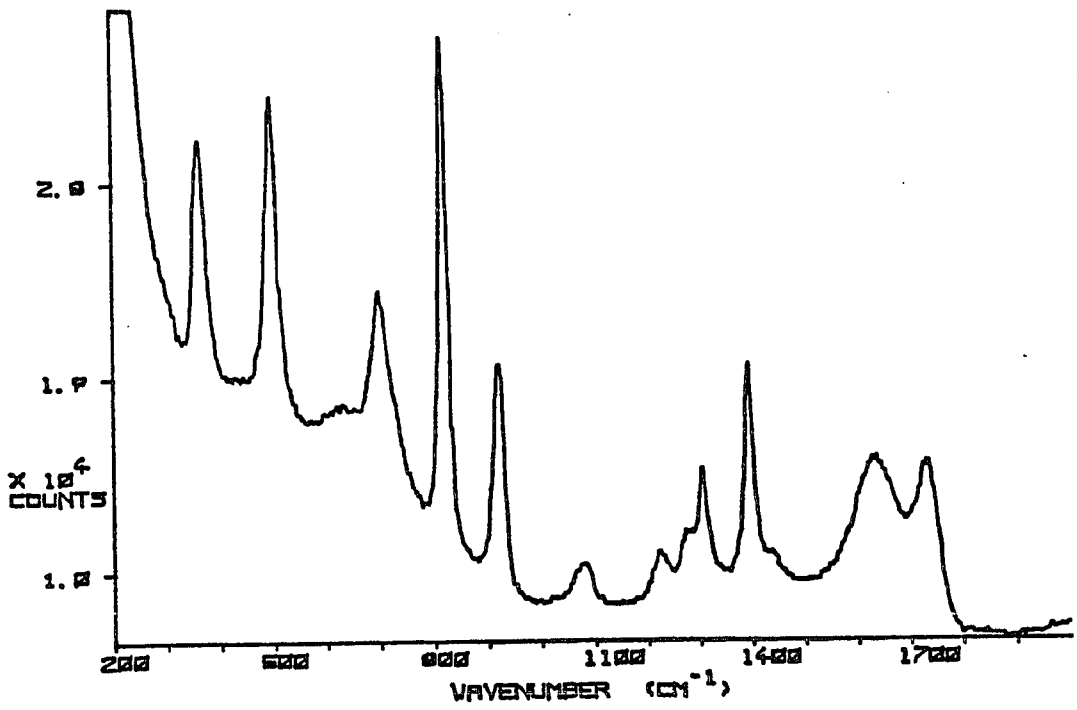

Figure 2-8. Mid-Frequency Raman Spectrum of Aqueous Acid

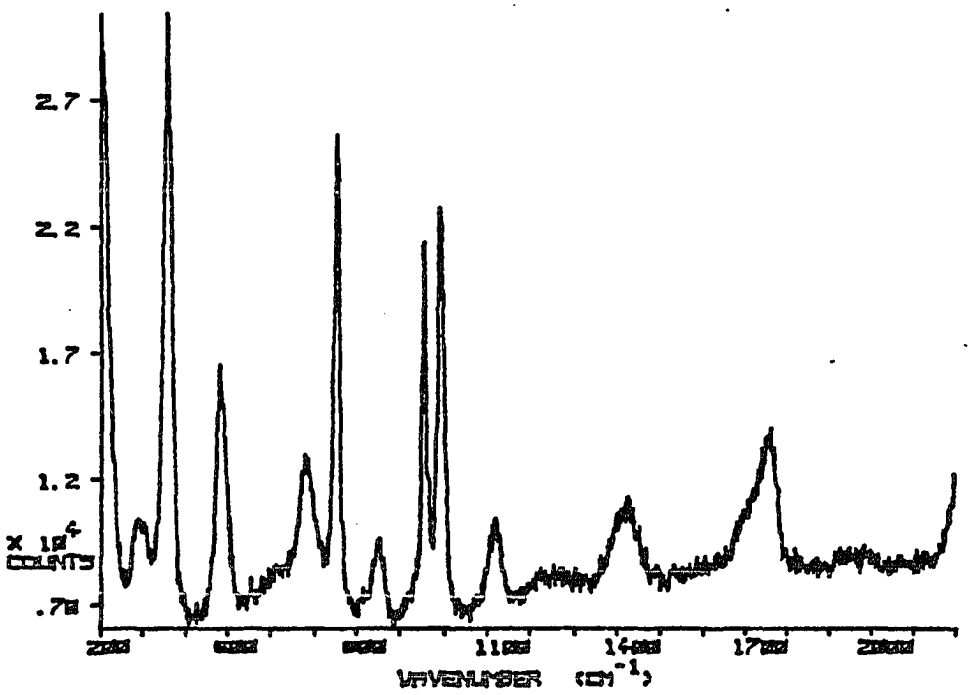

Figure 2-9. Mid-Frequency Depolarized Raman Spectrum of Neat Acid

Table 2-1. Depolarization Ratios for Deuterated Acid

Line Position (cm^{-1})	Value
3528 (acetonitrile solvent)	0.00
2212	0.19
1745	0.18
1424	0.26
1269	0.10
1121	0.26
991	0.48
957	0.15
844	0.06
755	0.28
682	0.09
611	0.11
481	0.14
358	0.43
287	0.33
270	-
205	0.88
120 (calculated)	-

Note: Depolarization values are identical to those for naturally polarized light. Maximum=0.86 (6/7). Mininum =0.0. The band at 205 cm^{-1} is completely depolarized and the value given is within the limits of experimental error.

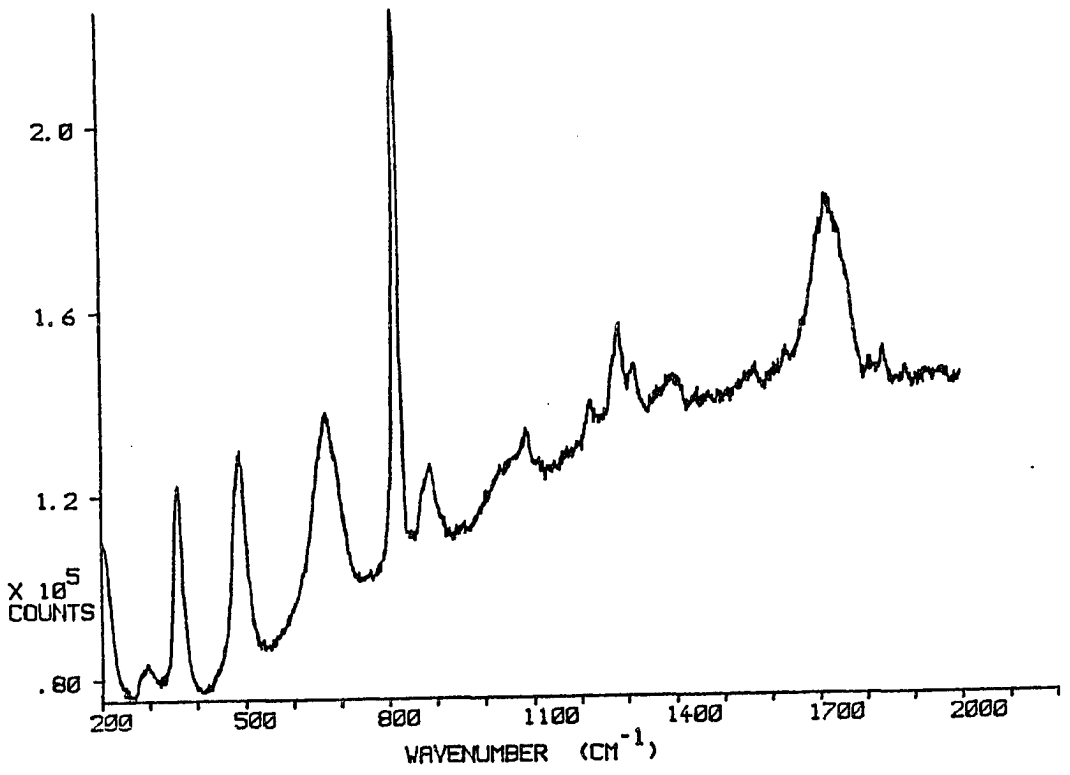

Figure 2-10. Raman Spectrum of Neat CHFClCOO-D

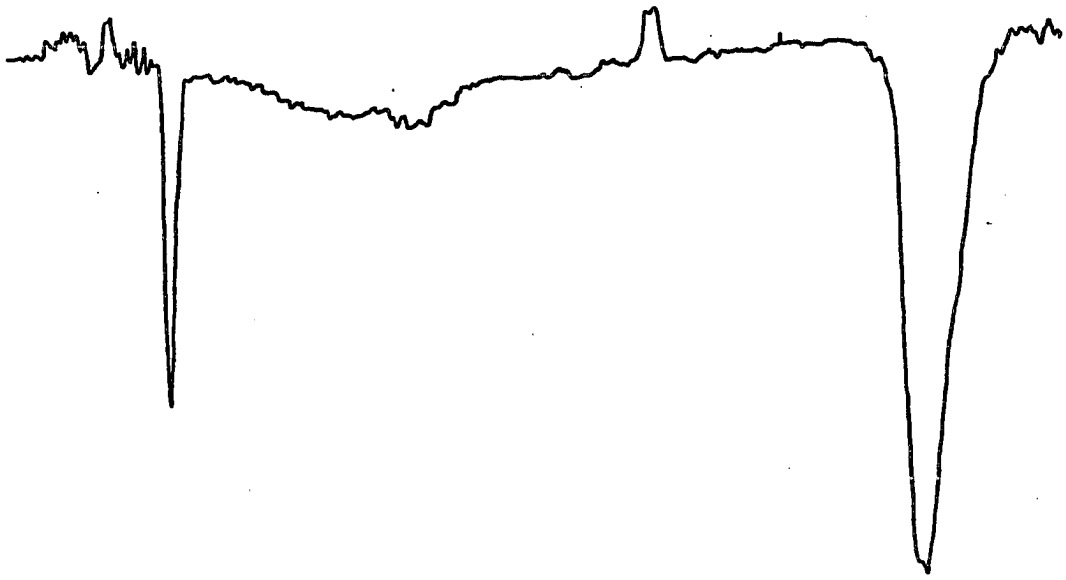

Figure 2-11. Gas Phase IR Spectrum of Chlorofluoroacetic Acid Between 4000 cm^{-1} and 1650 cm^{-1}

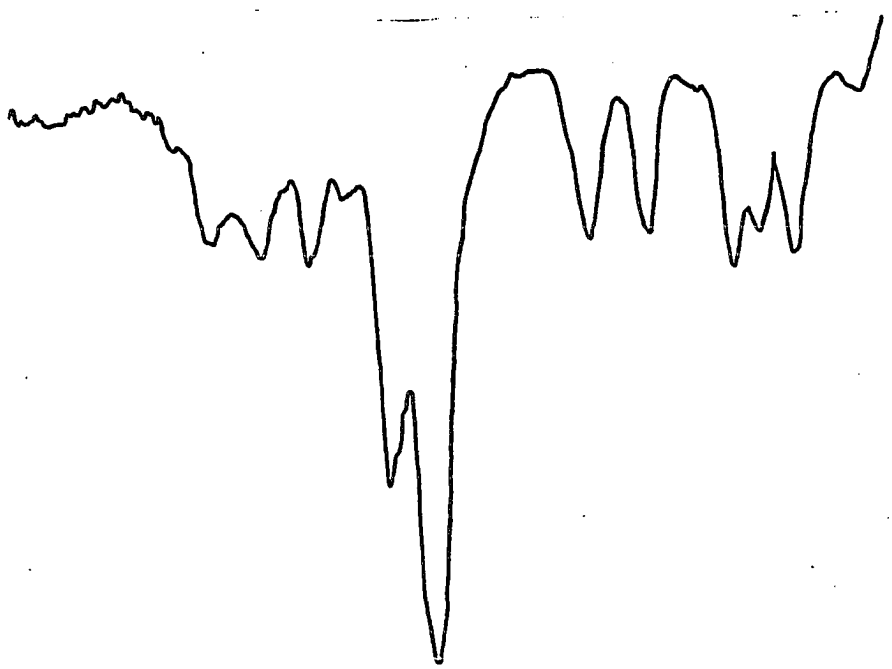

Figure 2-12. Gas Phase IR Spectrum of Chlorofluoroacetic Acid Between 1650 cm^{-1} and 500 cm^{-1}

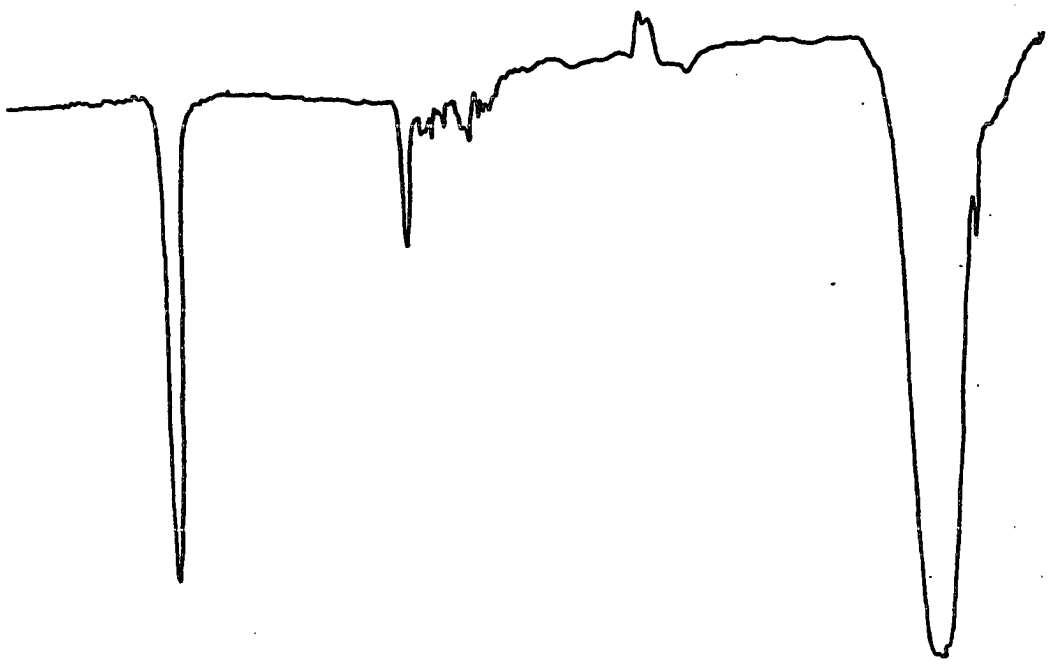

Figure 2-13. Gas Phase IR Spectrum of Deuterated Chlorofluoroacetic Acid Between 4000 cm^{-1} and 1650 cm^{-1}

Figure 2-14. Gas Phase IR Spectrum of Deuterated Chlorofluoroacetic Acid Between 1650 cm^{-1} and 500^{-1}

Table 2-2. Vapor Phase Acid IR Spectral Data

Line Position (cm^{-1})	Assignment	Relative Intensity
3578	O-H stretch	60
3000	C-H stretch	very weak
1805	C=O stretch	95
1392	C-O stretch	23
1325	Cl-C-H bend	26
1260	C-O-H bend	28
1160	C-C-H bend	71
1100	C-F stretch	100
894	C-C stretch	28
817	C-Cl stretch	28
705	Skeletal	34
670	?	28
625	COOH wag	31
540	Skeletal	5

Note: KRS-5 windows cut off lower frequency bands.

Table 2-3. Vapor Phase Acid (Deuterated) IR Spectral Data

Line Position (cm^{-1})	Assignment	Relative Intensity
3578	O-H stretch	75
2215	C-D stretch	3
1805	C=O stretch	97
1388	C-O stretch	31
1335	impurity	43
1265	C-O-H bend	62
1160	impurity	78
1090	C-F stretch	100
1000	Cl-C-H bend	79
900	C-C stretch	3
812	C-Cl Stretch	63
752	?	17
700	Skeletal	47
670	?	38
620	COOH wag	45
545	Skeletal	18

Note: Considerable material deposited on windows.

E. Outline of Normal Coordinate Analysis

The normal coordinate analysis (42) performed here uses a set of vibrational force constants, atomic position coordinates, and descriptions of the types of vibrations occurring (internal coordinates, such as bond stretches, angle bending motions, etc.) as input for the calculation of vibrational frequencies, the contribution of a given force constant to a given normal mode (force field), and relative displacement coordinates for each atom involved in a given vibration.

The analysis begins with consideration of atomic kinetic energies and potential energies between atoms in a vibration. The kinetic energy is given by:

$$2T=q^{t}q. \qquad [2\text{-}1]$$

T is the diagonal kinetic energy matrix and q's are mass weighted Cartesian displacement coordinates, given by:

$$q=M^{1/2}x. \qquad [2\text{-}2]$$

M is the atomic mass and x is a Cartesian displacement coordinate of the atom in question. Unless otherwise noted, all quantities given in this section are matrices. A superscript t denotes the transposed matrix. The matrix T is in diagonal form when mass weighted Cartesian coordinates are used. The potential energy can also be defined in terms of mass weighted Cartesian coordinates. However, it is set up in terms of internal coordinates because these are the most

easily visualized in a physical model. The potential energy is given by:

$$2V=R^{t}F_{R}R. \qquad [2-3]$$

V is the potential energy, F_R is the force constant matrix, and R's, the internal coordinates, are related to Cartesian displacement coordinates by:

$$R=Bx. \qquad [2-4]$$

B is the transformation matrix. Transposing [2-4], [2-3] can be written as:

$$2V=x^{t}B^{t}F_{R}Bx. \qquad [2-5]$$

$B^{t}F_{R}B$ is defined as F_x. Then,

$$2V=x^{t}F_{x}x. \qquad [2-6]$$

The force constant matrix is now given in terms of Cartesian displacement coordinates. This is physically meaningless in and of itself, but is useful in the transformations that follow.

Using [2-2] and its transpose, $x^{t}=q^{t}M^{-1/2}$, [2-7],the following equation is obtained:

$$2V=q^{t}M^{-1/2}F_{x}M^{-1/2}q. \qquad [2-8]$$

A matrix H can be defined as:

$$H=M^{-1/2}F_{x}M^{-1/2}. \qquad [2-9]$$

Eq. [2-9] can be rewritten as:

$$2V=q^{t}Hq. \qquad [2-10]$$

The matrix H is symmetric and represents the potential energy in mass weighted Cartesian displacements. In order to calculate vibrational frequencies (eigenvalues),

eigenvectors, and the potential energy distribution, H must be diagonalized. Let C be the matrix that diagonalizes H. C is a 3Nx3N unitary orthonormal matrix. The diagonal eigenvalue matrix is then given by:

$$C^{t}HC=\Lambda_{3N}. \qquad [2-11]$$

Six eigenvalues in this matrix will be zero.

Two matrix transformations must now be calculated. The first is the transformation between Cartesian and normal coordinates and is called the S matrix by Schellman (35). Such a transformation allows relative atomic displacement coordinates to be correlated with a given normal mode. The second transform, used to calculate the potential energy distribution, is that between internal and normal coordinates. In normal coordinates:

$$2V=Q^{t}Q. \qquad [2-12]$$

Using [2-11] for Λ,

$$Q^{t}C^{t}HCQ=2V. \qquad [2-13]$$

An examination of [2-10] shows that:

$$q=CQ. \qquad [2-14]$$

Since $q=M^{1/2}x$ (eq. 2-2),

$$x=M^{-1/2}CQ. \qquad [2-15]$$

Now, S is defined as:

$$S=M^{-1/2}C. \qquad [2-16]$$

Therefore,

$$x=SQ. \qquad [2-17]$$

From [2-15] and [2-4], it is found that $R=BM^{-1/2}CQ$. Setting $L=BM^{-1/2}C$,

$$R=LQ. \qquad [2-18]$$

The eigenvalue χ_i for a given normal mode i is given by: $\Sigma j,k \; L_{ji}L_{ki}F_{jk}$. [2-19]

The sum is taken over the jk pairs. The fractional contribution to χ_i for a given off-diagonal matrix element F is given by: $2L_{ji}L_{ki}F_{jk}/\lambda_i$. [2-21]

For diagonal terms, eq. 2-21 becomes:

$$L_{ji}^2F_{jj}/\lambda_i. \qquad [2\text{-}22]$$

Subscripts j and k denote force constant numbers (indices). When j does not equal k, an off diagonal interaction force constant or related off diagonal parameter is implied. Diagonal quantities are denoted by j=k.

Each column of the S matrix, described above, corresponds to relative displacements of atoms 1 through N for a given normal coordinate Q. Each of these columns can be decomposed into a 3xN matrix, called the SF matrix, given by:

$$\begin{matrix} S_{1x} & S_{1y} & S_{1z} \\ \cdot & \cdot & \cdot \\ S_{Nx} & S_{Ny} & S_{Nz} \end{matrix} \; . \qquad [2\text{-}23]$$

The relative Cartesian displacements for a given normal mode are normalized to one. In order to calculate the fractional contribution of a given atomic displacement, the appropriate SF matrix element is squared and multiplied by the atomic weight (43).

The advantage of using the above formalism to perform normal coordinate analysis of asymmetric molecules can best be understood when compared with an alternative form:

$$FG-E\lambda=0. \qquad [2\text{-}24]$$

In this equation (the Wilson FG form), the F and G matrices have to be diagonalized because internal coordinates are used instead of Cartesian coordinates. Unlike in the Cartesian form, the G matrix is no longer diagonal.

The product FG is, in general, an unsymmetical matrix and methods for its diagonalization are much more time consuming. Symmetric matrices can be diagonalized in a time proportional to k^3, where k is the order of the matrix. An unsymmetrical matrix requires a time proportional to k^4. Such time considerations are of the utmost importance if the calculations are to be carries out on a personal computer.

The input force field used in the analysis is the Urey-Bradley (44) type. Comparison with a different type of field, the generalized valence force field, shows why the former was used. For chlorofluoroacetic acid, a C_1 molecule with 8 atoms, the number of force constants needed for the analysis is given by n(n+1)/2, where n is the number of diagonal force constants. For the acid, 210 force constants are needed for the calculations. Since there are only 18 (+ isotopic) normal modes observable, a large indeterminacy is inherent in force constant selection. Often, many force constants must arbitrarily be set equal to zero.

The Urey-Bradley force field consists of diagonal force constants and interaction constants between non-bonded atoms. For the acid, a total of 30 force constants were

used in the calculations. Of these, 18 were diagonal, leaving a much smaller number of constants indeterminate. Isotopic substitution and use of literature values for certain constants can virtually eliminate the indeterminacy (and arbitrariness).

Calculations for the acid anion were done on an AT&T 6300 Personal Computer equipped with an Intel 8087 arithmetic co-processor and a 20 megabyte hard disk (Western Digital Hardcard). An IBM AT, using Intel 80286 and 80287 processors, was used for the acid calculations.

The programs written by J.H. Schachtschneider (45) (CART, GMAT, and UBZM) were used to calculate static Cartesian coordinates, the B matrix, and the Z matrix respectively. It was not necessary to calculate the G matrix in the above formalism. The Z matrix is the transformation matrix between Urey-Bradley input force constants and internal coordinate force constants. Eigenvalues, eigenvectors, and potential energy distributions were calculated using programs NCA and CRTFPC, written by M. Diem and adapted for AT&T and IBM machines by M.A. Davies and M. Diem.

Results of the calculations are given below. Force constants are given and compared with previously determined literature values. The full potential energy distributions, as well as summaries, for normal and isotopically substituted species, are presented. The full distributions are tables, the entries of which are the fractional contributions of each force constant to a given normal mode.

Entries in the distribution tables are numbered left to right and correspond to the force constant numbering given in the force constant listing. The molecular geometry, including principal Cartesian coordinates, and atom nubering scheme used in the normal coordinate calculations of the acid anion are shown in Figure 2-15. The corresponding axes and numbering scheme for the parent acid are given in Figure 3-12. Finally, Table 2-19 gives a comparison between force constants for chlorofluoroacetic acid used in this work and relevant force constants for bromochlorofluoro methane given in reference 53.

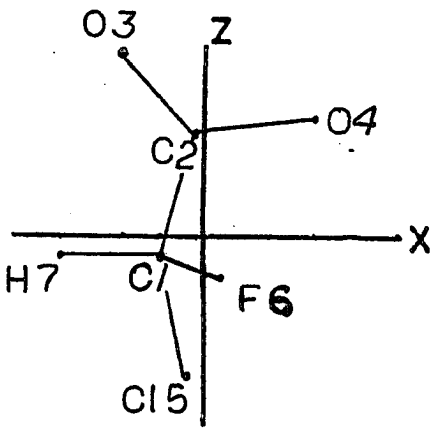

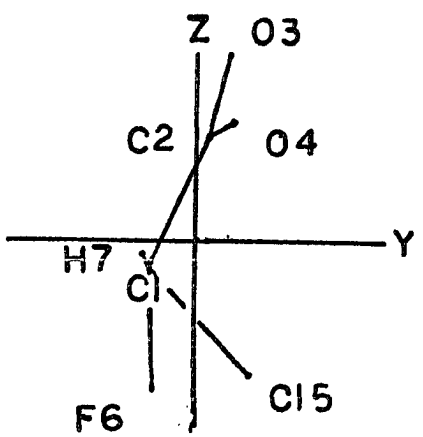

Note: 0.5 inch = 1 Å

Figure 2-15. Numbering Scheme and Principal Cartesian Coordinates for $CHFClCOO^-$

Table 2-4. Force Constants for Chlorofluoroacetic Acid

CHLOROFLUOROACETIC ACID
NORMAL COORDINATE ANALYSIS

1	1.900000	C*-Cl	2	4.000000	C*-F
3	1.700000	C*-Carb	4	3.800000	C*-H
5	6.700000	C-O	6	10.200000	C=O
7	6.700000	O-H	8	.480000	Cl-C*-F
9	.100000	Cl-C*-C	10	.200000	Cl-C*-H
11	.100000	F-C*-H	12	.150000	F-C*-C
13	.340000	H-C*-C	14	.300000	C*-C-O
15	.350000	C*-C=O	16	.150000	O-C-O
17	.500000	C-O-H	18	.065000	TCOOH
19	.035000	TOH	20	.300000	WCOOH
21	.650000	H.C*.Cl	22	1.300000	H.C*.F
23	.510000	H.C*.C	24	.800000	Cl.C*.F
25	1.000000	F.C*.C	26	1.100000	Cl.C*.C
27	1.300000	C*.C.O	28	2.900000	O.C.O
29	.500000	C.O.H	30	.000000	Rho C*

Table 2-5. Observed and Calculated Frequencies for Chlorofluoroacetic Acid

OBSERVED AND CALCULATED FREQUENCIES

	OBS.FREQ. (CM-1)	CALC.FREQ. (CM-1)	DIFFERENCE (CM-1)	PERCENT ERROR
1	3528.0	3531.2	-3.2	-.090
2	3007.0	3015.8	-8.8	-.292
3	1759.0	1765.3	-6.3	-.360
4	1439.0	1426.2	12.8	.888
5	1322.0	1328.3	-6.3	-.480
6	1253.0	1250.1	2.9	.229
7	1224.0	1208.9	15.1	1.238
8	1083.0	1102.9	-19.9	-1.833
9	927.0	931.8	-4.8	-.522
10	811.0	797.7	13.3	1.638
11	701.0	706.8	-5.8	-.823
12	620.0	617.7	2.3	.373
13	504.0	498.4	5.6	1.121
14	380.0	364.5	15.5	4.092
15	292.0	289.7	2.3	.788
16	270.0	268.2	1.8	.655
17	222.0	215.4	6.6	2.993
18	.0	120.1	.0	.000

AVERAGE ERROR= 7.4 CM-1 OR 1.02 PERCENT.

Table 2-6. Potential Energy Distribution for Chlorofluoroacetic Acid

FREQUENCY = 3531.2 CM-1								
.0000	.0000	.0000	.0000	.0003	.0000	.9614	.0000	.00
.0000	.0000	.0000	.0000	.0001	.0000	.0000	.0000	.0000
.0000	.0000	.0000	.0000	.0376	.0000	.0000	.0000	.0004
.0002	.0000	.0000						
FREQUENCY = 3015.8 CM-1								
.0001	.0001	.0001	.7545	.0000	.0001	.0000	.0001	.0000
.0001	.0000	.0000	.0004	.0001	.0001	.0000	.0000	.0001
.0000	.0000	.0513	.1477	.0442	.0001	.0001	.0001	.0007
.0000	.0000	.0000						
FREQUENCY = 1765.3 CM-1								
.0000	.0002	.0052	.0002	.1349	.7426	.0000	.0000	.0003
.0001	.0002	.0005	.0123	.0148	.0068	.0010	.0205	.0002
.0000	.0000	.0003	.0013	.0218	.0000	.0008	.0012	.0312
.0034	.0000	.0000						
FREQUENCY = 1426.2 CM-1								
.0000	.0000	.0594	.0005	.5911	.0613	.0008	.0000	.0001
.0000	.0000	.0001	.0009	.0002	.0168	.0092	.0029	.0000
.0000	.0000	.0000	.0003	.0495	.0000	.0308	.0299	.0161
.1297	.0000	.0000						
FREQUENCY = 1328.3 CM-1								
.0013	.0005	.0035	.0248	.0004	.0033	.0000	.0000	.0004
.0535	.0842	.0000	.0356	.0002	.0001	.0000	.0010	.0427
.0000	.0005	.1431	.5604	.0396	.0001	.0004	.0015	.0029
.0000	.0000	.0000						
FREQUENCY = 1250.1 CM-1								
.0005	.0029	.0239	.0000	.0119	.0238	.0050	.0007	.000C
.0035	.0000	.0001	.0056	.0025	.0025	.0046	.5304	.0003
.0000	.0000	.0065	.0006	.2346	.0004	.0030	.0038	.0250
.1076	.0000	.0000						

Table 2-6, continued

FREQUENCY = 1208.9 CM-1								
.0057	.0142	.0176	.0008	.0015	.0242	.0001	.0048	.0001
.1175	.0020	.0007	.2767	.0003	.0000	.0001	.0100	.0079
.0000	.0000	.2437	.0060	.2361	.0026	.0003	-.0002	.0218
.0053	.0000	.0000						
FREQUENCY = 1102.9 CM-1								
.0055	.6909	.0298	.0118	.0001	.0003	.0000	.0165	.0024
.0191	.0019	.0036	.0001	.0030	.0047	.0000	.0058	.0068
.0010	.0094	.0266	.0586	.0142	.0177	.0084	.0096	.0521
.0003	.0000	.0000						
FREQUENCY = 931.8 CM-1								
.0488	.0369	.2657	.0040	.0028	.0017	.0008	.0074	.0004
.0033	.0000	.0133	.0048	.0066	.0018	.0073	.0710	.0005
.0004	.0046	.0056	.0022	.1202	.0015	.0542	.0077	.2315
.0947	.0000	.0000						
FREQUENCY = 797.7 CM-1								
.3808	.0123	.0014	.0151	.0005	.0024	.0003	.0549	.0124
.0020	.0069	.0025	.0136	.0330	.0144	.0025	.0074	.0080
.0029	.0398	.1175	.0246	.0141	.0202	.0100	.0483	.1250
.0272	.0000	.0000						
FREQUENCY = 706.8 CM-1								
.0043	.0011	.0098	.0014	.0046	.0070	.0008	.0003	.0035
.0043	.0014	.0151	.0160	.0006	.0751	.0388	.0254	.0027
.0001	.0015	.0048	.0064	.0403	.0011	.0600	.0353	.2567
.3817	.0000	.0000						
FREQUENCY = 617.7 CM-1								
.0159	.0224	.0008	.0002	.0003	.0000	.0000	.0034	.0102
.0001	.0016	.0214	.0004	.0045	.0005	.0011	.0005	.0004
.0097	.5445	.0023	.0039	.0003	.0019	.1658	.1602	.0183
.0091	.0000	.0000						

Table 2-6, continued

FREQUENCY = 498.4 CM-1								
.1876	.0238	.0012	.0013	.0162	.0002	.0003	.0144	.0001
.0098	.0012	.0024	.0000	.0596	.0099	.0115	.0026	.0033
.0000	.0105	.0110	.0029	.0004	.1826	.0353	.1081	.2258
.0778	.0000	.0000						
FREQUENCY = 364.5 CM-1								
.0018	.0005	.0017	.0021	.0056	.0000	.0001	.2521	.0014
.0025	.0018	.0093	.0042	.0274	.0096	.0028	.0004	.0236
.0000	.0065	.0028	.0090	.0052	.4216	.0580	.0157	.1166
.0176	.0000	.0000						
FREQUENCY = 289.7 CM-1								
.0032	.0009	.0000	.0172	.0065	.0004	.0001	.0000	.0058
.0130	.0074	.0598	.0391	.0263	.0625	.0024	.0001	.0188
.0006	.0447	.0302	.0425	.0300	.0021	.3154	.0528	.2049
.0131	.0000	.0000						
FREQUENCY = 268.2 CM-1								
.0003	.0001	.0000	.0001	.0002	.0000	.0000	.0007	.0012
.0000	.0000	.0000	.0002	.0001	.0005	.0001	.0000	.0063
.9224	.0478	.0000	.0005	.0001	.0008	.0003	.0165	.0013
.0004	.0000	.0000						
FREQUENCY = 215.4 CM-1								
.0032	.0007	.0000	.0013	.0018	.0000	.0000	.0024	.0423
.0009	.0006	.0174	.0030	.0010	.0045	.0005	.0000	.0001
.0574	.2900	.0042	.0022	.0024	.0066	.0897	.4530	.0121
.0026	.0000	.0000						
FREQUENCY = 120.1 CM-1								
.0000	.0022	.0002	.0009	.0000	.0000	.0000	.0123	.0002
.0189	.0009	.0013	.0030	.0002	.0003	.0000	.0000	.8782
.0054	.0002	.0439	.0058	.0029	.0153	.0043	.0020	.0014
.0000	.0000	.0000						

Table 2-7. Potential Energy Distribution Summary for Chlorofluoroacetic Acid

```
FREQUENCY = 3531.2
    MODE COMPOSITION:
     .96 FORCE CONST #  7  O-H
FREQUENCY = 3015.8
    MODE COMPOSITION:
     .75 FORCE CONST #  4  C*-H
     .15 FORCE CONST # 22  H.C*.F
FREQUENCY = 1765.3
    MODE COMPOSITION:
     .13 FORCE CONST #  5  C-O
     .74 FORCE CONST #  6   C=O
FREQUENCY = 1426.2
    MODE COMPOSITION:
     .59 FORCE CONST #  5  C-O
     .13 FORCE CONST # 28  O.C.O
FREQUENCY = 1328.3
    MODE COMPOSITION:
     .14 FORCE CONST # 21   H.C*.Cl
     .56 FORCE CONST # 22  H.C*.F
FREQUENCY = 1250.1
    MODE COMPOSITION:
     .53 FORCE CONST # 17  C-O-H
     .23 FORCE CONST # 23  H.C*.C
     .11 FORCE CONST # 28  O.C.O
FREQUENCY = 1208.9
    MODE COMPOSITION:
     .12 FORCE CONST # 10  Cl-C*-H
     .28 FORCE CONST # 13  H-C*-C
     .24 FORCE CONST # 21   H.C*.Cl
     .24 FORCE CONST # 23  H.C*.C
FREQUENCY = 1102.9
    MODE COMPOSITION:
     .69 FORCE CONST #  2  C*-F
FREQUENCY =  931.8
    MODE COMPOSITION:
     .27 FORCE CONST #  3   C*-Carb

     .12 FORCE CONST # 23  H.C*.C
     .23 FORCE CONST # 27   C*.C.O
```

Table 2-7, continued

```
FREQUENCY =  797.7
    MODE COMPOSITION:
     .38 FORCE CONST #  1  C*-Cl
     .12 FORCE CONST # 21   H.C*.Cl
     .13 FORCE CONST # 27   C*.C.O
FREQUENCY =  706.8
    MODE COMPOSITION:
     .26 FORCE CONST # 27   C*.C.O
     .38 FORCE CONST # 28  O.C.O
FREQUENCY =  617.7
    MODE COMPOSITION:
     .54 FORCE CONST # 20  WCOOH
     .17 FORCE CONST # 25  F.C*.C
     .16 FORCE CONST # 26  Cl.C*.C
FREQUENCY =  498.4
    MODE COMPOSITION:
     .19 FORCE CONST #  1  C*-Cl
     .18 FORCE CONST # 24   Cl.C*.F
     .11 FORCE CONST # 26  Cl.C*.C
     .23 FORCE CONST # 27   C*.C.O
FREQUENCY =  364.5
    MODE COMPOSITION:
     .25 FORCE CONST #  8  Cl-C*-F
     .42 FORCE CONST # 24   Cl.C*.F
     .12 FORCE CONST # 27   C*.C.O
FREQUENCY =  289.7
    MODE COMPOSITION:
     .32 FORCE CONST # 25  F.C*.C
     .20 FORCE CONST # 27   C*.C.O
FREQUENCY =  268.2
    MODE COMPOSITION:
     .92 FORCE CONST # 19  TOH
FREQUENCY =  215.4
    MODE COMPOSITION:
     .29 FORCE CONST # 20  WCOOH
     .45 FORCE CONST # 26  Cl.C*.C
FREQUENCY =  120.1
    MODE COMPOSITION:
     .88 FORCE CONST # 18   TCOOH
```

Table 2-8. Observed and Calculated Frequencies for the Deuterated Acid

OBSERVED AND CALCULATED FREQUENCIES

	OBS.FREQ. (CM-1)	CALC.FREQ. (CM-1)	DIFFERENCE (CM-1)	PERCENT ERROR
1	3528.0	3531.2	-3.2	-.090
2	2212.0	2189.0	23.0	1.041
3	1745.0	1761.4	-16.4	-.941
4	1424.0	1426.0	-2.0	-.141
5	1269.0	1249.9	19.1	1.508
6	1121.0	1110.9	10.1	.900
7	991.0	990.7	.3	.035
8	957.0	958.8	-1.8	-.187
9	844.0	862.2	-18.2	-2.153
10	755.0	764.7	-9.7	-1.279
11	682.0	689.5	-7.5	-1.105
12	611.0	616.2	-5.2	-.858
13	481.0	495.3	-14.3	-2.976
14	358.0	364.1	-6.1	-1.707
15	287.0	287.6	-.6	-.219
16	270.0	268.2	1.8	.684
17	205.0	214.7	-9.7	-4.730
18	.0	119.8	.0	.000

AVERAGE ERROR= 8.3 CM-1 OR 1.14 PERCENT.

Table 2-9. Potential Energy Distribution for the Deuterated Acid

FREQUENCY = 3531.2 CM-1								
.0000	.0000	.0000	.0000	.0003	.0000	.9614	.0000	.0000
.0000	.0000	.0000	.0000	.0001	.0000	.0000	.0000	.0000
.0000	.0000	.0000	.0000	.0376	.0000	.0000	.0000	.0004
.0002	.0000	.0000						
FREQUENCY = 2189.0 CM-1								
.0005	.0006	.0003	.7704	.0000	.0003	.0000	.0005	.0001
.0003	.0000	.0002	.0008	.0003	.0005	.0000	.0000	.0003
.0000	.0000	.0464	.1342	.0405	.0003	.0004	.0004	.0028
.0000	.0000	.0000						
FREQUENCY = 1761.4 CM-1								
.0000	.0002	.0056	.0005	.1375	.7528	.0000	.0000	.0003
.0000	.0000	.0005	.0069	.0150	.0069	.0010	.0208	.0001
.0000	.0000	.0001	.0001	.0147	.0000	.0009	.0013	.0314
.0034	.0000	.0000						
FREQUENCY = 1426.0 CM-1								
.0000	.0000	.0605	.0012	.5890	.0629	.0008	.0000	.0001
.0000	.0000	.0001	.0015	.0003	.0166	.0092	.0030	.0000
.0000	.0000	.0001	.0001	.0482	.0000	.0309	.0299	.0154
.1301	.0000	.0000						
FREQUENCY = 1249.9 CM-1								
.0002	.0025	.0215	.0001	.0114	.0278	.0051	.0004	.0000
.0001	.0002	.0000	.0012	.0026	.0024	.0046	.5384	.0000
.0000	.0000	.0001	.0005	.2389	.0002	.0033	.0039	.0232
.1112	.0000	.0000						
FREQUENCY = 1110.9 CM-1								
.0013	.6529	.0591	.0030	.0007	.0036	.0000	.0219	.0030
.0012	.0082	.0014	.0411	.0029	.0041	.0000	.0101	.0047
.0009	.0077	.0011	.0347	.0190	.0203	.0000	.0118	.0855
.0000	.0000	.0000						

Table 2-9, continued

FREQUENCY = 990.7 CM-1								
.0063	.0551	.0847	.0316	.0020	.0008	.0001	.0005	.0010
.0003	.0560	.0065	.0647	.0022	.0004	.0004	.0150	.0090
.0000	.0002	.0133	.4805	.0392	.0024	.0268	.0037	.0917
.0056	.0000	.0000						
FREQUENCY = 958.8 CM-1								
.1098	.0404	.0885	.0024	.0022	.0005	.0001	.0144	.0008
.1365	.0275	.0102	.0314	.0000	.0022	.0010	.0149	.0289
.0012	.0140	.1950	.1374	.0174	.0020	.0230	-.0034	.0887
.0129	.0000	.0000						
FREQUENCY = 862.2 CM-1								
.0092	.0000	.0800	.0000	.0002	.0072	.0009	.0014	.0011
.0276	.0015	.0002	.1589	.0162	.0017	.0137	.0536	.0001
.0001	.0008	.0467	.0115	.2958	.0008	.0243	.0260	.0562
.1644	.0000	.0000						
FREQUENCY = 764.7 CM-1								
.3155	.0076	.0000	.0062	.0004	.0008	.0001	.0436	.0105
.0364	.0024	.0012	.0007	.0221	.0198	.0002	.0010	.0212
.0022	.0319	.2982	.0075	.0021	.0175	.0032	.0363	.1096
.0018	.0000	.0000						
FREQUENCY = 689.5 CM-1								
.0105	.0013	.0153	.0000	.0049	.0099	.0006	.0006	.0025
.0002	.0001	.0164	.0519	.0001	.0700	.0326	.0177	.0017
.0002	.0050	.0011	.0003	.0902	.0022	.0604	.0256	.2631
.3156	.0000	.0000						
FREQUENCY = 616.2 CM-1								
.0191	.0210	.0011	.0003	.0002	.0001	.0000	.0034	.0103
.0002	.0026	.0202	.0000	.0039	.0002	.0012	.0006	.0002
.0095	.5433	.0024	.0075	.0006	.0013	.1591	.1647	.0167
.0105	.0000	.0000						

Table 2-9, continued

FREQUENCY = 495.3 CM-1								
.1780	.0238	.0015	.0012	.0159	.0003	.0003	.0153	.0001
.0115	.0021	.0025	.0006	.0597	.0091	.0122	.0027	.0035
.0000	.0089	.0096	.0068	.0015	.1811	.0374	.1054	.2266
.0822	.0000	.0000						
FREQUENCY = 364.1 CM-1								
.0018	.0005	.0018	.0017	.0057	.0001	.0001	.2528	.0014
.0026	.0016	.0096	.0043	.0267	.0089	.0029	.0004	.0238
.0000	.0064	.0031	.0080	.0055	.4221	.0598	.0165	.1137
.0183	.0000	.0000						
FREQUENCY = 287.6 CM-1								
.0033	.0009	.0000	.0155	.0063	.0003	.0001	.0000	.0054
.0122	.0066	.0605	.0450	.0270	.0614	.0021	.0001	.0190
.0012	.0482	.0289	.0386	.0361	.0018	.3164	.0486	.2030
.0115	.0000	.0000						
FREQUENCY = 268.2 CM-1								
.0002	.0002	.0000	.0001	.0002	.0000	.0000	.0007	.0012
.0001	.0000	.0000	.0003	.0001	.0006	.0001	.0000	.0066
.9238	.0455	.0000	.0004	.0003	.0008	.0001	.0165	.0017
.0004	.0000	.0000						
FREQUENCY = 214.7 CM-1								
.0034	.0007	.0000	.0012	.0019	.0000	.0000	.0023	.0428
.0012	.0005	.0168	.0037	.0011	.0048	.0005	.0000	.0001
.0555	.2877	.0053	.0017	.0030	.0066	.0868	.4568	.0130
.0026	.0000	.0000						
FREQUENCY = 119.8 CM-1								
.0000	.0022	.0002	.0008	.0000	.0000	.0000	.0124	.0002
.0185	.0008	.0014	.0029	.0002	.0003	.0000	.0000	.8807
.0054	.0001	.0427	.0052	.0028	.0154	.0044	.0018	.0013
.0000	.0000	.0000						

Table 2-10. Potential Energy Distribution Summary for the Deuterated Acid

```
FREQUENCY = 3531.2
    MODE COMPOSITION:
     .96 FORCE CONST #  7  O-H
FREQUENCY = 2189.0
    MODE COMPOSITION:
     .77 FORCE CONST #  4  C*-H
     .13 FORCE CONST # 22  H.C*.F
FREQUENCY = 1761.4
    MODE COMPOSITION:
     .14 FORCE CONST #  5  C-O
     .75 FORCE CONST #  6   C=O
FREQUENCY = 1426.0
    MODE COMPOSITION:
     .59 FORCE CONST #  5  C-O
     .13 FORCE CONST # 28  O.C.O
FREQUENCY = 1249.9
    MODE COMPOSITION:
     .54 FORCE CONST # 17  C-O-H
     .24 FORCE CONST # 23  H.C*.C
     .11 FORCE CONST # 28  O.C.O
FREQUENCY = 1110.9
    MODE COMPOSITION:
     .65 FORCE CONST #  2  C*-F
FREQUENCY =  990.7
    MODE COMPOSITION:
     .48 FORCE CONST # 22  H.C*.F
FREQUENCY =  958.8
    MODE COMPOSITION:
     .11 FORCE CONST #  1  C*-Cl
     .14 FORCE CONST # 10  Cl-C*-H
     .19 FORCE CONST # 21   H.C*.Cl
     .14 FORCE CONST # 22  H.C*.F
FREQUENCY =  862.2
    MODE COMPOSITION:
     .16 FORCE CONST # 13  H-C*-C
     .30 FORCE CONST # 23  H.C*.C
     .16 FORCE CONST # 28  O.C.O
FREQUENCY =  764.7
    MODE COMPOSITION:
     .32 FORCE CONST #  1  C*-Cl
     .30 FORCE CONST # 21   H.C*.Cl
     .11 FORCE CONST # 27   C*.C.O
FREQUENCY =  689.5
    MODE COMPOSITION:
     .26 FORCE CONST # 27   C*.C.O
     .32 FORCE CONST # 28  O.C.O
```

Table 2-10, continued

```
FREQUENCY -  616.2
    MODE COMPOSITION:
      .54 FORCE CONST # 20   WCOOH
      .16 FORCE CONST # 25   F.C*.C

      .16 FORCE CONST # 26   Cl.C*.C
FREQUENCY -  495.3
    MODE COMPOSITION:
      .18 FORCE CONST #  1   C*-Cl
      .18 FORCE CONST # 24    Cl.C*.F
      .11 FORCE CONST # 26   Cl.C*.C
      .23 FORCE CONST # 27    C*.C.O
FREQUENCY -  364.1
    MODE COMPOSITION:
      .25 FORCE CONST #  8   Cl-C*-F
      .42 FORCE CONST # 24    Cl.C*.F
      .11 FORCE CONST # 27    C*.C.O
FREQUENCY -  287.6
    MODE COMPOSITION:
      .32 FORCE CONST # 25   F.C*.C
      .20 FORCE CONST # 27    C*.C.O
FREQUENCY -  268.2
    MODE COMPOSITION:
      .92 FORCE CONST # 19   TOH
FREQUENCY -  214.7
    MODE COMPOSITION:
      .29 FORCE CONST # 20   WCOOH
      .46 FORCE CONST # 26   Cl.C*.C
FREQUENCY -  119.8
    MODE COMPOSITION:
      .88 FORCE CONST # 18    TCOOH
```

Table 2-11. Force Field for the Acid Anion

CHLOROFLUOROACETIC ACID ANION (H)
NORMAL COORDINATE ANALYSIS

1	1.900000	C*-Cl	2	3.800000	C*-F
3	1.400000	C*-Carb	4	3.900000	C*-H
5	7.400000	Carb-O	6	.430000	Cl-C*-F
7	.100000	Cl-C*-Carb	8	.200000	Cl-C*-H
9	.100000	F-C*-H	10	.150000	F-C*-Carb
11	.340000	H-C*-Carb	12	.300000	C*-Carb-O
13	.450000	O-Carb-O	14	.065000	TCO2
15	.340000	WCO2	16	.850000	H.C*.Cl
17	1.100000	H.C*.F	18	.495000	H.C*.Carb
19	.800000	Cl.C*.F	20	1.000000	F.C*.Carb
21	.940000	Cl.C*.Carb	22	1.200000	C*.Carb.O
23	2.500000	O.Carb.O	24	.000000	Rho C*

Table 2-12. Observed and Calculated Frequencies for the Acid Anion

OBSERVED AND CALCULATED FREQUENCIES

	OBS.FREQ. (CM-1)	CALC.FREQ. (CM-1)	DIFFERENCE (CM-1)	PERCENT ERROR
1	3007.0	3034.5	-27.5	-.916
2	1597.0	1600.2	-3.2	-.201
3	1392.0	1391.3	.7	.048
4	1305.0	1325.5	-20.5	-1.573
5	1224.0	1212.9	11.1	.909
6	1057.0	1072.8	-15.8	-1.498
7	928.0	945.1	-17.1	-1.840
8	828.0	807.3	20.7	2.505
9	726.0	719.5	6.5	.899
10	636.0	630.8	5.2	.825
11	497.0	497.7	-.7	-.144
12	357.0	360.2	-3.2	-.896
13	290.0	287.2	2.8	.974
14	220.0	214.3	5.7	2.583
15	.0	121.9	.0	.000

AVERAGE ERROR= 9.4 CM-1 OR 1.05 PERCENT.

Table 2-13. Potential Energy Distribution for the Acid Anion

FREQUENCY = 3034.5 CM-1								
.0001	.0002	.0001	.7677	.0000	.0001	.0000	.0000	.0000
.0000	.0004	.0002	.0000	.0001	.0000	.0699	.1179	.0424
.0001	.0001	.0001	.0006	.0000	.0000			
FREQUENCY = 1600.2 CM-1								
.0001	.0003	.0001	.0000	.8943	.0001	.0004	.0005	.0003
.0007	.0212	.0282	.0000	.0002	.0000	.0013	.0013	.0194
.0001	.0037	.0044	.0386	-.0151	.0000			
FREQUENCY = 1391.3 CM-1								
.0001	.0009	.0472	.0004	.6416	.0001	.0000	.0020	.0003
.0000	.0090	.0108	.0324	.0000	.0000	.0061	.0016	.0370
.0001	.0279	.0208	.0176	.1441	.0000			
FREQUENCY = 1325.5 CM-1								
.0022	.0014	.0005	.0017	.0029	.0001	.0001	.1375	.0532
.0002	.0040	.0000	.0001	.0538	.0007	.4169	.3213	.0021
.0000	.0004	.0004	.0000	.0006	.0000			
FREQUENCY = 1212.9 CM-1								
.0015	.0060	.0279	.0122	.0633	.0021	.0005	.0296	.0381
.0008	.2943	.0004	.0008	.0010	.0000	.0682	.1929	.2349
.0013	.0012	.0017	.0146	.0067	.0000			

Table 2-13, continued

FREQUENCY = 1072.8 CM-1								
.0045	.7072	.0333	.0103	.0006	.0170	.0024	.0064	.0005
.0037	.0029	.0081	.0009	.0031	.0116	.0088	.0796	.0068
.0202	.0058	.0089	.0552	.0021	.0000			
FREQUENCY = 945.1 CM-1								
.0278	.0253	.2197	.0034	.0216	.0038	.0003	.0028	.0000
.0080	.0013	.0218	.0636	.0004	.0030	.0041	.0026	.0645
.0010	.0609	.0188	.1853	.2601	.0000			
FREQUENCY = 807.3 CM-1								
.4091	.0131	.0035	.0158	.0041	.0531	.0092	.0003	.0084
.0078	.0107	.0350	.0161	.0026	.0576	.0922	.0262	.0039
.0216	.0204	.0266	.1050	.0577	.0000			
FREQUENCY = 719.5 CM-1								
.0028	.0008	.0448	.0072	.0116	.0001	.0081	.0040	.0044
.0160	.0264	.0614	.0828	.0037	.0000	.0137	.0183	.0571
.0000	.0365	.0313	.3276	.2414	.0000			
FREQUENCY = 630.8 CM-1								
.0210	.0264	.0013	.0004	.0006	.0038	.0084	.0003	.0023
.0190	.0007	.0062	.0030	.0003	.5886	.0030	.0047	.0002
.0021	.1597	.1185	.0222	.0073	.0000			

Table 2-13, continued

FREQUENCY = 497.7 CM-1								
.1825	.0231	.0036	.0019	.0127	.0127	.0003	.0105	.0015
.0031	.0001	.0761	.0198	.0037	.0170	.0128	.0035	.0000
.1791	.0500	.1133	.2338	.0390	.0000			
FREQUENCY = 360.2 CM-1								
.0017	.0006	.0021	.0021	.0044	.2377	.0014	.0019	.0023
.0111	.0037	.0347	.0054	.0225	.0089	.0025	.0101	.0050
.4429	.0704	.0146	.1043	.0098	.0000			
FREQUENCY = 287.2 CM-1								
.0020	.0010	.0000	.0163	.0053	.0000	.0036	.0088	.0090
.0626	.0384	.0891	.0065	.0156	.0563	.0249	.0464	.0280
.0009	.3314	.0289	.2142	.0108	.0000			
FREQUENCY = 214.3 CM-1								
.0013	.0008	.0001	.0021	.0020	.0045	.0547	.0012	.0014
.0150	.0054	.0075	.0017	.0020	.2561	.0046	.0052	.0037
.0095	.0741	.5259	.0183	.0029	.0000			
FREQUENCY = 121.9 CM-1								
.0000	.0018	.0001	.0013	.0000	.0105	.0003	.0147	.0009
.0008	.0042	.0006	.0000	.8912	.0002	.0421	.0053	.0037
.0154	.0025	.0028	.0014	.0000	.0000			

Table 2-14. Acid Anion Potential Energy Distribution Summary

```
FREQUENCY = 3034.5
    MODE COMPOSITION:
     .77 FORCE CONST #  4   C*-H
     .12 FORCE CONST # 17   H.C*.F
FREQUENCY = 1600.2
    MODE COMPOSITION:
     .89 FORCE CONST #  5   Carb-O
FREQUENCY = 1391.3
    MODE COMPOSITION:
     .64 FORCE CONST #  5   Carb-O
     .14 FORCE CONST # 23   O.Carb.O
FREQUENCY = 1325.5
    MODE COMPOSITION:
     .14 FORCE CONST #  8   Cl-C*-H
     .42 FORCE CONST # 16   H.C*.Cl
     .32 FORCE CONST # 17   H.C*.F
FREQUENCY = 1212.9

    MODE COMPOSITION:
     .29 FORCE CONST # 11   H-C*-Carb
     .19 FORCE CONST # 17   H.C*.F
     .23 FORCE CONST # 18    H.C*.Carb
FREQUENCY = 1072.8
    MODE COMPOSITION:
     .71 FORCE CONST #  2   C*-F
FREQUENCY =  945.1
    MODE COMPOSITION:
     .22 FORCE CONST #  3    C*-Carb
     .19 FORCE CONST # 22   C*.Carb.O
     .26 FORCE CONST # 23   O.Carb.O
FREQUENCY =  807.3
    MODE COMPOSITION:
     .41 FORCE CONST #  1   C*-Cl
     .11 FORCE CONST # 22   C*.Carb.O
FREQUENCY =  719.5
    MODE COMPOSITION:
     .33 FORCE CONST # 22   C*.Carb.O
     .24 FORCE CONST # 23   O.Carb.O
FREQUENCY =  630.8
    MODE COMPOSITION:
     .59 FORCE CONST # 15    WCO2
     .16 FORCE CONST # 20   F.C*.Carb
     .12 FORCE CONST # 21    Cl.C*.Carb
```

Table 2-14, continued

```
FREQUENCY =  497.7
    MODE COMPOSITION:
     .18 FORCE CONST #  1  C*-Cl
     .18 FORCE CONST # 19  Cl.C*.F
     .11 FORCE CONST # 21   Cl.C*.Carb
     .23 FORCE CONST # 22  C*.Carb.O
FREQUENCY =  360.2
    MODE COMPOSITION:
     .24 FORCE CONST #  6   Cl-C*-F
     .44 FORCE CONST # 19  Cl.C*.F
     .10 FORCE CONST # 22  C*.Carb.O
FREQUENCY =  287.2
    MODE COMPOSITION:
     .33 FORCE CONST # 20  F.C*.Carb
     .21 FORCE CONST # 22  C*.Carb.O
FREQUENCY =  214.3
    MODE COMPOSITION:
     .26 FORCE CONST # 15   WCO2
     .53 FORCE CONST # 21   Cl.C*.Carb
FREQUENCY =  121.9
    MODE COMPOSITION:
     .89 FORCE CONST # 14  TCO2
```

Table 2-15. Deuterated Anion Observed and Calculated Frequencies

OBSERVED AND CALCULATED FREQUENCIES

	OBS.FREQ. (CM-1)	CALC.FREQ. (CM-1)	DIFFERENCE (CM-1)	PERCENT ERROR
1	2212.0	2203.2	8.8	.397
2	1599.0	1595.0	4.0	.250
3	1393.0	1386.4	6.6	.477
4	1112.0	1078.9	33.1	2.974
5	985.0	981.0	4.0	.410
6	960.0	953.0	7.0	.727
7	876.0	890.1	-14.1	-1.611
8	778.0	785.6	-7.6	-.972
9	709.0	694.9	14.1	1.985
10	620.0	629.0	-9.0	-1.447
11	490.0	494.8	-4.8	-.972
12	358.0	359.9	-1.9	-.538
13	290.0	285.3	4.7	1.622
14	220.0	213.5	6.5	2.935
15	.0	121.6	.0	.000

AVERAGE ERROR= 8.4 CM-1 OR 1.15 PERCENT.

Table 2-16. Potential Energy Distribution for the Deuterated Anion

FREQUENCY = 2203.2 CM-1								
.0005	.0008	.0003	.7836	.0002	.0005	.0001	.0002	.0000
.0002	.0008	.0007	.0000	.0002	.0000	.0629	.1069	.0387
.0003	.0004	.0003	.0025	.0000	.0000			
FREQUENCY = 1595.0 CM-1								
.0001	.0002	.0001	.0000	.9169	.0001	.0005	.0000	.0000
.0007	.0105	.0285	.0000	.0002	.0000	.0000	.0000	.0092
.0000	.0041	.0048	.0395	-.0154	.0000			
FREQUENCY = 1386.4 CM-1								
.0000	.0009	.0533	.0014	.6679	.0000	.0000	.0000	.0000
.0000	.0006	.0111	.0332	.0000	.0000	.0002	.0001	.0166
.0001	.0283	.0210	.0144	.1508	.0000			
FREQUENCY = 1078.9 CM-1								
.0027	.6684	.0587	.0015	.0045	.0193	.0033	.0033	.0108
.0020	.0404	.0067	.0014	.0067	.0113	.0050	.0320	.0118
.0203	-.0027	.0121	.0783	.0022	.0000			
FREQUENCY = 981.0 CM-1								
.0647	.0310	.1171	.0011	.0042	.0085	.0000	.1348	.0066
.0106	.0718	.0040	.0120	.0219	.0098	.2705	.0241	.0208
.0016	.0303	.0002	.1113	.0430	.0000			

Table 2-16, continued

FREQUENCY = 953.0 CM-1								
.0011	.0443	.0705	.0148	.0048	.0000	.0008	.0248	.0585
.0028	.0118	.0071	.0155	.0213	.0000	.1081	.4410	.0016
.0026	.0341	.0072	.0653	.0621	.0000			
FREQUENCY = 890.1 CM-1								
.0061	.0022	.0253	.0029	.0255	.0010	.0000	.0115	.0177
.0004	.1542	.0210	.0614	.0011	.0004	.0201	.1181	.2229
.0002	.0178	.0180	.0240	.2482	.0000			
FREQUENCY = 785.6 CM-1								
.3779	.0085	.0022	.0149	.0012	.0459	.0105	.0078	.0096
.0042	.0002	.0334	.0031	.0074	.0549	.2165	.0343	.0047
.0209	.0105	.0279	.0923	.0111	.0000			
FREQUENCY = 694.9 CM-1								
.0000	.0012	.0483	.0005	.0155	.0000	.0053	.0004	.0004
.0174	.0738	.0557	.0684	.0033	.0024	.0008	.0011	.1331
.0002	.0403	.0199	.3203	.1917	.0000			
FREQUENCY = 629.0 CM-1								
.0248	.0243	.0019	.0005	.0003	.0038	.0086	.0004	.0037
.0175	.0000	.0051	.0038	.0001	.5857	.0030	.0099	.0009
.0014	.1515	.1223	.0212	.0092	.0000			

Table 2-16, continued

FREQUENCY = 494.8 CM-1								
.1738	.0229	.0042	.0018	.0123	.0133	.0003	.0115	.0026
.0032	.0002	.0758	.0212	.0036	.0151	.0116	.0080	.0012
.1769	.0522	.1115	.2351	.0417	.0000			
FREQUENCY = 359.9 CM-1								
.0016	.0006	.0022	.0017	.0044	.2384	.0014	.0020	.0021
.0113	.0038	.0336	.0055	.0228	.0089	.0028	.0094	.0053
.4438	.0716	.0150	.1018	.0100	.0000			
FREQUENCY = 285.3 CM-1								
.0020	.0011	.0000	.0147	.0051	.0001	.0034	.0080	.0083
.0634	.0441	.0887	.0059	.0158	.0585	.0230	.0431	.0338
.0008	.3325	.0262	.2119	.0097	.0000			
FREQUENCY = 213.5 CM-1								
.0014	.0007	.0001	.0020	.0021	.0043	.0551	.0014	.0012
.0144	.0065	.0081	.0017	.0020	.2529	.0057	.0043	.0046
.0094	.0715	.5281	.0194	.0028	.0000			
FREQUENCY = 121.6 CM-1								
.0000	.0018	.0001	.0013	.0000	.0105	.0003	.0143	.0008
.0009	.0041	.0006	.0000	.8937	.0002	.0409	.0047	.0036
.0156	.0026	.0025	.0014	.0000	.0000			

Table 2-17. Deuterated Anion Potential Energy Distribution Summary

```
FREQUENCY = 2203.2
    MODE COMPOSITION:
     .78 FORCE CONST #  4   C*-H
     .11 FORCE CONST # 17   H.C*.F
FREQUENCY = 1595.0
    MODE COMPOSITION:
     .92 FORCE CONST #  5   Carb-O
FREQUENCY = 1386.4
    MODE COMPOSITION:
     .67 FORCE CONST #  5   Carb-O
     .15 FORCE CONST # 23   O.Carb.O
FREQUENCY = 1078.9
    MODE COMPOSITION:
     .67 FORCE CONST #  2   C*-F
FREQUENCY =  981.0
    MODE COMPOSITION:
     .12 FORCE CONST #  3    C*-Carb
     .13 FORCE CONST #  8   Cl-C*-H

     .27 FORCE CONST # 16   H.C*.Cl
     .11 FORCE CONST # 22   C*.Carb.O
FREQUENCY =  953.0
    MODE COMPOSITION:
     .11 FORCE CONST # 16   H.C*.Cl
     .44 FORCE CONST # 17   H.C*.F
FREQUENCY =  890.1
    MODE COMPOSITION:
     .15 FORCE CONST # 11   H-C*-Carb
     .12 FORCE CONST # 17   H.C*.F
     .22 FORCE CONST # 18    H.C*.Carb
     .25 FORCE CONST # 23   O.Carb.O
FREQUENCY =  785.6
    MODE COMPOSITION:
     .38 FORCE CONST #  1   C*-Cl
     .22 FORCE CONST # 16   H.C*.Cl
FREQUENCY =  694.9
    MODE COMPOSITION:
     .13 FORCE CONST # 18    H.C*.Carb
     .32 FORCE CONST # 22   C*.Carb.O
     .19 FORCE CONST # 23   O.Carb.O
FREQUENCY =  629.0
    MODE COMPOSITION:
     .59 FORCE CONST # 15    WCO2
     .15 FORCE CONST # 20   F.C*.Carb
     .12 FORCE CONST # 21    Cl.C*.Carb
```

Table 2-17, continued

```
FREQUENCY =  494.8
    MODE COMPOSITION:
     .17 FORCE CONST #  1  C*-Cl
     .18 FORCE CONST # 19  Cl.C*.F
     .11 FORCE CONST # 21   Cl.C*.Carb
     .24 FORCE CONST # 22  C*.Carb.O
FREQUENCY =  359.9
    MODE COMPOSITION:
     .24 FORCE CONST #  6   Cl-C*-F
     .44 FORCE CONST # 19  Cl.C*.F
     .10 FORCE CONST # 22  C*.Carb.O
FREQUENCY =  285.3
    MODE COMPOSITION:
     .33 FORCE CONST # 20  F.C*.Carb
     .21 FORCE CONST # 22  C*.Carb.O
FREQUENCY =  213.5
    MODE COMPOSITION:
     .25 FORCE CONST # 15   WCO2
     .53 FORCE CONST # 21   Cl.C*.Carb
FREQUENCY =  121.6
    MODE COMPOSITION:
     .89 FORCE CONST # 14  TCO2
```

The SF matrix for the chlorofluoroacetic acid anion is given in Table 2-18. The corresponding data for the parent acid are presented in Chapter 3 in conjunction with the discussion of ROA data. In certain cases, reference to the SF matrix allows better visualization of a given vibration than is possible through examination of the potential energy distribution alone. The bands occurring near 500 cm^{-1} and 700 cm^{-1} are cases in point.

The fractional contribution of a given atom to the total (relative) atomic motion during a given vibration is calculated by squaring the appropriate SF matrix element and multiplying by the atomic weight of the atom in question. The table is arranged so that motions of atoms along the molecule fixed axes are given by row, with motions along the x axis in row 1, motions along y in row 2, and those along z in row 3 of the table. The atoms are numbered from 1 through 7. Each column represents the x, y, and z motions of a given atom. The atomic numbering scheme is given in Figure 2-15.

In the 700 cm^{-1} band, the chiral carbon contributes 0.49 (49%) to the total relative atomic motion. Oxygen atoms 3 and 4 contribute 0.17 and 0.24, respectively, and the H atom contributes 0.05. It can be seen that the individual atomic motions span the entire molecule.

Oxygen 1 contibutes 0.28, chlorine contributes 0.30, and fluorine contributes 0.22 to the 500 cm^{-1} band.

In other cases, the SF matrix confirms what is already

easily visualized, as in the case of the C-H stretch, in which the H atom has a fractional contribution of 0.94 and the carbon to which it is bound contributes 0.05, for a total of 0.99 of the atomic motion.

Table 2-18. Acid Anion SF Matrix

NORMAL MODE NU 1	3034.5 CM-1	3007.0 CM-1				
SF MATRIX						
.0639	.0027	.0002	-.0008	.0016	.0065	-.9639
.0088	.0020	.0000	-.0003	.0017	-.0045	-.0991
-.0002	.0042	.0000	-.0007	-.0018	-.0009	.0418
NORMAL MODE NU 2	1600.2 CM-1	1597.0 CM-1				
SF MATRIX						
-.0133	.2259	-.0660	-.0918	-.0004	-.0004	-.0061
.0039	.0032	.0156	-.0184	-.0003	.0011	-.0519
.0122	-.0794	.0660	-.0122	.0014	.0017	-.1349
NORMAL MODE NU 3	1391.3 CM-1	1392.0 CM-1				
SF MATRIX						
-.0086	.0548	.0804	-.1131	-.0013	.0005	.0052
.0030	.0768	-.0234	-.0252	.0004	-.0085	-.0334
.0084	.1785	-.0922	-.0226	-.0033	-.0057	-.1822
NORMAL MODE NU 4	1325.5 CM-1	1305.0 CM-1				
SF MATRIX						
.0063	-.0072	-.0027	.0095	-.0128	.0245	-.1055
-.0439	.0007	-.0031	.0044	-.0062	-.0073	.8507
.0264	-.0104	.0046	.0006	.0058	-.0016	-.4479
NORMAL MODE NU 5	1212.9 CM-1	1224.0 CM-1				
SF MATRIX						
-.0140	.0313	.0019	-.0484	.0053	.0194	-.0190
-.0463	.0142	.0015	-.0086	.0031	-.0021	.4270
-.0863	.0221	.0051	-.0048	-.0015	.0011	.7906
NORMAL MODE NU 6	1072.8 CM-1	1057.0 CM-1				
SF MATRIX						
-.1134	-.0015	.0077	-.0047	.0025	.0686	-.0576
.1871	-.0262	-.0018	.0043	-.0012	-.1069	.0994
.0702	-.0197	-.0213	.0050	-.0011	-.0224	.1176
NORMAL MODE NU 7	945.1 CM-1	928.0 CM-1				
SF MATRIX						
-.0786	.0458	-.0984	.1110	-.0023	.0171	-.0500
.0045	.0459	.0033	.0098	-.0023	-.0361	-.0451
-.1367	.1311	.0394	-.0222	.0017	-.0064	-.1450
NORMAL MODE NU 8	807.3 CM-1	828.0 CM-1				
SF MATRIX						
.1059	-.0210	.0438	-.0546	-.0214	-.0088	.0780
.1273	-.0686	.0279	.0076	-.0327	-.0084	.0460
-.1711	-.0089	.0277	.0056	.0407	.0176	-.1478

Table 2-18, continued

NORMAL MODE NU	9	719.5 CM-1		726.0 CM-1			
SF MATRIX							
-.1597	.0121	.1027	-.0161	.0068	.0146	-.1332	
-.0727	-.0235	.0138	.0396	.0062	.0093	-.0945	
-.0933	-.0593	-.0076	.1150	.0004	.0131	-.1492	
NORMAL MODE NU	10	630.8 CM-1		636.0 CM-1			
SF MATRIX							
-.0295	.0466	-.0209	.0090	.0039	-.0064	-.0311	
.0065	-.2293	.0308	.0417	.0069	.0642	.0507	
.0296	.0891	-.0433	-.0234	-.0287	.0333	.0255	
NORMAL MODE NU	11	497.7 CM-1		497.0 CM-1			
SF MATRIX							
.0434	-.0488	.0269	-.0517	.0058	.0107	.0504	
-.0555	-.0404	.0571	.0058	.0627	-.1065	-.0514	
.0022	.0483	.1175	.0003	-.0687	.0009	-.0710	
NORMAL MODE NU	12	360.2 CM-1		357.0 CM-1			
SF MATRIX							
.0414	.0445	-.0144	.0344	-.0202	-.0351	.0315	
-.0045	.0020	-.0595	.0055	.0670	-.0792	.0220	
-.0339	-.0499	-.0995	.0066	-.0029	.1367	-.0027	
NORMAL MODE NU	13	287.2 CM-1		290.0 CM-1			
SF MATRIX							
.0780	.0668	-.0149	.0309	-.0189	-.0728	.0570	
-.0041	-.0051	.0067	.0966	-.0146	-.0566	.0469	
.0251	.0299	-.0418	.1288	-.0057	-.1019	.0852	
NORMAL MODE NU	14	214.3 CM-1		220.0 CM-1			
SF MATRIX							
-.0150	-.0100	-.0043	-.0162	.0168	.0023	-.0122	
-.0886	-.0359	.0809	.0521	.0210	-.0682	-.0826	
.0016	-.0242	-.0511	-.0996	.1012	-.0469	-.0147	
NORMAL MODE NU	15	121.9 CM-1		.0 CM-1			
SF MATRIX							
.0340	.0106	-.0261	.0253	-.0589	.0806	.0376	
-.0234	-.0086	.1265	-.1338	.0127	.0058	-.0607	
.0011	.0016	-.0655	.0724	.0022	-.0121	.0103	

Table 2-19. Comparison of Force Constants with Previous Data for Bromochlorofluoromethane (53)

Force Constant	This Work	Ref. 53
C-Cl	1.90	2.0398
C-F	4.00	4.0867
C-H	3.80	3.9207
Cl-C-F	0.48	0.4814
Cl-C-H	0.20	0.1132
F-C-H	0.10	0.0272
Cl.C.F	0.80	0.8430
Cl.C.H	0.65	0.6418
F.C.H	1.30	1.3763
Rho C*	0.00	-0.2307

Note: Non-bonded interactions are denoted by atoms separated periods. Rho C* is the intramolecular tension constant around the chiral carbon atom. Force constants are in units of mdyne/Å.

CHAPTER 3. MEASUREMENT OF RAMAN OPTICAL ACTIVITY

A. Introduction to ROA Measurement

ROA measurements seem, given the proper equipment, to be fairly straightforward and not much more difficult to make than a conventional Raman spectrum. The major components needed to make such a measurement are a laser, a modulator with which to create circularly polarized light and to modulate the light between left and right handed states, a monochromator, and a detection apparatus. There are two ways to perform the experiment. The first method makes use of a photomultiplier tube with dual channel data storage capability. In this experiment, the monochromator is scanned over the spectral region of interest. The scanning is done with a stepping motor drive controlled by a microcomputer. The grating of the monochromator is moved into position and a signal is generated by the computer, initiating data collection. Raman scattered radiation is detected by the phototube and the information is stored in the first channel of the dual channel device. Data collection stops, the modulator is switched to the second polarization state, and the second channel of the storage device is readied for use. Data collection begins again and Raman scattering induced by the second polarization state of the laser light is collected and stored. When one such

cycle is completed, the grating of the monochromator is scanned to the next position. This is repeated until the entire spectral range of interest is covered. It is usually necessary to scan the spectral region a number of times in order to improve signal to noise ratio. Finally, data in one channel is subtracted from data in the other channel and the ROA spectrum is obtained.

The second method takes advantage of multichannel detectors to survey an entire spectral region at one time. The exit slit of the monochromator is removed and the grating is not moved during a data acquisition period. A typical multichannel detector, consisting of 1024 diodes in a linear array, is capable of covering about 650 cm^{-1} at a time. The modulator is switched to the first polarization state, and the diode array is then turned on for a given time period. The Raman spectrum is collected and the array then shut off and cleared for the next cycle. The modulator switches and the process is repeated. Data from each polarization state are stored in separate data arrays in the microcomputer's memory. The spectrum has to be collected many times and the data for each polarization state added together in order to obtain acceptable signal to noise ratios. As before, data from one polarization state is subtacted from data of the other, yielding ROA spectra.

B. Circularly Polarized Light

Barron, in his early experiments, attempted to reproduce the ROA spectra reported by Moskovits, Bosnich, and Ozin and by Diem, Fry, and Burow. He was unable to reproduce these experiments and, upon further investigation, found that the data acquired depended strongly upon the orientation of the plane of polarization of the small linear component which was contaminating the otherwise circularly polarized laser beam. This slight ellipticity in the beam caused spurious ROA signals to appear in the spectra. These signals could be much larger than the actual ROA signal. It was patently clear that successful ROA experiments could be performed only if the device producing circular polarization, the electro-optic modulator, was carefully aligned. In order to do this, the nature of circular polarization must be well understood.

Two optical waves, polarized perpendicular to each other, can be represented by two equations:

$$E_x(z,t)=iE_{0x}\cos(kz-\omega t) \qquad [3\text{-}1]$$

and

$$E_y(z,t)=jE_{0y}\cos(kz-\omega t+\delta). \qquad [3\text{-}2]$$

E_x and E_y are the electric field vectors at time t, d is the relative phase difference between the two waves, and ω is the frequency of light. Subscripts i and j denote unit vectors along the x and y directions, respectively and k is the unit vector along the propagation direction z. E_{0x} and E_{0y} are the scalar amplitudes for each wave. If the

relative phase difference between the two waves is 0 or some integral multiple of 2π, the waves are said to be in phase and the resultant wave is plane polarized and oriented at 45 degrees with respect to the positive x axis. The wave equation is:

$$E(z,t)=(iE_{0x}+jE_{0y})\cos(kz-\omega t). \qquad [3-3]$$

If the phase difference is some odd integral multiple of π, the waves are out of phase and the wave equation is:

$$E(z,t)=(iE_{0x}-jE_{0y})\cos(kz-\omega t). \qquad [3-4]$$

The type of radiation of interest in ROA is obtained when both linearly polarized components have equal amplitudes; i.e., $E_{0x}=E_{0y}=E_0$ and have a relative phase difference of $-\pi/2+2m\pi$ where m=0,+ or - 1,2, etc.. . Then:

$$E_x=iE_0\cos(kz-\omega t) \qquad [3-5]$$

$$\text{and } E_y=jE_0\sin(kz-\omega t). \qquad [3-6]$$

As a result:

$$E=E_0(i\cos(kz-\omega t)-j\sin(kz-\omega t)). \qquad [3-7]$$

The scalar amplitude E_0 is constant. However, the direction of E is time varying (Fig.3-1). In this case, the resultant electric vector appears to be moving clockwise when viewed by an observer toward whom the wave is travelling. As mentioned in Chapter 1, such a wave is said to be right circularly polarized. If the phase factor is $+\pi/2+(2m\pi)$, the resultant appears to rotate counterclockwise and this wave is said to be left circularly polarized.

The description of circular polarization given above suggests that circularly polarized light can be produced if

one component of a linearly polarized beam can be slowed down relative to the other component and if both components are of equal amplitude and mutually perpendicular. This, in fact, is how all retardation-based optical devices work. Light is sent through a crystal whose indices of refraction for the two linearly polarized components are different. This is done by aligning the plane of polarization of the incident beam so that one of the mutually perpendicular components of the plane polarized beam has its plane of polarization parallel to the so-called "fast axis" of the crystal. The other component lies along the "slow axis". The fast and slow axes of the polarizing device must then be interchanged in order to change the handedness of the resulting circular polarization. In an electro-optic modulator, this is accomplished by reversing the polarity of a voltage applied to a crystal. The details of alignment and operation of an electro-optic modulator, will be discussed in section D.

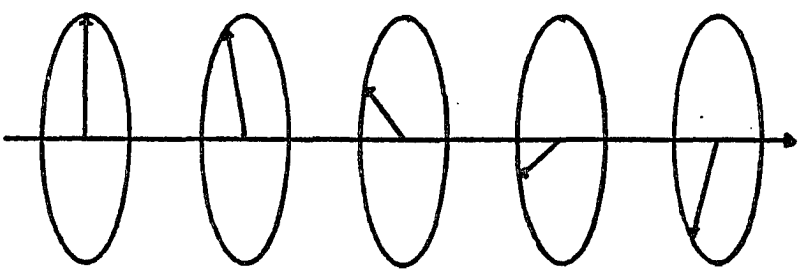

Figure 3-1. Circularly Polarized Light

C. Instrumental Artefacts in ROA Measurements

Hug (27) and Barron (28) were the first to analyze the source of instrumental artefacts in ROA measurements. Hug's treatment of the problem was based upon analysis of the angular distribution of Raman scattering in terms of scattering cross sections. Barron's treatment, more straightforward than Hug's, was based upon the molecular theory of scattering of polarized light developed with Atkins (16).

The geometry of an ROA experiment is shown in Figure 3-2. A laser beam, assumed to contain slight linear contamination in the otherwise circular polarization;i.e., an elliptically polarized beam, travels along the z axis. The major axis of the polarization ellipse, shown in Figure 3-3, is inclined at an angle θ to the x axis. The light is scattered by a molecule at the origin and the scattering is detected at a point d at a distance R from the origin. The scattering direction is arbitrary and is specified by a polar angle α and an azimuthal angle ξ. Unit vectors i, j, and k are attached to the space fixed axes x, y, and z, respectively. The scattered wave, a plane wave at the point of detection, is described by a set of unit vectors i^d, j^d, and k^d, where k is parallel to the scattering direction and i^d and j^d are always perpendicular and parallel, respectively, to the scattering plane described as the plane containing the incident and scattered directions. The follow-

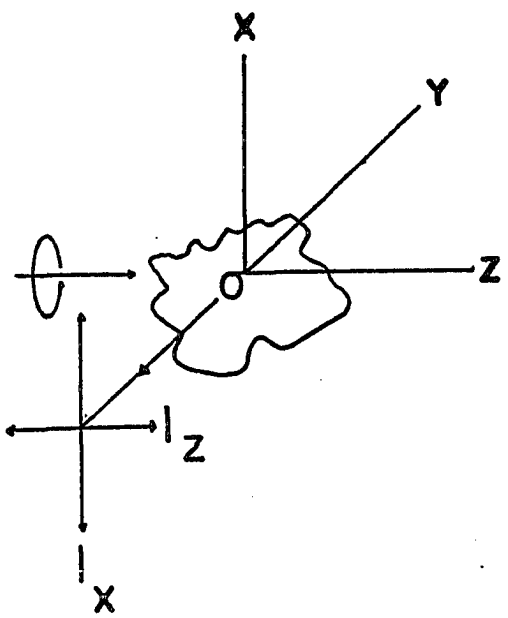

Figure 3-2. ROA Scattering Geometry

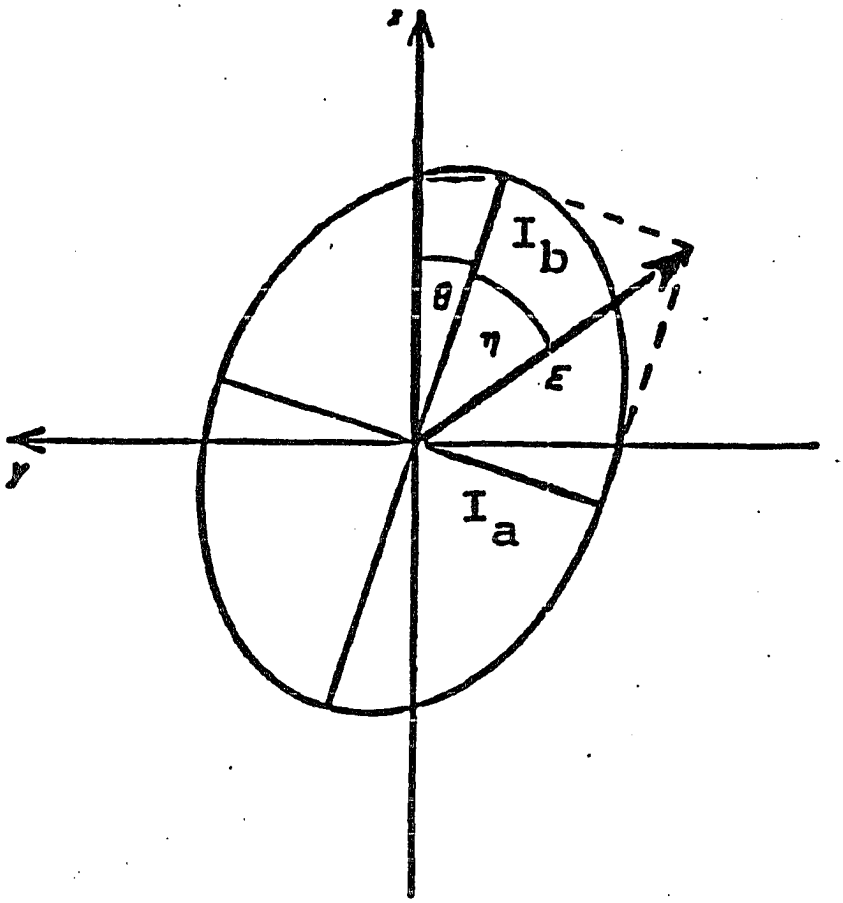

Fig. 3-3. The Polarization Ellipse

ing equations can be written:

$i^d = i \sin\alpha - j \cos\alpha$, [3-8a]

$j^d = i \cos\xi \cos\alpha - j \cos\xi \sin\alpha - k \sin\xi$, and [3-8b]

$k^d = i \sin\xi \cos\alpha + j \sin\xi \sin\alpha + k \cos\xi$. [3-8c]

The polarization of the incident beam is characterized by a parameter P, the degree of polarization. P=1 for a polarized (in this case, circular) and P=0 for an unpolarized beam. The elliptical polarization of the beam is described by the angles η and θ (Fig.3-3). The scattered intensity components at point d in the scattering axis system, polarized perpendicular and parallel to the scattering plane, as functions of the distance R, the scattering angles α and ξ, the polarization parameters of the incident beam, and the molecular property tensors, need to be calculated. For a freely rotating molecule, the intensities are given by (28):

$$I_x^d = k/2((A+B(P\cos2\eta\ \cos2\theta))\sin^2\alpha) + (A-B(P\cos2\eta\ \cos2\theta))\cos^2\alpha + 2B(P\cos2\eta\ \sin2\theta)\sin\alpha\ \cos\alpha \quad [3\text{-}9a]$$

and

$$I_y^d = k/2((A+B(P\cos2\eta\ \cos2\theta))\cos^2\alpha\ \cos^2\xi) + (A-B(P\cos2\eta\ \cos2\theta))\sin^2\alpha\ \cos^2\xi - 2B(P\cos2\eta\ \sin2\theta)\sin\alpha\ \cos\alpha\ \cos^2\xi + (2C\sin^2\xi), \quad [3\text{-}9b]$$

$$k = 1/30(\epsilon\epsilon_0/\mu\mu_0)^{1/2}(\omega^2\mu E^0/4\pi R)^2, \quad [3\text{-}10a]$$

$$A = 15\alpha^2 + 7/3\beta(\alpha)^2 + 5/3\beta(\alpha')^2, \quad [3\text{-}10b]$$

$$B = 15\alpha^2 + 1/3\beta(\alpha)^2 - 5/3\beta(\alpha')^2, \quad [3\text{-}10c]$$

$$C=\beta(\alpha)^2+5/3\beta(\alpha')^2. \qquad [3\text{-}10d]$$

ϵ, ϵ_0, μ, and μ_0 are SI constants, ω is the angular frequency of the light beam, and E_0 is the electric vector amplitude of the incident beam. α^2, $\beta(\alpha)^2$, and $\beta(\alpha')^2$ are the isotropic, anisotropic, and antisymmetric molecular polarizability tensor invariants, given by:

$$\alpha^2=1/9(\alpha_{ii}\alpha_{jj}^*), \qquad [3\text{-}11a]$$

$$\beta(\alpha)^2=1/2(3\alpha_{ij}\alpha_{ij}^*-\alpha_{ii}\alpha_{jj}^*), \qquad [3\text{-}11b]$$

$$\beta(\alpha')^2=3/2(\alpha'_{ij}\alpha'_{ij}^*), \qquad [3\text{-}11c]$$

where α_{ij} and α_{ij}^* are the symmetric and antisymmetric parts, respectively, of the complex electric dipole-electric dipole molecular polarizability tensor. The antisymmetric part is an imaginary quantity. Interference terms between the molecular polarizabilities and electric dipole-magnetic dipole and electric dipole-electric quadrupole tensors, which are the terms responsible for ROA have been omitted because only the spurious intensities are being calculated. In these equations, subscripts i and j denote Cartesian coordinates, but do not necessarily represent x and y, as is usually the case.

The amount of light energy passing across a surface element $A^2d\Omega$ in unit time in a cone of solid angle $d\Omega=\sin\xi\, d\xi\, d\alpha$ is calculated by multiplying the intensity by A^2. If the scattering takes place along the y axis, the total radiant energy passing the given surface element per unit time is obtained by integrating over $\Delta\xi$ and $\Delta\alpha$ (Fig. 3-4). The spurious scattering differences are then given by:

$$W^R_x - W^L_x = A^2 kC((1/\rho)-1)(P\cos 2\eta_R \cos 2\theta_R - P_L \cos 2\eta_L \cos 2\theta_L)\sin\Delta\alpha \sin(\Delta\xi/2), \quad [3\text{-}12a]$$

and

$$W^R_z - W^L_z = -1/3(A^2 kC)((1/\rho)-1) - (P_R \cos 2\eta_R \cos 2\theta_R - P_L \cos 2\eta_L \cos 2\theta_L) \sin\Delta\alpha \sin^3(\Delta\xi/2), \quad [3\text{-}12b]$$

where R and L denote right and left circular polarization states and ρ is the depolarization ratio. The subscripts z and x denote scattering collected with a polarization analyzer, the transmission axis of which is oriented parallel to the axis indicated by the subscript. Scattering polarized parallel to the z axis is the depolarized component.

The equations above show clearly why artefacts for strongly polarized bands will be larger than those for depolarized bands; for a strongly polarized band, $(1/\rho)-1$ approaches infinity. The equations also show an explicit dependence upon the angles defining the scattering cone; the equations imply that the smallest possible collection apertures should be used. Also apparent from the equations is that artefacts for the depolarized component due to the finite collection angle used will be smaller due to the $\sin^3 \Delta\xi/2$ term. Hug (27) proposed two major strategies for further reduction of artefacts. Since both equations have a $\sin\Delta\alpha$ dependence, collection in a complete semicircle ($\Delta\alpha$ = 180 degrees) should completely eliminate these artefacts. This, in practice, is very difficult.

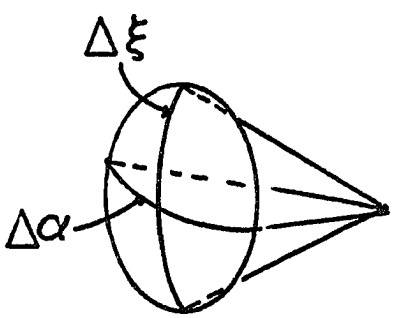

Figure 3-4. ROA Collection Angles

Another way to achieve the same goal is evident from the equations. If the major axis of the polarization ellipse is oriented at + or - 45 degrees to the y axis, the artefacts will disappear. This assumes, of course, that the intensities of the linearly polarized contaminants of each polarization state are identical. If a collection lens is placed at + 45 degrees to the y axis, the effective azimuth θ is equal to $\theta'-45$ degrees; similarly, if another collection lens is placed at +45 to the y axis, the effective azimuth is $\theta'+45$ degrees. Assuming that the initial azimuth for both left and right polarization states were equal,

$$(\cos 2(\theta'_R-45^o)-\cos 2(\theta'_L-45^o))$$
$$-(\cos 2(\theta'_R+45^o)-\cos 2(\theta'_L+45^o))=0.$$

Hug then demonstrated the utility of the twin lens collection system. Such a scheme is used in the optical system of the Hunter College ROA unit (Fig. 3-5).

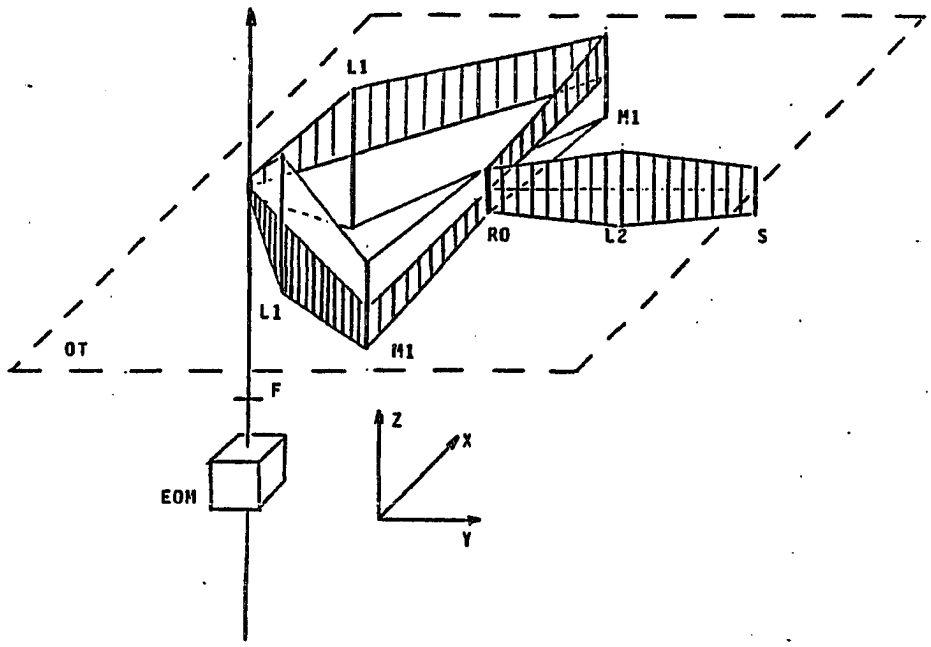

Figure 3-5. Optical Layout of the Hunter College ROA Unit

D. The Electro-optic Modulator

In order to achieve probe beam radiation which will not lead to false ROA signals, the electro-optic modulator (EOM) must be carefully aligned. Proper alignment using a trial and error procedure is virtually impossible, and a stepwise procedure, leading to reproducible polarization parameters, is needed. In order to develop and execute such a procedure, a thorough knowledge of the electro-optic effect is required.

The EOM, or Pockels cell, is a crystal along which an electric field is applied. The crystal, usually made of $NH_4H_2PO_4$, KH_2PO_4, or KD_2PO_4, is optically anisotropic. This means that its effect on a beam of light passing through it depends upon the direction of the electric vector relative to the crystallographic axes.

An ideal EOM crystal is optically uniaxial, that is, there is only one axis, the optic axis, along which two beams of light, polarized mutually perpendicular, have the same refractive index. The optic axis will be the Z axis.

The change of refractive index with direction in uniaxial crystals can be described using an ellipsoidal figure termed an indicatrix (46) (Fig. 3-6), the axes of which lie along the X, Y, and Z axes. The index of refraction along a given direction is proportional to the length of the ellipse axis along that direction. The equation for the indicatrix is:

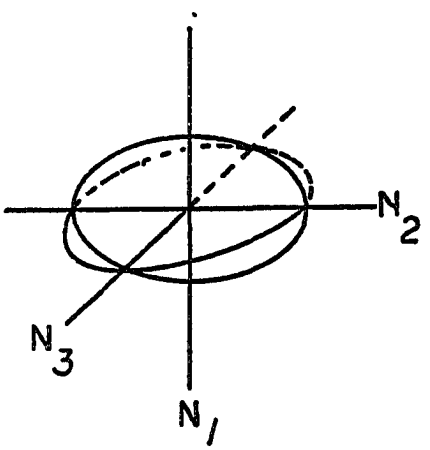

Figure 3-6. The Index Ellipsoid (Indicatrix)

$$(x^2/n_1^2)+(y^2/n_2^2)+(z^2/n_3^2)=1. \qquad [3\text{-}13]$$

In a uniaxial crystal, $n_1=n_2$, so that this equation becomes: $$((x^2+y^2)/n_1^2)+(z^2/n_3^2)=1. \qquad [3\text{-}14]$$

When the crystal is subjected to an electric field, the indicatrix is given by the more general equation:

$$a_{11}x^2+a_{22}y^2+a_{33}z_2+2a_{23}yz+2a_{13}xz+2a_{12}xy=1. \qquad [3\text{-}15]$$

The deformation of the indicatrix represents a change in the optical properties of the crystal. The indices a_{ij} are called the polarization constants. They are given by: $a_{ij}-\delta_{ij}(1/n_in_j)=r_{ijk}E_k$, $(i,j,k=1,2,3)$. The subscripts on r are usually contracted so that ijk=mk, ij=m. Then 11=1, 22=2, 33=3, 23=4, 13=5, 12=6 (47). The equations, in which δ denotes the Kronecker function, describe changes of the length of the principal axes of the indicatrix; i.e., changes in the refractive indices of the crystal. They are:

$$a_{11}-(1/n_1^2)=r_{11}E_1+r_{12}E_2+r_{13}E_3, \qquad [3\text{-}15a]$$

$$a_{22}-(1/n_2^2)=r_{21}E_1+r_{22}E_2+r_{23}E_3, \qquad [3\text{-}15b]$$

$$a_{33}-(1/n_3^2)=r_{31}E_1+r_{32}E_2+r_{33}E_3, \qquad [3\text{-}15c]$$

$$a_{23}=r_{41}E_1+r_{42}E_2+r_{43}E_3, \qquad [3\text{-}15d]$$

$$a_{13}=r_{51}E_1+r_{52}E_2+r_{53}E_3, \qquad [3\text{-}15e]$$

$$a_{12}=r_{61}E_1+r_{62}E_2+r_{63}E_3, \qquad [3\text{-}15f]$$

in which the r coefficients are the electro-optic coefficients. The last three of eqn. [3-15] describe how the indicatrix is rotated about its axis when an electric field is applied.

These equations take into account only optical changes which are linear in the electric field E. There can also be

mechanical strain, but this can be eliminated by mechanically constraining the crystal. If the crystal is modulated at a frequency corresponding to an acoustic resonance of the lattice, the effect produced may be larger than that induced by an electric field. Such an effect is eliminated by modulating at very low frequencies (<10Hz). Quadratic and higher order effects are also present, but these are quite small and can be ignored.

Eq. 3-14 must remain unchanged when the crystal is subjected to symmetry operations. If the crystal is rotated through π about the x axis, x will be unchanged. Y and z will change sign. E_1, the electric field component parallel to the x axis, will be unchanged. Y and z will change sign. E_2 and E_3, parallel to the y and z axes, respectively, change sign. The coefficients a_{11}, a_{22}, a_{33}, and a_{23} must be positive while a_{12} and a_{13} must be negative. In order that these criteria are met in the general case, some of the electro-optic coefficients must be zero. In fact, all of the coefficients except r_{41}, r_{52}, and r_{63} are zero. When the crystal is rotated about the y axis, x and z change sign, as do the corresponding electric field components. a_{12} and a_{23} are negative, all other a values are positive. As before all r values with the exception of r_{41},r_{52}, and r_{63} are zero.

An improper rotation of $\pi/2$ about the z axis, followed by inversion through the center of symmetry yields the same result as rotation through an angle θ about the y axis.

For crystals of tetragonal symmetry, such as the KD_2PO_4 used in the experiments described herein, r_{41} and r_{52} are equal, but very small compared to r_{63}. Therefore, the electro-optic equation for a uniaxial crystal subjected to an electric field E_3 along the z axis becomes:

$$((x^2+y^2)/n_1^2)+(z^2/n_3^2)+2r_{63}E_3xy=1. \qquad [3\text{-}16]$$

The cross term in xy indicates that the indicatrix has been rotated with respect to the original position with major and minor axes parallel to the coordinate system. The rotation takes place only in the x-y plane. The angle of rotation can be computed by first taking z=0, since the rotation takes place about the z axis. The indicatrix axes, indicated with primes, can be transformed into the original x-y-z axis system using:

$$x=x'\cos\theta - y'\sin\theta \qquad [3\text{-}17a]$$

and

$$y=x'\sin\theta + y'\cos\theta. \qquad [3\text{-}17b]$$

The electro-optic equation now becomes:

$$(1+n_1^2r_{63}E_3\sin^2\theta)(x'^2)+(1-n_1^2r_{63}E_3\sin^2\theta)(y'^2)$$
$$+(2n_1^2r_{63}E_3(\cos^2\theta - \sin^2\theta)x'y')=n_1^2. \qquad [3\text{-}18a]$$

The angle θ is the angle of rotation in the x-y plane. Now, if the x and y axes are rotated so that they are parallel to the x'-y' system, the cross term containing x'y' disappears. This occurs when $\sin^2\theta = \cos^2\theta$. Therefore, θ is 45 degrees. The major axis of the indicatrix is rotated so that its major axis in the x-y plane lies at either + or - 45 degrees with respect to the crystallographic axes before application of the electric field.

The sign of the angle is a function of the applied voltage. For example, if a negative rotation angle is obtained with a positive voltage, a positive rotation will be obtained with a negative voltage. Note that the orientation of the indicatrix axis is independent of the applied voltage. Only values of the refractive index along axes perpendicular to the applied field are functions of the applied field strength. The equation for the indicatrix can now be written:

$$(x'/n_1)^2(1+n_1^2r_{63}E_3)+(y'/n_1)^2(1-n_1^2r_{63}E_3)+(z'/n_3)^2=1. \quad [3\text{-}18b]$$

The new principal indices of refraction are:

$$n_1'=(n_1^2/1+n_1^2r_{63}E_3)^{1/2} \text{ and } n_2'=(n_1^2/1-n_1^2r_{63}E_3)^{1/2}. \quad [3\text{-}19]$$

Finally, the induced birefringence, Δn, is given by (48):

$$\Delta n=n_1^3r_{63}E_3. \quad [3\text{-}20]$$

After application of an electric field, the indicatrix has three indices of refraction. One of the indices corresponds to an indicarix axis parallel to the beam. However, incident light plane polarized perpendicular to the beam direction will now be phase shifted because light polarized parallel to the minor axis of the polarization ellipse (the indicatrix as viewed along the z axis) travelsfaster than that polarized parallel to the major axis. The phase shift can be written: $\phi=2\ \pi/\lambda t_3\ \Delta n$, where t_3 is the thickness of the crystal. Using $V_3=E_3t_3$, in which V_3 is the applied voltage parallel to the z axis, the phase shift can be written as:

$$\phi=2\pi/\lambda(n_1^3 r_{63} E_3). \qquad [3\text{-}21]$$

λ is the wavelength of the incident light. Circular polarization is obtained when ϕ=+ or - 45 degrees. This is termed quarter wave retardation. The correlation between the sign of the phase shift angle and the sign of the applied voltage depends upon the orientation of the fast and slow indicatrix axes relative to the plane of polarization of the incident beam.

E. EOM Alignment

Proper EOM alignment begins by making certain that the laser beam travelling through the modulator crystal is parallel to the optic axis. Since the geometry of the EOM is vertical, the beam must also be vertical. A plumb line, with a conical plumb bob tied to one end, is used to establish a reference point. The bob is suspended above the hole in the optical table through which the laser beam passes. When the bob is centered above the hole, the other end of the line is attached to the ceiling. The hole in the table establishes the first reference point; the point at which the other end of the plumb line contacts the ceiling is the second. An index card placed above the hole can be used as an aide in determining if the laser beam is indeed centered. Because a plumb line was used, the vertical position of the second reference point relative to the

hole in the table is assured. The mirror, 45 degrees to the vertical path defined by the plumb line, is adjusted using pitch and yaw controls until the laser beam hits the reference point on the ceiling, (approximately 2.5 meters away), while remaining centered in the hole in the optical table.

If desired, two small pinholes (0.1-0.5 mm) can be introduced into the optical path and used as reference points after the initial procedure using the plumb line has been completed. They are simply adjusted using translation controls on their respective mounts until the laser passes through both.

It is important that the second reference point be as far away from the first as possible, because small deviations from vertical beam direction do not become apparent to the experimenter until the beam has deviated from the reference point; the long path acts as a "optical lever arm". Small deviations become more apparent the farther the beam travels.

When it has been established that the beam direction is correct, a beam expander is placed into the beam and the image of the beam is projected onto the ceiling using a short focal length lens. The beam expander used in this experiment is a simple Galilean telescope with an expansion ratio of 3:1. It is used to prevent localized heating of the EOM crystal due to absorption of laser radiation by the crystal. Such heating can cause mechanical strain in

the crystal and consequently introduce unwanted residual birefringence. If a defect exists in the crystal, its effect upon the beam may vitiate the entire EOM alignment. By spreading out the beam, such a difficulty is minimized. The beam should be centered in both the beam expander and the short focal length lens. Concentric rings, due to Fraunhofer diffraction, should be observed on the ceiling. The center of the set of rings should fall on the reference point discussed earlier. Using pitch and yaw controls on the beam expander mount, the expander is adjusted until the intensity of each ring is uniform; i.e., the intensity is the same for each point on each diffraction ring.

A linear polarizer is now placed in the optical path. This polarizer serves to optically isolate the laser from the rest of the system. When laser radiation passes through the EOM crystal (with 1/4 wave retardation applied) and is reflected back through the EOM, the resulting beam is retarded by 90 degrees, resulting in linear polarization perpendicular to the original incident beam. Such radiation cannot pass through the polarizer. The beam is centered in the polarizer and the polarizer aligned by superimposing back reflected light from the polarizer itself onto the mirror used to direct the beam upward.

All optical components used to steer and modulate the laser radiation should now be properly aligned. The EOM is removed from the beam path and the spinning polarizer is rotated until its transmission axis is perpendicular to the

plane of laser polarization (minimum transmission position). The EOM is now put back into the beam and its pitch and yaw controls are adjusted until transmission is again minimized. This operation serves to select a good starting position for the actual EOM alignment by eliminating or minimizing residual birefringence in the crystal. A spinning polarizer is used to measure the circularity of the beam and polarization ellipse orientation. This is done using a series of four intensity measurements. The first of these, I_0 is made with no electric field applied to the crystal. This is done to determine the plane of laser polarization. The major axis of the polarization ellipse should lie in this plane when retardation voltages are applied. The second measurement, I_a is made with the electric field applied. The polarizer is rotated until the intensity minimum (minor axis of the polarization ellipse) is found. A computer prompts the operator to input this value (read from a digital voltmeter). The third value measured, I_b, is the intensity value of the major axis of the polarization ellipse;i.e., the intensity maximum. The polarizer is rotated until this value is found.

At this point, the degree of ellipticity of the beam, η, is computed. η is defined as the arc $\tan(I_b/I_a)^{1/2}$ (see Fig. 3-2). For perfectly circularly polarized light, η=45 degrees. The fourth and final reading, I_c, is now made by first turning off the EOM electric field. The polarizer is not moved. The intensity profile of the

polarized laser beam - polarizer combination varies as the $\cos^2\phi$, with ϕ being the angle through which the polarizer is rotated away from its original orientation. ϕ is defined as the $\cos(I_c/I_0)^{1/2}$. Measurement of beam parameters using the procedure described above will take place after the remaining optics have been aligned.

The orientation of the spinning polarizer can be seen by referring to Figure 3-3. The first intensity measurement (I_0) is made with the polarizer transmission axis parallel to the x axis of the figure. The second, I_a, is made to determine the position of the minor axis of the polarization ellipse. The third, I_b, measures the major axis of the ellipse. The fourth and final measurement is made with the voltage turned off and parallel to I_b. This measurement determines the orientation of the ellipse.

The spinning polarizer is aligned by first centering the laser beam inside of it. It is leveled by first attaching the output terminal of the digital voltmeter to an oscilloscope (the voltmeter is, in turn, connected to the laser power meter head). The scope is set to dual channel operation with channel 1 at DC. The spinning polarizer is now geared to a synchronous AC motor. A $\cos^2\phi$ waveform should now be observed on scope channel 2. The straight line DC level of channel 1 can be adjusted until it contacts the maxima of the $\cos^2$ waveform. Pitch and yaw controls are adjusted until the $\cos^2$ maxima touch the DC level. An improper adjustment is indicated when only

maxima 360 degrees apart touch the DC level.

A voltage of 1000 volts is now applied to the crystal and the intensity value detected by the power meter head is read off of the digital voltmeter. This procedure is repeated for a voltage of -1000 volts. The polarization ellipses should not be rotated at this point. Intensities for both voltage polarities are equalized by slightly adjusting pitch and yaw controls if necessary.

The voltage polarities are adjusted to + and - 1500 volts. Circularities (ellipticities) for each polarization handedness are still the same and the ellipses are overlapped; however, they are rotated by 10-15 ^{o} from the plane of laser polarization. At + and - 1550 volts, the ellipses are rotated far from the desired orientation. The ellipses can be rotated into the proper orientation and the circularities improved by carefully adjusting pitch and yawand rotation controls on the EOM mount. This is done in an "iterative" fashion. The pitch and yaw control is adjusted. Rotation of the polarization ellipses can be checked manually by disengaging the teeth at the base of the rotating polarizer mount from the gear of the AC motor. If circularity is improved, the EOM rotation control is adjusted in order to orient the polarization ellipses. Then, the pitch and yaw controls are re-adjusted, followed by rotation of the EOM. It may be possible to get very close to optimum alignment using this procedure. Final fine adjustment of beam circularities and ellipse rotation can be

made by changing the voltages applied to the EOM in + or - 5 volt increments. Care must be taken that the ellipses are not over-rotated by this voltage adjustment. With practice, a badly aligned modulator can be aligned in less than 1 hour.

F. Details of the ROA Unit Optical Layout

A Spectra-Physics Model 166-4 argon ion laser, tuned to the 5145 Å line, was used as the light source for all experiments except ROA measurements of chlorofluoroacetic acid, in which a Lexel Model 95-3 argon ion laser, tuned to the 4880 Å line was used. It was found that the Lexel laser had much better power stability. Furthermore, it was noticed that the beam of the Spectra-Physics laser had a tendency to "walk". When viewed from the positive Z axis in Figure 3-5 (looking into the vertically travelling beam), the beam appeared to drift in the positive Y direction after one or two days. This was attributed to insufficient thermal control of the prism assembly; when the prism moved, the beam leaving the laser no longer travelled horizontally. When the beam then reflected off of the 45° mirror, it did so at a point away from the center of the mirror and at an angle of slightly more than 45°. Such problems were not encountered with the Lexel laser. After reflection from the 45° mirror, the beam travelled

vertically along an optical rail (Ardel Kinematics) through the beam expander, constructed using two asymmetric lenses. The beam then passes through the prism polarizer (Karl Lamprecht) used to optically isolate the laser and into the 10mm aperture of a KD_2PO_4 electro-optic modulator (Lasermetrics, Model 1057). The crystal is surrounded by index matching fluid. The circularly polarized beam created by the EOM the is focused with a 20 cm focal length achromatic lens into the sample. A 75 mm long, 1.5 mm i.d. pyrex tube with a flat window cemented to it was used as the sample cell for the pinene studies; a quartz tube was used in the chlorofluoroacetic acid study. The window of the quartz cell was attached by sintering. The sample tubes were mounted in a chuck, which in turn was mounted to the optical rail. The chuck can be rotated out of the laser beam path for EOM alignment. The final element mounted on the vertical optical rail is the rotating prism polarizer used to measure beam circularity parameters. This is mounted just before the laser power meter head.

The Raman scattered radiation is collected with two f/1.2 Canon FD series 50 mm camera lenses. They are mounted with their optic axes 90^{o} apart and at 45^{o} with respect to the Y-Z plane (Figure 3-5). As explained earlier, such a collection configuration was pioneered by Hug and was found by him to drastically reduce ROA artifacts. The adjustable diaphragm of these lenses may be closed down to further reduce artefacts; however, because light throughput is

crucial to the success of ROA experiments, this feature is rarely used. Furthermore, the quality of EOM alignment makes such lens stop-downs uneccessary. The separate images produced by the two lenses are directed to a recombination optic using two flat mirrors, M1, shown in Fig. 3-5. The recombination optic, RO, shown in the above mentioned figure, consists of two flat mirrors, one on top of the other, oriented at 45^{o} to the Y-Z plane. The vertex of the right angle defined by the two mirrors is the common focus of the two separate images collected through each arm. The image of the sample, now recombined, travels parallel to the Y axis in the figure through a third camera lens, L2, which is identical to the other two and is focused onto the slit of a monochromator. Image magnification at the monochromator slit is x5.

The spectrograph consists of a 64 cm focal length Czerny-Turner single monochromator equipped with a 1800 groove/mm holographically ruled diffraction grating (Instruments S.A., Model HR640). The superior optical properties of holographically ruled gratings allow use of a single monochromator in Raman measurements, thus dramatically increasing total light throughput. The exit slit of the monochromator was removed, allowing spectral segments of approximately 650 cm^{-1} to be studied. A 25 mm focal length cylindrical lens was placed at the exit of the monochromator with its long axis oriented parallel to the diode array. The image produced by this lens is about 4mm

high and shows a center line running along its horizontal length. This line is due to the two image collection system.

G. Signal Detection and Processing

Signals were detected using a Tracor Northern Model 6122 intensified diode array, consisting of 1024 diodes. A schematic detailing the interrelationships between the various electronic components of the ROA unit is given in Figure 3-7. The instrument is controlled by a microcomputer(Columbia Data Systems Model 964). The computer communicates with an interface module (Instruments S.A. Spectralink). The Spectralink contains the monochromator stepping motor control (used to move the grating), two high voltage power supplies used to operate the EOM, and the diode array detector controller. Details of the design of the detector controller have been published (49).

An ROA data acquisition cycle is initiated by switching on one of the EOM high voltage power supplies. The EOM reaches quarter wave retardation in about 25 ms. The diode array is cleared and data acquisition is started. After a preset exposure time has elapsed, the diode array is read and the data stored. The first high voltage supply is turned off, the second is turned on, and after a suitable

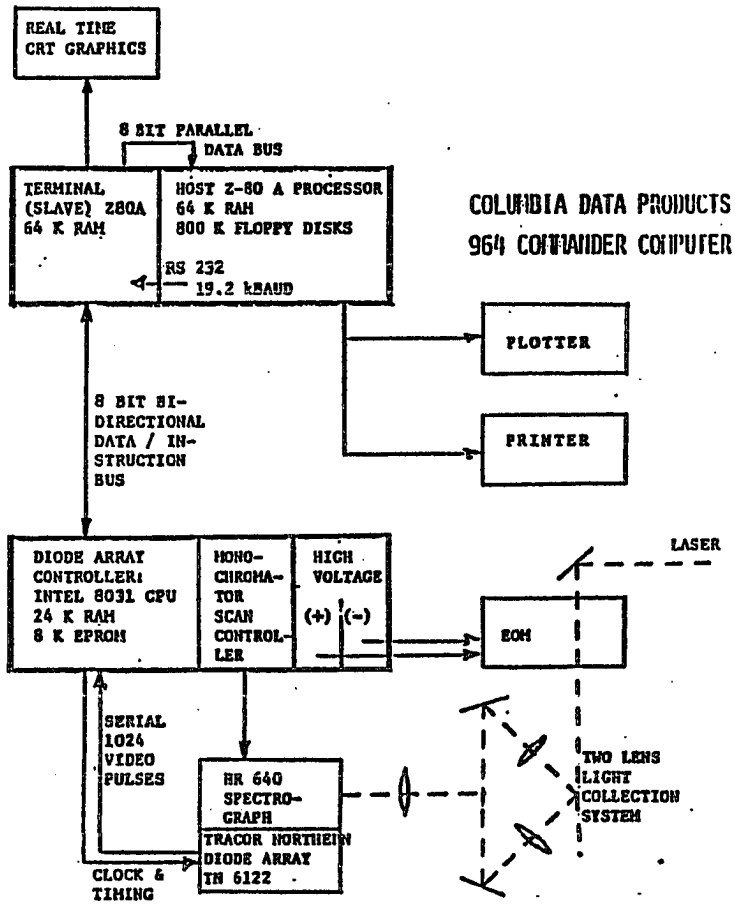

Figure 3-7. Electronic Layout of the Hunter College ROA Unit

delay time and several clearing cycles, data acquisition begins for the next polarization state. The sum of the Raman spectra for both polarization states, as well as the ROA spectrum, are displayed on the computer terminal screen simultaneously, allowing the experimenter to follow improvement of the signal to noise ratio in real time. Further details of the operation and design of this "first generation" ROA unit can be found in reference (30).

The electronic scheme outlined above was operational during development of the EOM alignment procedures and the pinene studies. Since that time, several major improvements have been made. First, the Columbia computer has been replaced with an AT&T 6300 Personal Computer, equipped with an Intel 8086 processor and an Intel 8087 arithmetic coprocessor, 640 kbyte of RAM and two megabyte hard disks (Iomega Bernoulli Box).

The software used to control the instrument, previously written in Z-80 assembly language, has been entirely rewritten in Magic/L.

The output of the laser power meter head is no longer connected to a digital voltmeter. It is now passed to a current-to-frequency converter. A signal proportional to the light intensity sensed by the detector is produced by a fast 32 bit counter and the counter output is, in turn, read by the computer.

A sintered glass scatter plate has been placed in front of the laser power meter head to eliminate the effect of

any polarization sensitivity of the power meter.

Rotation of the polarizer used to measure probe beam parameters is now automated. The polarizer is rotated 360 ^{o}in 200 steps. Each of the 200 intensity measurements is stored in an array and the array is searched for maximum and minimum values. The four intensity measurements are made in the same fashion as in the earlier ROA unit. Now, however, the $\cos^2$ waveform is displayed on the CRT as an intensity vs. angle plot. Using the display, the experimenter can determine if the maximum of the waveform is shifted; i.e., if the ellipse is rotated. Perfectly circularly polarized light would, of course, yield a straight line.

EOM crystals are known to cause small (approximately 20-50μ) beam deflections. While such a deflection seems small, the consequence of such beam movement is the introduction of first derivative-shaped artefacts into ROA spectra. Such artefacts arise because the image of the scattered radiation of one polarization handedness is moved across the diode array with respect to the image formed during the other half of the modulation cycle. Corresponding portions of the Raman spectrum then fall on different diodes. First derivative shaped artefacts occur when the Raman spectra are subtracted to yield ROA signals. Beam expansion drastically minimizes this effect. First derivative shapes occurring in all Raman peaks are a telltale sign of beam deflection during modulation.

A 1 mm pinhole, mounted permanently in front of the detector head, allows measurement of beam deflections to be made. The spinning polarizer is rotated through 360 ^{o} and the 200 intensity measurements are integrated. This is done to eliminate the necessity of removing the rotating polarizer from the beam in order to make an intensity measurement. This procedure is repeated when the opposite polarization handedness is selected. If a difference in intensity is seen, it means that one beam has moved and is either better centered relative to the pinhole or, more commonly, is less well aligned with the hole. The EOM can be realigned, if necessary, to minimize these deflections. As explained earlier, beam deflections cause "first derivative shapes" to appear in the ROA spectrum. Further details can be found in (50).

H. Total ROA of α - Pinene

Pinene is a colorless, high boiling liquid at room temperature and is readily available in enantiomeric form. It has become the universal standard used in evaluation of ROA instrument performance.

Normally, only depolarized ROA of this molecule has been collected. If ROA is to be used to study relatively dilute solutions (1M or less) of biomolecules, for example, collection of only the depolarized component may not be

feasible, because signal levels may be far too low. Collection of total ROA, that is, without a polarization analyzer, may be necessary. Total ROA contains the polarized scattering component, making it more susceptible to polarization artefacts. However, a successful total ROA experiment provides a good test of the alignment of the system. The EOM alignment procedure described above allows the experimenter to achieve EOM alignment good enough to permit the total ROA spectrum, once though to be unobtainable, to be collected. Such a spectrum, as well as the corresponding Raman spectrum, is shown in Figure 3-8. Table 3-1 gives the line positions and values for both total and depolarized ROA measurements made on the "first generation" Hunter College ROA unit. Note that the signs of all total and depolarized Δ values agree. Furthermore they are in agreement with theoretical predictions (10^{-3}-10^{-4}). Acquisition times for total ROA measurement are much shorter than those for depolarized measurements (5 hrs. vs. 10hrs. per enantiomer). Signal to noise ratios for total ROA are also much better.

It is gratifying to note that in their recent, thorough analysis of ROA artefacts in terms of Stokes Mueller calculus, Hecht et.al. (51) point out the importance of total ROA measurements. In addition to greatly increased radiation throughput, the authors point out that use of a polarization analyzer has the disadvantage of being highly susceptible to orientation error due to the dependence of

polarizer orientation on optical rotation of the sample. If, for example, the sample decomposes slightly during a long experiment, with consequent change in the optical rotation, data acquired with an analyzer will be erroneous.

I. ROA of Chlorofluoroacetic Acid

Though pinene is a convenient standard for ROA diagnostics, it is not an ideal sample for ROA model studies due to the large number of vibrations and the difficulty of interpreting ROA signals in terms of a normal coordinate analysis for this molecule. It is clear that at this point in time, studies on smaller molecules, with a relatively small number of vibrations, are needed. The molecule selected for such a study was (-)-S-chlorofluoroacetic acid. Its small number of normal modes and low vapor pressure make it an excellent model system.

The ROA spectrum of chlorofluoroacetic acid is shown in Figure 3-10. Because a neat liquid with a number of highly polarized Raman bands was selected, the depolarized spectrum was recorded. Acquisition time was 15 hours at a laser power of 650 mW at 4880 Å. It was found that this sample was photochemically unstable at this laser wavelength and had begun to decompose after 3 days of exposure to the laser beam. The line at 5145 Å should be used for any future studies. The frequency region from 276.2 cm^{-1} to 982.1 cm^{-1}

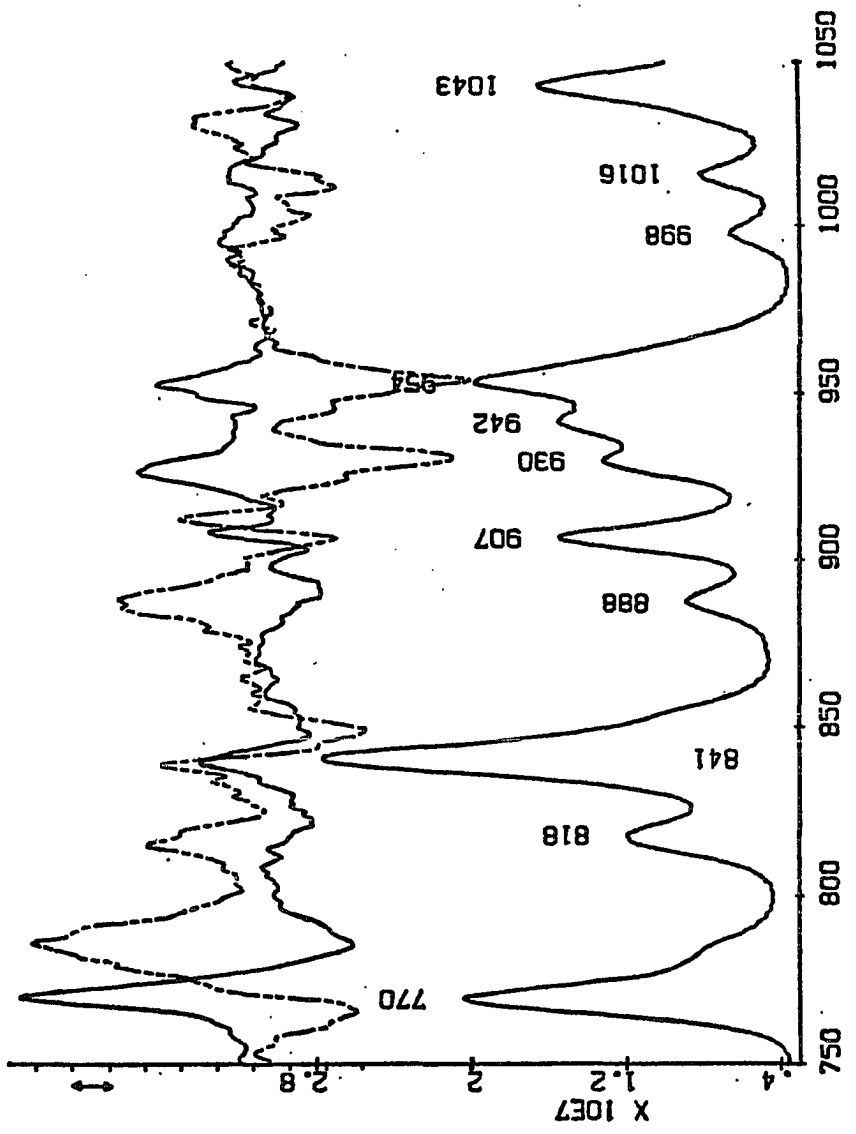

Figure 3-8. Raman and Total ROA Spectra of α-Pinene

Table 3-1. Total ROA Data for α-Pinene

Line Position (cm^{-1})	10^3x Δ Value
770	-0.6
787	2.7
819	0.4
841	-
886	1.0
906	-
929	-0.7
941	0.0
953	-0.5
997	-
1015	-
1043	-

Note: Intensities are in arbitrary units. Dashes indicate signals too small to be distinguished from noise or obscured by spurious signals or other bands.

has two large ROA bands. The first, occurring at 380 cm^{-1}, is associated with the Cl-C-F deformation. The other, at 701 cm^{-1}, corresponds to a skeletal mode.

The ROA is interpreted in terms of relative atomic displacements, given in Table 3-2. As explained in Ch. 2, the fractional contribution to the total of all atomic displacements is found by squaring each term in the matrix and multiplying by the appropriate atomic weight. Atoms are numbered left to right from 1 to 8 (see Fig. 3-9). The first row of numbers for a given vibration corresponds to movement along the molecule fixed x-axis. The second column represents movement along the y axis, and the third, along the z axis. The low frequency mode shows a very large fluorine displacement component; in fact, this fractional contribution to the total of all relative displacements is .49. Also of note is the 22% contribution of the carbonyl oxygen. Thus, these two atoms alone contribute 71% of the total atomic motion in this vibration. Chlorine contributes significantly (0.17) as well.

The high frequency ROA band has, in contrast, a relatively small F motion (2.0%). However, the carbonyl oxygen contributes 17% and the acidic oxygen has a 28% contribution. Other Raman bands in the spectral region studied, with the exception of the 292 cm^{-1} mode, lack any appreciable oxygen atom motion. Though small by comparison with O atom displacements, the H atoms make a relatively large contribution (13%) to the 701 cm^{-1} band when compared to

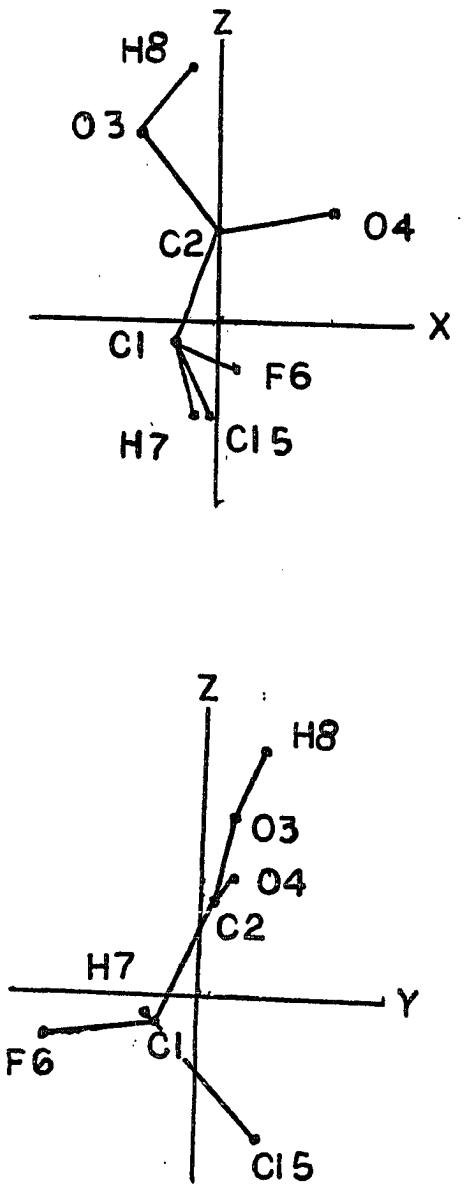

Note: 0.5 inch = 1 Å

Figure 3-9. Geometry and Atom Numbering of Chlorofluoroacetic Acid With Principal Cartesian Coordinates

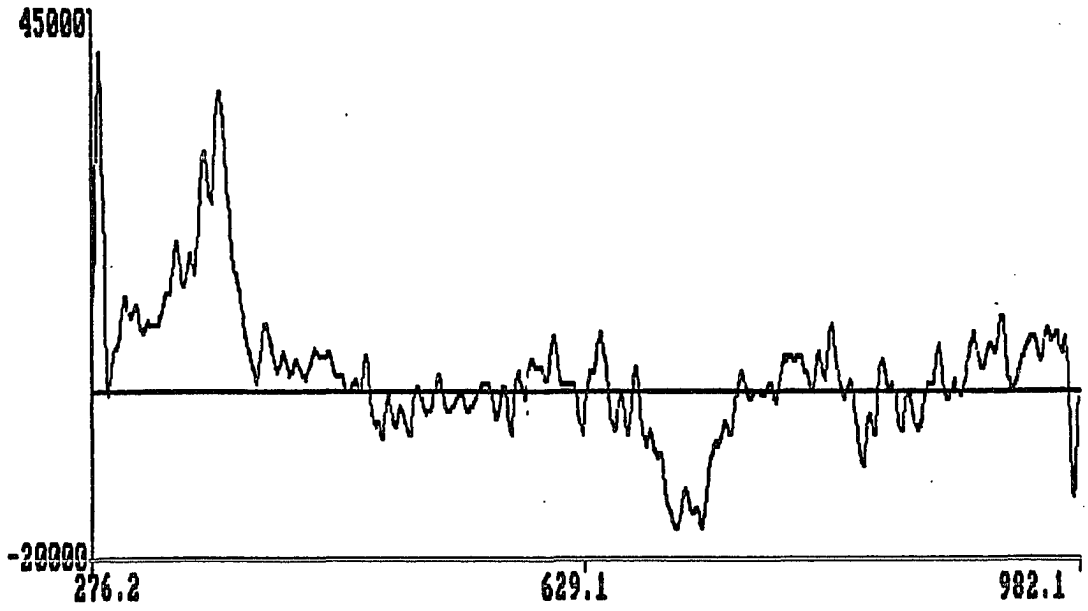

Figure 3-10. ROA Spectrum of (-)-S-Chlorofluoroacetic Acid

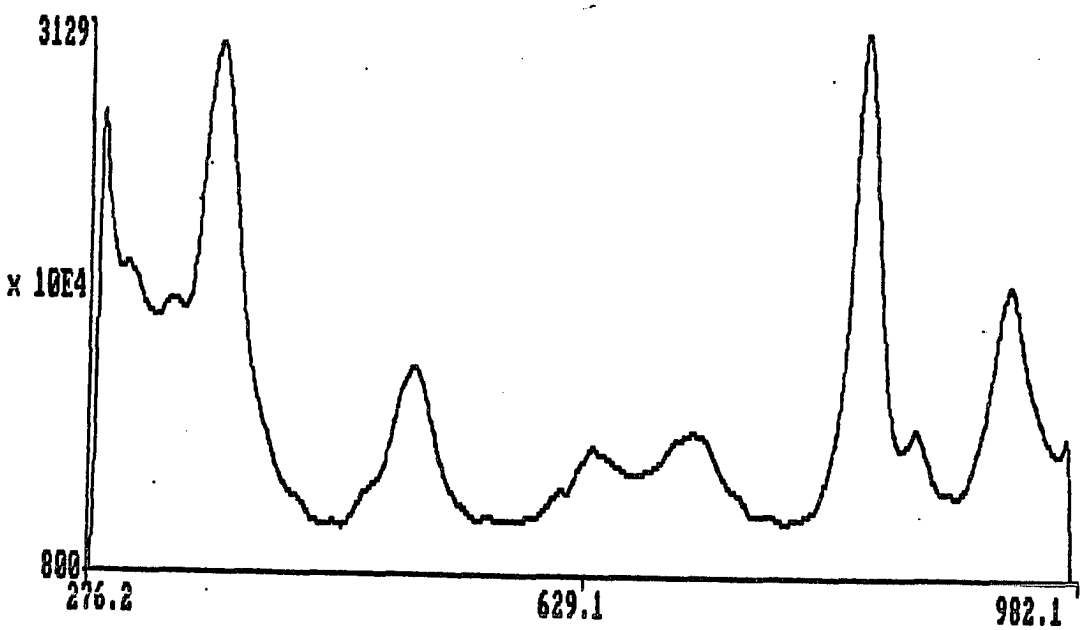

Figure 3-11. Multichannel Raman Spectrum of (-)-S-Chlorofluoroacetic Acid

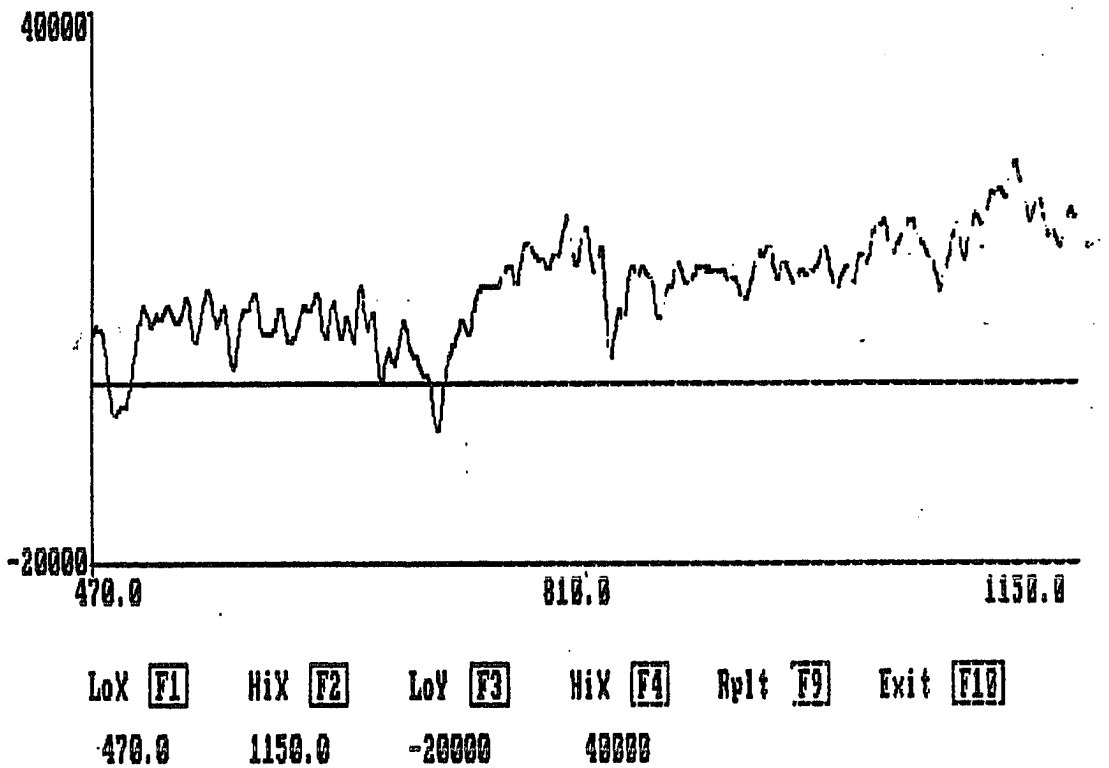

Figure 3-12. ROA Spectum of Chlorofluoroacetic Acid Between 470 cm^{-1} and 1150 cm^{-1}

Table 3-2. SF Matrix for Chlorofluoroacetic Acid

NORMAL MODE NU 1 3531.2 CM-1 3528.0 CM-1							
SF MATRIX							
.0003	-.0009	.0278	-.0002	.0000	.0000	-.0007	-.4294
-.0003	.0009	.0214	.0001	.0000	.0000	.0000	-.3480
-.0008	.0028	.0483	.0002	.0000	.0000	.0001	-.7936
NORMAL MODE NU 2 3015.8 CM-1 3007.0 CM-1							
SF MATRIX							
-.0630	-.0032	-.0001	.0011	-.0012	-.0080	.9676	-.0012
-.0088	-.0021	.0001	.0004	-.0013	.0057	.0614	-.0004
.0007	-.0044	.0000	.0008	.0013	.0012	-.0367	-.0006
NORMAL MODE NU 3 1765.3 CM-1 1759.0 CM-1							
SF MATRIX							
-.0127	.2301	-.0341	-.1334	.0000	-.0004	.0020	.0764
.0018	.0315	.0043	-.0258	.0002	-.0005	-.0493	-.0023
.0066	-.0036	.0248	-.0189	.0001	.0001	-.1006	-.0361
NORMAL MODE NU 4 1426.2 CM-1 1439.0 CM-1							
SF MATRIX							
.0015	.0348	-.0925	.0712	.0001	.0001	-.0130	-.0861
.0039	-.0674	.0256	.0147	-.0013	.0066	.0149	.0205
.0115	-.2026	.1067	.0132	.0046	.0054	.0187	.0902
NORMAL MODE NU 5 1328.3 CM-1 1322.0 CM-1							
SF MATRIX							
.0230	-.0075	.0049	.0096	.0067	-.0370	.0749	-.0279
.0552	-.0069	.0028	-.0010	.0025	.0136	-.9508	.0022
.0134	-.0027	-.0045	.0006	-.0027	.0030	-.0409	.0133
NORMAL MODE NU 6 1250.1 CM-1 1253.0 CM-1							
SF MATRIX							
-.0071	.0076	-.1119	.0701	.0013	-.0037	.0026	.6755
-.0193	.0232	-.0096	.0066	.0011	.0033	-.0529	-.0470
-.0441	.0625	.0161	-.0081	-.0016	.0002	.1007	-.3925

Table 3-2, continued

NORMAL MODE NU 7	1208.9 CM-1	1224.0 CM-1					
SF MATRIX							
-.0058	-.0098	-.0108	.0368	-.0092	.0024	-.0402	.0950
.0264	.0021	-.0080	.0062	-.0040	-.0118	.0632	-.0121
.0999	.0043	-.0133	-.0007	.0015	-.0054	-.8992	-.0696
NORMAL MODE NU 8	1102.9 CM-1	1083.0 CM-1					
SF MATRIX							
-.1087	-.0002	-.0036	-.0023	.0039	.0646	-.0363	.0733
.1891	-.0204	-.0038	.0024	-.0007	-.1051	.0225	-.0050
.0678	-.0104	-.0216	.0025	-.0018	-.0247	.2146	-.0646
NORMAL MODE NU 9	931.8 CM-1	927.0 CM-1					
SF MATRIX							
.0937	-.0484	.0329	-.0769	.0035	-.0192	.0609	.3380
-.0127	-.0273	-.0152	-.0128	.0040	.0399	.0600	-.0332
.1677	-.0982	-.0465	.0009	-.0051	.0039	.2062	-.2065
NORMAL MODE NU 10	797.7 CM-1	811.0 CM-1					
SF MATRIX							
.1437	-.0325	.0174	-.0529	-.0228	-.0110	.1072	.1403
.1382	-.0595	.0180	-.0012	-.0331	-.0097	.1192	.0227
-.1310	-.0092	.0256	-.0155	.0397	.0160	-.1433	-.0428
NORMAL MODE NU 11	706.8 CM-1	701.0 CM-1					
SF MATRIX							
-.1210	.0007	.0982	-.0341	.0023	.0078	-.1054	.2936
-.0352	-.0428	.0082	.0397	-.0034	.0194	-.0761	-.0017
-.0915	-.0834	-.0252	.1212	.0129	.0193	-.1293	-.1269
NORMAL MODE NU 12	617.7 CM-1	620.0 CM-1					
SF MATRIX							
.0261	-.0454	.0185	-.0093	-.0028	.0051	.0273	.0588
-.0144	.2311	-.0289	-.0383	-.0068	-.0636	-.0483	-.0307
-.0247	-.0892	.0345	.0222	.0325	-.0358	-.0257	.0133

Table 3-2, continued

NORMAL MODE NU 13		498.4 CM-1		504.0 CM-1				
SF MATRIX								
.0372	-.0513	.0291	-.0562	.0058	.0108	.0426	.1501	
-.0573	-.0415	.0504	.0072	.0645	-.1056	-.0534	.0368	
-.0014	.0337	.1122	.0136	-.0687	.0033	-.0764	.0511	
NORMAL MODE NU 14		364.5 CM-1		380.0 CM-1				
SF MATRIX								
-.0425	-.0479	.0144	-.0385	.0200	.0368	-.0318	.0922	
.0050	-.0036	.0558	-.0070	-.0664	.0818	-.0284	.0345	
.0308	.0461	.1007	-.0039	-.0005	-.1326	-.0022	.0662	
NORMAL MODE NU 15		289.7 CM-1		292.0 CM-1				
SF MATRIX								
-.0806	-.0675	.0121	-.0338	.0201	.0735	-.0584	.0754	
-.0021	.0048	-.0055	-.0905	.0172	.0487	-.0615	.0283	
-.0250	-.0322	.0338	-.1329	.0126	.1013	-.0820	-.0172	
NORMAL MODE NU 16		268.2 CM-1		270.0 CM-1				
SF MATRIX								
.0017	.0029	.0101	.0045	.0004	-.0095	.0003	-.1247	
.0188	.0065	-.0755	-.0157	-.0002	.0145	.0229	.8580	
.0009	.0057	.0329	.0242	-.0199	.0007	.0046	-.3034	
NORMAL MODE NU 17		215.4 CM-1		222.0 CM-1				
SF MATRIX								
.0117	.0059	.0029	.0155	-.0183	.0062	.0100	.0153	
.0854	.0462	-.0648	-.0606	-.0192	.0680	.0768	-.2602	
-.0033	.0148	.0418	.0882	-.0971	.0574	.0089	.1213	
NORMAL MODE NU 18		120.1 CM-1		.0 CM-1				
SF MATRIX								
-.0344	-.0115	.0238	-.0254	.0588	-.0795	-.0379	.0412	
.0249	.0114	-.1219	.1357	-.0141	-.0041	.0605	-.1411	
-.0007	-.0019	.0613	-.0694	-.0054	.0157	-.0066	.0597	

their movement in other bands in the region. H atoms make a large contribution to the 927 cm^{-1} band as well (20% for both atoms), but there is little motion of the O atoms and no ROA signal.

Thus, it appears that motions of electronegative or electropositive atoms throughout the molecule can be correlated with significant ROA intensity. The Δ values are $1.2x10^{-3}$ for the low frequency band and $5x10^{-4}$ for the high frequency band.

Different types of molecular multipole interference terms can contribute to different vibrations, and such may be the case in chlorofluoroacetic acid. The Δ value for depolarized ROA is given by:

$$I_z^R - I_z^L = 2K(3\alpha_{ij}G'_{ij} - \alpha_{ii}G'_{jj} - (1/3)\alpha_{ij}\epsilon_{ilm}A_{mlj}), \qquad [3\text{-}22]$$

where K is a constant.

α is the electric dipole-electric dipole polarizability tensor, G' is the electric dipole-magnetic dipole tensor, and A is the electric dipole-electric quadrupole tensor. For most bands, the isotropic contribution $\alpha_{ii}G'_{jj}$ is negligible. This is not so for highly polarized bands, such as the one at 701 cm^{-1}, with a depolarization ratio of 0.09. The depolarization ratio for the low frequency Raman band is 0.43. Note that the isotropic part is opposite in sign to the anisotropic ($\alpha_{ij}G'_{ij}$) part and that the ROA bands observed have opposite signs. These facts, coupled with the large difference in depolarization ratios, allow speculation on the nature of the dominant terms

contributing to ROA intensity. Barron and Escribano (52) point out that "such contributions will be responsible for any ROA in strongly polarized bands,...". It should be pointed out that the context in which this statement was made was in reference to ROA intensity of a strongly polarized band in β-pinene. Available data do not allow speculation on the relative importance of the quadrupole term, though its relative importance could be deduced if either polarized or total ROA, recorded under condtions identical to those in depolarized measurements, were available. One must be certain, however, that the instrument response is the same for both polarized and depolarized measurements. In any case, it appears that depolarized ROA intensity in chlorofluoroacetic acid is generated by motions of either electronegative (F) or electropositive (H) atoms coupled with motions of the oxygen atoms (and their associated pairs of non-bonded electrons).

It is hoped that further studies such as these will, by expanding the limited ROA data base, allow empirical correlation of ROA intensity with atomic motions and conformational changes and assist in development of improved ROA computational techniques.

BIBLIOGRAPHY

1. Pease, L. and Watson, C., J. Amer. Chem. Soc. 100, 1279 (1978)

2. Greenfield, N. and Fasman, G.D., Biochemistry 8, 4108 (1969)

3. Blout, E.R., in "Optical Rotatory Dispersion: Applications to Organic Chemistry", C. Djerassi, ed., McGraw-Hill, New York (1960)

4. Ronich, F.W. and Krim, W.S., Biopolymers 20, 1919 (1972)

5. Biot, J.-B., Mem. de l'Inst. 13, part 1, 218 (1812)

6. Arago, D.F.J., Mem. de l'Inst. 12, part 1, 93 (1811)

7. Biot, J.-B., Mem. de l'Inst. 2:41, 136 (1817)

8. Haidinger, W., Ann. Phys. 70, 531 (1847)

9. Pasteur, L., Ann. Chim. 24, 457 (1848)

10. Cotton, A., Compt. Rend. 120, 989, 1044 (1895)

11. Kuhn, W., Trans. Faraday Soc. 26, 293 (1930)

12. Moffit, W., Woodward, R.B., Moscowitz, A., Klyne, W., and Djerassi, C., J. Amer. Chem. Soc. 83, 4013 (1961)

13. Gans, R., Z. Phys. 17, 353 (1923)

14. de Mallemann, R., Compt. Rend. 181, 371 (1925)

15. Kastler, A., Compt. Rend. 191, 565 (1930)

16. Atkins, P.W., and Barron, L.D., Molec. Phys. 16, 453 (1969)

17. Barron, L.D., and Buckingham, A.D., Molec. Phys. 20, 1111 (1971)

18. Bosnich, B., Moskovits, M.,and Ozin, G.A., J. Amer. Chem. Soc. 94, 4350 (1972)

19. Diem, M., Fry, J.L., and Burow, D.F., J. Amer. Chem. Soc. 95, 253 (1973)

20. Barron, L.D., Bogaard, M.P., and Buckingham, A.D., J. Amer. Chem. Soc. 95, 603 (1973)

21. Hug, W., Kint, S., Bailey, G.F., and Scherer, J.R., J. Amer. Chem. Soc. 97, 5509 (1975)

22. Barron, L.D., and Buckingham, A.D., J. Chem. Soc. Chem. Comm., 192 (1973)

23. Hug, W., Kamatari, A., Srinivasan, K., Jansen,H.-J., and Sliwka, H.-R., Chem. Phys. Lett. 76, 3, 469 (1980)

24. Barron, L.D., and Buckingham, A.D., J. Chem. Soc. Chem. Comm., 192 (1973)

25. Barron, L.D., J. Chem. Soc. Perkin II, 1074 (1976)

26. Barron, L.D., Meehan, C., and Vrbancich, J., J. Raman Spectrosc. 12, 251 (1982)

27. Hug W., Applied Spectrosc. 35, 1, 115 (1981)

28. Barron, L.D., and Vrbancich, J., J Raman Spectrosc. 15, 1, 47 (1984)

29. Hug, W., and Surbeck, H., Chem. Phys. Lett. 60, 186 (1979)

30. Oboodi, M.R., Davies, M.A., Gunnia, U., Blackburn, M.B., and Diem, M., J. Raman Spectrosc. 16, 366 (1985)

31. Landau, L.D., Lifschitz, E.M., and Pitaevskii, L.P., "Electrodynamics of Continuous Media", Pergamon Press (1984)

32. Barron, L.D., "Molecular Light Scattering and Optical Activity", Cambridge (1982), and references therein

33. Wigner, E.P., Z. Phys. 43, 624 (1927)

34. Barron, L.D., Nature 238, 5358, 17 (1972)

35. Schellman, J.A., J. Chem. Phys. 44, 1, 55 (1966)

36. Young, J.A., and Tarrant, P., J. Amer. Chem. Soc. 71, 2432 (1949)

37. Diem, M., Computer Enhanced Spectroscopy 1, 4, 191 (1983)

38. Katon, J.E., and Sinha, D., Spectrochim. Acta 33A, 45 (1977)

39. Wilmshurst, J.K., J. Chem. Phys. 25, 6, 1171 (1956)

40. Durig, J.R., Wurrey, C.J., Bucy, W.E., and Sloan, A.E., Spectrochim. Acta 32A, 175 (1976)

41. Koehler, J.S., and Dennison, D.M., Phys. Rev. 57, 1006 (1940), quote of unpublished data of Lawson, J., and Randall, H.M.

42. Wilson, E.B., Decius, J.C., and Cross, P., "Molecular Vibrations", McGraw-Hill, New York, 1955

43. Herzberg, G., "Infrared and Raman Spectra", Van Nostrand Reinhold, New York, 1945

44. Urey, H.C., and Bradley, C., Phys. Rev. 38, 1969 (1931)

45. Schachtschneider, J.H., "Vibrational Analysis of Polyatomic Molecules", Report No. 231-64, Shell Development Co., Emeryville, CA 94608, 1964

46. Born, M. and Wolf, E., "Principles of Optics", 6th ed., Pergamon Press, Oxford (1980)

47. Kaminow, I.P. and Turner, E.H., Appl. Optics 5, 10 (1966)

48. Hecht, E. and Zajac, A., "Optics", Addison Wesley, Reading, MA, 1974

49. Diem, M. and Ludl, H., Computer Enhanced Spectroscopy, in press

50. Gunnia, U., Diem, M., and Davies, M.A., J. Raman Spectrosc., in press

51. Hecht, L., Jordanov, B., and Schrader, B., Applied Spectrosc. 41, 2, 295 (1987)

52. Barron, L.D., and Escribano, J.R., Chem. Phys. Lett. 126,5 (1986)

53. Diem, M. and Burow, D.F., J. Phys. Chem. 81, 476 (1977)